UNIVERSIDADE D
COIMBRA

Carolina Rodrigues Duro

UNRAVELLING THE ROLE OF THE VENTRAL PREMAMMILLARY NUCLEUS OF THE HYPOTHALAMUS IN FEMALE SEXUAL BEHAVIOR

Dissertação no âmbito do Mestrado em Biologia Celular e Molecular, com especialização em Neurociências, orientada pela Doutora Susana Quelhas Lima e pelo Professor Doutor João Peça Silvestre apresentada ao Departamento de Ciência da Vida da Universidade de Coimbra.

Setembro de 2021

Faculdade de Ciências e Tecnologias
da Universidade de Coimbra

Unravelling the role of the ventral premammillary nucleus of the hypothalamus in female sexual behavior

Carolina Rodrigues Duro

Dissertação no âmbito do Mestrado em Biologia Celular e Molecular, com especialização em Neurociências, orientada pela Doutora Susana Quelhas Lima e pelo Professor Doutor João Peça Silvestre apresentada ao Departamento de Ciência da Vida da Universidade de Coimbra.

Setembro de 2021

1 2 9 0

UNIVERSIDADE D
COIMBRA

Affiliation:

Champalimaud Foundation

Champalimaud Centre for the Unknown

Champalimaud Research

Avenida Brasília, 1400-038 Lisbon, Portugal

Funding:

FCT Fundação para a Ciência e a Tecnologia

erc European Research Council

Acknowledgements/Agradecimentos

A realização da tese de mestrado é uma longa viagem marcada por inúmeros desafios, tristezas, incertezas e alegrias. Apesar do processo individual a que qualquer investigador está destinado, há pessoas indispensáveis para encontrar o melhor rumo em cada momento da caminhada. Trilhar este caminho só foi possível com o apoio, energia e força de vários familiares e amigos, a quem dedico especialmente esta dissertação.

À orientadora, Susana Lima, agradeço a orientação exemplar pautada por um elevado nível científico, um interesse permanente e uma visão crítica e oportuna, os quais contribuíram para enriquecer, passo por passo, todas as etapas subjacentes ao trabalho realizado.

Ao meu co-orientador, António Dias, pelo empenho inexcedível em cada passo da minha aprendizagem, pela paciência e disponibilidade diária, pelas orientações mestreais, pelo auxílio a ultrapassar todos os problemas que foram surgindo durante este percurso e por nunca desistir de mim!

A todos os elementos do Lima Lab pela ótima integração, espírito de equipa e sentimento de companheirismo que me proporcionaram muito bons momentos.

A todos os colegas de curso, em especial à colega e amiga sempre presente Jéssica Silva, sempre disponível para ouvir as minhas preocupações e dúvidas, mas também para celebrar cada vitória, ao longo deste processo.

Às amigas de Pombal Elsa Ferreira, Laura Carreira, Carolina Estrela, Liliana Freire, Mariana Gomes, Isabel, Constança e Flávia Rodrigues, entre outros, que estiveram ao meu lado durante este período, pelo companheirismo, pelo apoio nos momentos difíceis e por festejarem cada pequena vitória como o se fosse o fim da guerra!

À minha família, que sempre me apoiou todas as minhas decisões e fez inúmeros sacrifícios para que eu pudesse hoje terminar o meu percurso académico. Em especial, à tia Martinha e aos avós Maria e Hilário por serem o meu porto de abrigo em todas as ocasiões, por estarem sempre presentes e por terem a capacidade de desmitificar todos os aparentes problemas em aspetos positivos.

Por último, tendo consciência que sem eles nada disto teria sido possível, dirijo um agradecimento especial aos meus pais e irmã. Por todas as viagens a Lisboa para não me deixarem só, por serem modelos de perseverança, pelo apoio incondicional, incentivo e paciência demonstrados na superação dos obstáculos que ao longo deste ano. A eles dedico este trabalho!

Por fim, o meu profundo agradecimento a todas as pessoas aqui não mencionadas que contribuíram para a concretização desta dissertação, estimulando-me intelectual e emocionalmente.

“Ever tried. Ever failed. No matter. Try again. Fail again. Fail better”, *Samuel Beckett*

Abstract

The ventral premammillary nucleus (PMv) of the hypothalamus receives strong olfactory inputs and is highly connected to the brain's social behavior network, suggesting that it plays a central role in mouse social behavior. In male mice, Dopamine Active Transporter (DAT) gene expressing neurons of the PMv have been shown to be important for male social and aggressive behavior. In females, the role of these PMv-DAT neurons is still poorly understood. Preliminary results from our lab suggest that this population is also specifically activated by male-derived cues. The fact that PMv-DAT cell activation is related with opposite sex cues suggests that this population may be involved in male directed behaviors in the female as well, namely in sexual behavior. However, its role in this fundamental behavior has never been addressed.

To shed light into the role of the PMv-DAT population in females, we took a two-way approach: first, since the PMv-DAT population is active when exposed to the same cues (male derived signals) in both sexes, but the behavioral output can be drastically different, we hypothesize that these neurons might project to different target regions in male versus females. Consequently, we determine the output regions of the PMv-DAT population in females. To address this, we used a combination of Cre-expressing mice (DAT-Cre) together with an anterogradely travelling Cre-dependent viral vector expressing synaptophysin-GFP, which specifically labels the presynaptic terminals of this population. Second, in order to determine the role of this population in female sexual behavior, we performed a genetic ablation study, using a Diphtheria Toxin receptor and its ligand. Afterwards, a sexual behavioral study in the PMv neuronal ablated females was carried out to clarify the role of the PMv in the sexual circuits.

Mapping the architecture of this circuit and test the function of the PMv-DAT cells in sexual behavior will ultimately help us to better understand the role of the PMv in female sexual behavior.

Keywords: Ventral Premammillary Nucleus; Sexual Behavior; Neuronal Tracing; Neuronal Ablation.

Resumo

O núcleo pré-mamilar ventral (PMv) do hipotálamo recebe fortes *inputs* olfativos e está conectado à rede neuronal que regula os comportamentos socias do cérebro, sugerindo que desempenha um papel central no comportamento social em roedores. Em ratinhos machos, o gene *Dopamine Active Transporter* (DAT), expresso pelos neurónios do PMv, demonstrou ser importante para o comportamento social e agressivo masculino. Nas mulheres, o papel dessa população neuronal ainda é pouco compreendido. Resultados preliminares de nosso laboratório sugerem que os neurónios PMv-DAT são especificamente ativados por estímulos sensoriais provenientes do sexo masculino. O facto de a ativação das células PMv-DAT estar relacionada com estímulos do sexo oposto sugere que esta população pode estar envolvida em comportamentos femininos direcionados ao macho, nomeadamente no comportamento sexual. No entanto, a sua função e estrutura neste comportamento fundamental nunca foi abordada.

De forma a esclarecer o papel da população PMv-DAT em fêmeas, estabelecemos dois objetivos fundamenteis: estudar a conectividade deste núcleo, através da marcação dos seus outputs, e testar a sua função no comportamento sexual, utilizando uma ablação neuronal genética. Para o primeiro propósito, uma vez que a população PMv-DAT é ativa quando exposta aos mesmos sinais (sinais derivados do sexo masculino) em ambos os sexos, mas o comportamento gerado pode ser diferente, propusemos que estes neurónios podem projetar para diferentes regiões do cérebro em machos e fêmeas. Consequentemente, decidimos determinar os *outputs* da população PMv-DAT em fêmeas. Para isso, usámos uma combinação de ratinhos que expressam Cre (DAT-Cre) simultaneamente com um vetor viral anterógrado dependente de Cre, que expressa sinaptofisina-GFP, de forma a marcar especificamente os terminais pré-sinápticos da população. Para o segundo objetivo, a fim de compreender o papel as células PMv-DAT no controlo do comportamento sexual feminino, uma ablação neuronal, usando o recetor e a toxina Difteria, foi realizada especificamente para células PMv-DAT. Posteriormente, foi realizado um estudo comportamental sexual nas fêmeas submetidas à ablação neuronal PMv para esclarecer o papel do PMv nos circuitos sexuais femininos. Em suma, o mapeamento da arquitetura deste circuito e o teste funcional das células PMv-DAT ajudará a compreender o papel do PMv no comportamento sexual feminino.

Palavras-chave: Núcleo Pré-Mamilar Ventral; Comportamento Sexual; Marcação Neuronal; Ablação Neuronal.

Content

List of Figures

List of Tables

Abbreviations

AAV – Adeno-associated Virus;

AHN - Anterior Hypothalamus Nucleus;

AHA - Anterior Hypothalamic Area;

AHC - Anterior Hypothalamic Area, central;

AHP - Anterior Hypothalamic Area, posterior;

AHiPM - Amygdalohippocampal Posteromedial, posterior part;

AOB - Accessory Olfactory Bulb;

AON - Anterior Olfactory Nucleus;

ARC – Arcuate Nucleus;

BNST - Bed Nucleus of the Stria Terminalis;

BNSTpd – Bed Nucleus of the Stria Terminalis, postero-dorsal part;

BNSTpm - Bed Nucleus of the Stria Terminalis, posteromedial part;

BNSTpr - Principal Nucleus of the Bed Nucleus of the Stria Terminalis;

BNSTpv - Bed Nucleus of the Stria Terminalis, ventral part;

BrdU – Bromodeoxyuridine;

BSL – Biosafety Level;

Casp3 – Caspase-3;

ChR2 - Channelrhodopsin-2;

CNO - Clozapine N-oxide;

CoA - Cortical Amygdala;

CoAa - Cortical Amygdala, anterior part;

CoApl - Cortical Amygdala, posterolateral part;

CoApm - Cortical Amygdala, posteromedil part;

CTb - Subunit B of the Cholera Toxin;

CTb-ir - CTb Immunoreactive Neurons;

DAT – Dopamine Active Transporter;

DIO - Double-Floxed Inverse Open Reading Frame;

DM - Dorsomedial Hypothalamic Nucleus;

DREADDs - Designer Receptors Exclusively Activated by Designer Drugs;

DTR - Diphtheria Toxin Receptor;

DTx - Diphtheria Toxin;

EnvA-RVDG - EnvA pseudotyped, glycoprotein-deleted RV;

EPSC - Excitatory Postsynaptic Currents;

ERα - Estrogen Receptor Alpha;

FACS - Fluorescence-Activated Cell Sorting;

FSH - Follicle-Stimulating Hormone;

fx – fornix;

GCaMP - Genetically Encoded Calcium Indicator;

GFP – Green Fluorescence Protein;

GnRH - Gonadotropin-Releasing Hormone;

I - Intercalate Nucleus of the Amygdala;

ICj - Island of Calleja;

IEG - Immediate Early Gene;

IPACM - Interstitial Nucleus of the Posterior Limb of the Anterior Commissure, medial;

IPACL - Interstitial Nucleus of the Posterior Limb of the Anterior Commissure, lateral;

IPSC - Inhibitory Postsynaptic Current;

KO – Knockout;

LA - Lateroanterior Hypothalamic Nucleus;

LH - Luteinizing Hormone;

LO - Lateral Olfactory Tract;

LPAG - Lateral Periadeductal Grey;

LSI - Lateral Spetal Nucleus, intermediate part;

LSV - Lateral Septal Nucleus, ventral part;

LV – Lateral Ventricle;

MeA – Medial Amygdala;

MeAAHi - Medial Amygdala, amygdalo-hippocampal part;

MePD – Medial Amygdala, posterodorsal part;

MePV - Medial Amygdala, posteroventral part;

MFB - Medial Forebrain Bundle;

MOB - Main Olfactory Bulb;

MOE - Main Olfactory Epithelium;

MOI – Multiplicity of Infection;

MPN – Medial Preoptic Nucleus;

MPOA – Medial Preoptic Area;

mt - mammillothalamic tract;

M1 - Primary Motor Cortex;

M2 - Secondary Motor Cortex;

NAc - Nucleus Accumbens;

NMDA - N-methyl-D-aspartate;

Opt - Optic Tract;

Or - Stratus Oriens;

OSN - Olfactory Sensory Neurons;

OT – Olfactory Tubercle;

OVX – Ovariectomized;

PA - Posterior Amygdala;

PAG – Midbrain Periaqueductal Gray;

PaV - Paraventricular Hypothalamic Nuclei, ventral part;

PaAP - Paraventricular Hypothalamic, anterior parvicell;

PaMP - Paraventricular Hypothalamic, medial parvicell;

PB - Phosphate Buffered;

PBS - Phosphate Buffered Saline;

PFA – Paraformaldehyde;

PFC – Prefrontal Cortex;

PHAL - Phaseolus Vulgaris

Leucoagglutinin;

plCOA - Posterolateral Cortical Amygdala;

PLH - Peduncular Lateral Hypothalamic Nuclei;

PMv – Ventral Premammillary Nucleus;

PMd – Dorsal Premammillary Nucleus;

PR – Progesterone Receptor;

PVN - Paraventricular Nucleus of Hypothalamus;

RABV - Rabies Virus;

RCh - Retrochiasmatic Area;

RChl - Retrochiasmatic Area, lateral part;

retroAAV – Retrograde Adeno-associated Virus;

RG - Rabies Envelope Glycoprotein;

RML - Retromammillary Nucleus lateral;

RMM - Retromammilary Nucleus, medial;

Rt - Reticular Thalamic Nucleus;

Shy - Septohypothalamic Nuclei;

SM - Stria Medullaris;

SN – Substantia Nigra;

StA - Strial Part Preoptic Area;

StHy - Striohypothalamic Nuclei;

TEVp - Heterologous Enzyme Tobacco Etch Virus Protease;

Trpc2 - Channel mediating VNO Signaling.

TVA - Avian Tumor Virus Receptor A;

vGlut - Vesicular Glutamate Transporter;

VLPAG: Ventrolateral Periaqueductal Grey;

vLSN - Ventral Lateral Septal Nucleus;

VMH - Ventromedial Nucleus of the Hypothalamus;

VMHdm - Dorsomedial Ventromedial Nucleus of the Hypothalamus;

VMHvl - Ventromedial Nucleus of the Hypothalamus, ventrolateral part;

VMHvll – Ventromedial Nucleus of the Hypothalamus, lateral part;

VMHvlm - Ventromedial Nucleus of the Hypothalamus, ventrolateral medial part;

VNO - Vomeronasal Organ;

VP – Ventral Pallidum;

VSV - Vesicular Stomatitis Virus;

VTA – Ventral Tegmental Area.

VTM - Ventral Tuberomammilary Nucleus.

Introduction

Introduction

1. Sexual Behavior

Sexual behavior is an example of a social interaction, a very particular one that is not only necessary for reproduction and, consequently, for species survival, but also for species evolution (Georgiadis et al., 2012; Kudwa et al., 2005; James G. Pfaus et al., 2016). Not surprising, nature reinforced mechanisms that, similarly to other instinctive behaviors, turned sex into a pleasurable endeavor across different taxa, from humans to rodents (Georgiadis et al., 2012; Kudwa et al., 2005; James G. Pfaus et al., 2016).

Rodents are some of the most established mammalian model systems in biology. Within the different rodent species, particularly the rat was fundamental for early studies on the neurobiological basis for sexual behavior. A notable shift has taken place over the past decades, with mice taking a more prominent role. This shift was primarily instigated by the availability of a larger genetic toolbox for mice, particularly for manipulation and monitoring of specific cell populations. In this way, mice became fundamental to stablishes a causal relationship between the activity of specific cell groups and behavior. Accordingly, it was the model used in this study.

Given the fact that sexual behavior is widespread across different animal species, efforts have been made to unravel the neuronal systems controlling this behavior, taking into consideration the anatomical connections (James G. Pfaus, 1999). Nevertheless, the current knowledge about the specific neural mechanisms underlying sexual behavior is limited. In order to understand the neurobiological regulation of this behavior, it is important to recognize the phases of the sexual interactions (Snoeren, 2018). Overall, sexual behaviors follow a conserved pattern and can be divided in five phases: detection, approach, investigation, consummatory or action and post-consummatory phase (fig. 1) (Wei et al., 2021). The first three phases can be considered together as an **appetitive phase,** which brings the animals into close proximity (K. Hashikawa et al., 2016).

In the detection phase, rodents aim to identify the presence and location of a distant social target via sensory cues emitted by the target. These cues are mainly olfactory, i.e., vaginal secretions and male urine markings. Upon sensing conspecific olfactory cues, a rodent decreases its velocity, twitches its nose rhythmically, while changing its orientation (Kurnikova et al., 2017). Volatiles emitted from animals are detected by olfactory sensory neurons (OSNs) in the main olfactory epithelium (MOE) and information is relayed to the main olfactory bulb (MOB) (Baum & Cherry, 2015), where the signal is distributed to multiple regions, including the olfactory tubercle (OT), anterior olfactory nucleus (AON) and amygdala (Spehr et al., 2006; Wei et al., 2021). On the other hand, non-volatile compounds, such as pheromones (Dulac & Torello, 2003), induce behavioral responses through the activation of related neural pathways (Baum & Cherry, 2015). Pheromones

are detected by vomeronasal sensory neurons (VSNs) (Martel & Baum, 2009) and gain access to the brain via the vomeronasal organ (VNO), which sends input to the accessory olfactory bulb (AOB) (Belluscio et al., 1999). From there, most olfactory information arrives at the medial nucleus of the amygdala (MeA), which in turn innervates hypothalamic nuclei such as the medial preoptic nucleus (MPN), the ventromedial nucleus (VMH) and the ventral premammillary nucleus (PMv) (Belluscio et al., 1999; A. Chen et al., 2020). The approach and investigation phase are defined as close exploration, usually through sniffing, of the social target (Jänig et al., 2018). Sniffing is directed toward facial or anogenital areas, where pheromones are released, which leads to an increase in sexual arousal (Liberles, 2014). The appetitive phase provides a gateway that reflect an individual's internal readiness to engage with a social stimulus (Jänig et al., 2018). Accordingly, while the male mouse usually is very eager to explore the female mouse to copulate, the female behavior can vary as she decides whether to accept or reject the male, depending on her internal state (Golden et al., 2016; Trezza et al., 2011). If the female is receptive, the consummatory phase will follow.

The **consummatory phase** in rodents consists in mounting, where the male grabs the female flank with his forelimbs and performs pelvic thrusts to insert the penis inside the female vagina. A receptive female allows the male to mount her, by performing a position known as lordosis. Lordosis posture is a stereotypic female copulatory behavior performed in response to a stimulus (male touching the flanks), and characterized by a posture of a hollow back and deflected tail to give the male access to her vagina (Flanagan-Cato, 2011; Snoeren, 2018). The lordosis behavior reflects the female's receptivity and varies according to the hormonal state of the female. After several cycles of mounting and dismounting, where a variable number of penile intromissions are performed, ejaculation occurs, which is easily identified as the male starts shivering and eventually falls to the side of the female, where he stays immobile for around 25 seconds (Hull & Dominguez, 2007; Johansen et al., 2008; T. E. McGill & Coughlin, 1970; Thomas E. McGill, 1961). The consummatory phase ends with the ejaculation, which also sets the start of the **post-consummatory phase**. This last stage is characterized by the absence of sexual drive for a period of time, the refractory period, which varies according to the mice strain (Hulla & Dominguez, 2007; Johansen et al., 2008; Valente et al., 2021). Sexual behavior has been characterized in both male and female rats. However, mouse reproductive behavior has been mostly described for males (Burns-Cusato et al., 2004). Even though, the internal and external states modulate sexual receptivity in both male and female mice, my master thesis focuses exclusively on the female's perspective of sexual behavior and the underlying neuronal mechanisms.

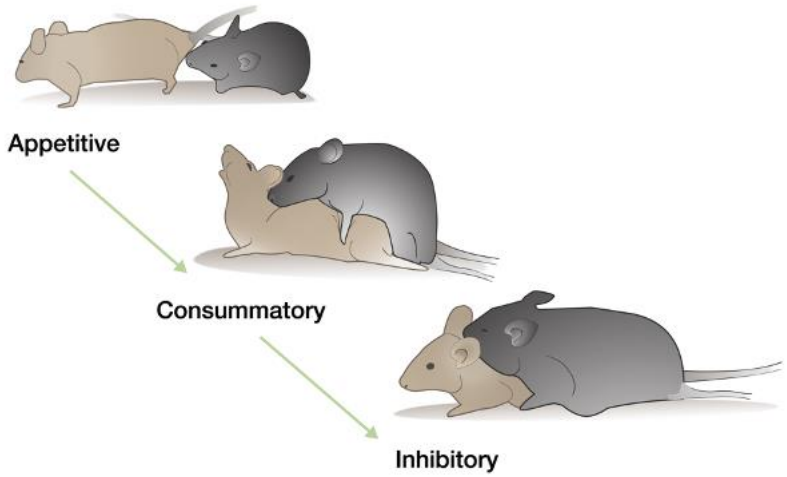

Figure 1. Sexual behavior follows the typical structure of motivated behaviors. During the appetitive phase both male and female perform different types of investigations, such as anogenital, nose to nose or body to body. The second phase consists in the stereotypic behavior, made up of mounts with or without intromissions, which allows ejaculation to occur. Sexual behavior ends with a post-consummatory phase, which is characterized by the absence of sexual drive for a variable time. Adapted from: Lima *et al*, 2015.

1.1. Reproductive Cycle in Female Mice and Hormonal Dependence

As mentioned earlier, in female mice, the willingness to engage in a sexual behavior can vary, depending on her internal state, which is dictated by reproductive cycle, known as estrous cycle in rodents, and lasts approximately 4-5 days (Snoeren, 2018). In general, the estrous cycle is regulated by the hypothalamus-pituitary-gonads axis and the synthesis of the gonadotropin-releasing hormone (GnRH), as the GnRH released by the hypothalamus induces the secretion of luteinizing hormone (LH) and follicle-stimulating hormone (FSH) by the anterior pituitary, leading to ovulation (Butcher et al., 1974; Sarkar et al., 1976). Ovulation in females is the most crucial event during the cycle and is a timed process governed both centrally, by theses GnRH neurons in the hypothalamus, and locally, by two sex hormones: estrogen/estradiol released by the ovarian follicles and progesterone released by the corpora lutea (Miller & Takahashi, 2014) (fig. 2). Thus, fluctuations in these hormones are well defined across the estrous cycle, which can be divided in four stages:

1. **Metestrus:** is the recovery period that occurs in the absence of fertilization from the past cycle. It consists in the generation of corpus luteum and, normally, the plasma circulating levels of progesterone, estrogen, LH and FSH are low;

2. **Diestrus:** corresponds with the maturation of follicles. Hormonal LH and FSH levels are low. However, estrogen concentration increases progressively (Butcher et al., 1974; Snoeren, 2018; Walmer et al., 1992);

3. **Proestrus:** consists in the period when LH, FSH, progesterone, and estrogen reach the maximum concentration, which corresponds to the preovulatory state. Females are usually receptive in a late phase of this stage, namely in the transition proestrus/estrus;

4. **Estrus:** is characterized by ruptured follicles and formation of corpus luteum. The levels of estrogen concentrations start to decline and the concentrations of LH and FSH are the lowest during all cycle.

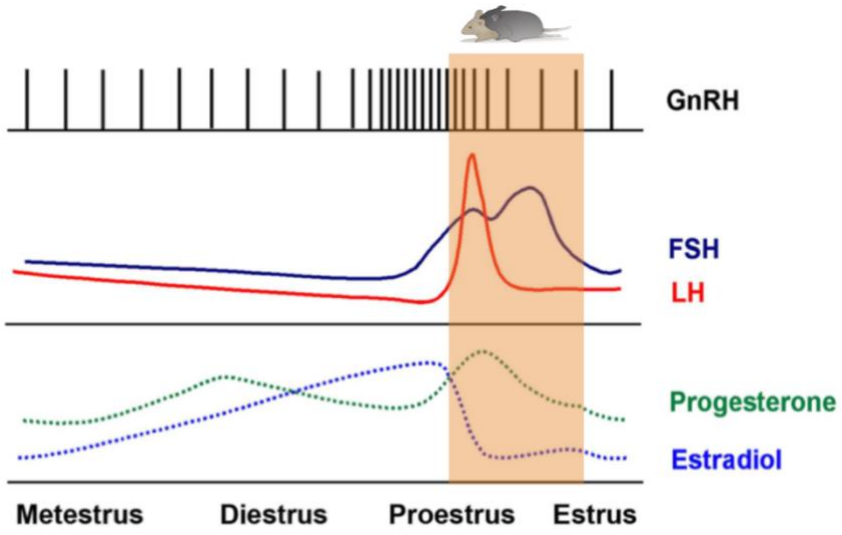

Figure 2. Hormonal fluctuations across the typical estrous cycle in rodents and correlation with sexual behavior. In the mouse, the estrous cycle repeats every 4–5 days. Metestrus and diestrus are characterized by low but slowly increasing levels of estradiol. Proestrus starts with an increase in GnRH release from the hypothalamus and a peak of LH and FSH is also observed. Estrogen reaches the higher concentration in the pre-ovulatory period, while progesterone peak overlaps the ovulation. In orange is represented the period of female sexual receptivity. Adapted from: Miller & Takahashi, 2014.

The duration of each stage is well characterized in the rat, with a total duration of 4-5 days: proestrus lasts for 12 to 14 hours, estrus for 25 to 27 hours, metestrus for 6 to 8 hours and diestrus, for 55 to 57 hours (Snoeren, 2018). On the other side, mice do not display such regular cycles. The identification of each stage in mice can be done by vaginal smear cytology, according to the cell types present in female vaginal secretion (fig. 3). By this method, it is possible to correlate the phase of the estrous cycle, which allow the use of each stage as a variable and to correlate it with the behaviors performed by the female.

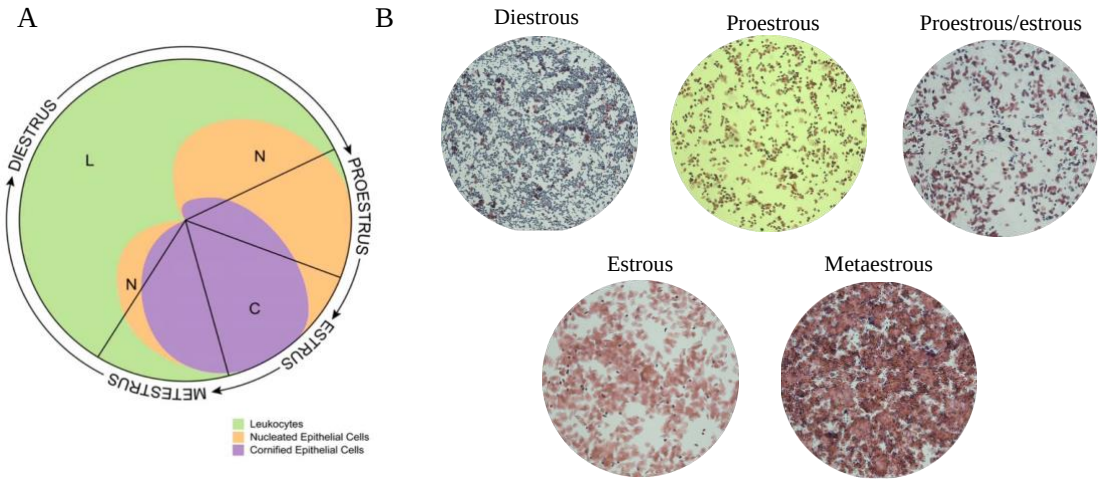

Figure 3. Estrous cycle stage identification. (A) Visual representative map of the cell types and their relative proportion during the four stages. The lines in the circle mark where the stage of estrous changes. The total cycle takes about 4–5 days, consequently the size of each quadrant (between 2 lines) consists in an estimation of the length of each stage. (B) Representative images of vaginal secretions, with 10x magnification, that illustrate different cell types during the estrous cycle. Adapted from Byers *et al*, 2012.

The propensity of a female mice for the sexual behavior changes during the cycle stages and, consequently, they perform different behaviors towards a male copulatory attempt (Nomoto & Lima, 2015). On one hand, during the receptive phase, which corresponds to the transition of proestrus to estrus stage, estrogen and progesterone reach the highest concentration (fig. 3), and females are likely to allow the male to mount and to adopt the lordosis posture. On the other hand, during the non-receptive phase female mice will reject the mount attempts by escaping and performing kicking behaviors towards the male (rearing up, lunging, turning, biting or chasing) (Johansen et al., 2008). In non-naturally cycling females without ovaries, known by ovariectomized (OVX), sexual receptivity can be induced by the combination of hormonal injection of estrogen and progesterone (Levine et al., 1992; Miller & Takahashi, 2014; Simonian et al., 1999).

2. Neuronal Circuits Underlying Sexual Behaviors

Sexual behavior is coordinated by an orchestra of neural circuits, which integrate incoming sensory information with the internal state (Georgiadis et al., 2012). Our knowledge regarding the neuronal mechanisms underlying sexual behavior originates from studies using a variety of different techniques. For example, neuronal activity can be measured in different ways, from electrophysiological techniques to using calcium indicators or by the activation of immediate-early gene products, such as c-Fos (Coolen et al., 1996; Hudson, 2018; Polston & Erskine, 1995; Rowe & Erskine, 1993; Tian et al., 2009, 2012). In the last decade, new techniques have entered the field of behavioral neuroscience which could be very helpful to address the complexity of female sexual behavior, including tools that allow the manipulation of neurons in a genetically delineated way, such as optogenetics and chemogenetics (Berglund et al., 2016; Nectow & Nestler, 2020; Snoeren,

2018; Song & Knöpfel, 2016). Overall, these methods revealed a number of brain regions whose activity has an impact on female sexual behavior, such as medial preoptic area (mPOA), the bed nucleus of the stria terminalis (BNST), the medial amygdala (MeA), the ventromedial hypothalamus (VMH), and the periaqueductal gray (PAG) (fig. 4) (Erskine, 1993; J. G. Pfaus et al., 1993; Polston & Erskine, 1995; Rowe & Erskine, 1993; Snoeren, 2018; Tetel et al., 1993). Moreover, different regions of the brain areas become activated during the different phases of sexual behavior. For example, chemosensory investigation (appetitive phase) induced c-Fos activation in the female posteromedial part of the BNST (BNSTpm) (Coolen et al., 1996) and posterodorsal part of MeA (MeApd) (Coolen et al., 1996; Tetel et al., 1993).

Despite the importance of many brain regions in the expression of females sexual behavior, one of the most relevant brain regions controlling this fundamental behavior is the **ventral portion of the ventromedial hypothalamus (VMHvl)** (Canteras et al., 1994; Eugene Millhouse, 1973). The VMHvl has been shown to be an extremely relevant hypothalamic nucleus in numerous of social behaviors (Falkner et al., 2016; Lee et al., 2014; D. Lin et al., 2011; C. F. Yang et al., 2013). Suppression of VMHvl activity can decrease the frequency of attack, investigatory and sexual behaviors (Falkner et al., 2016, 2020; Lee et al., 2014; Lin et al., 2011; Yang et al., 2013).

The VMHvl is known as the major site for the regulation of lordosis, as lordosis behavior in response to mounts leads to specific activation of the VMHvl (Coolen et al., 1996), while lesions reduce lordosis posture (Pfaff & Sakuma, 1979a) and electrical stimulation facilitates the expression of lordosis (Pfaff & Sakuma, 1979b). Importantly, recent studies have shown that the VMHvl is not a homogenous structure. In fact, the VMHvl seems to be composed of several different neuronal populations expressing different markers (Y. Hashikawa et al., 2017; Yang et al., 2013) with different connectivity (Lo et al., 2019; Zha et al., 2020), corresponding to variable functions (Falkner et al., 2014; K. Hashikawa et al., 2017; Y. Hashikawa et al., 2017; Karigo et al., 2020; Kim et al., 2019; Lee et al., 2014; Nomoto & Lima, 2015), which are spatially segregated across its anterior-posterior axis (Dias et al., 2021; K. Hashikawa et al., 2017; Y. Hashikawa et al., 2017; Inoue et al., 2019). For instance, optogenetic activation of VMHvl estrogen receptor expressing ($Esr1^+$) neurons in females triggers either attack (in lactating females) or mounting (in virgin females) in individual animals. Thus, VMHvl $Esr1^+$ neurons may constitute a heterogeneous population. Consequently, Hashikawa *et al* found that the VMHvl appears to contain compartments that preferentially drive specific behaviors: neurons associated with female-type mounting are mostly located in the lateral part of the VMHvl (VMHvll), whereas neurons associated with attack are located in a more medial part (VMHvlm) in females (K. Hashikawa et al., 2017) (P. Chen & Hong, 2018). Another VMHvl subpopulation that controls sex-typical behaviors is the progesterone receptor (PR)-expressing neurons, which largely overlaps with the $Esr1^+$ population (Blaustein, 2008; Cohen & Pfaff, 1992; Flanagan-Cato, 2011; Quadros et al., 2008; Yang et al., 2013). This

subpopulation is required for the normal display of mating in both sexes (Yang et al., 2013). Ablation of PR^+ VMHvl neurons led to a profound decrease in female sexual receptivity and in male sexual behavior and aggression (Yang et al., 2013; Zilkha et al., 2021).

The VMH receives neuronal inputs from the MeA and the BNST (Canteras et al., 1995; Gu et al., 2003; Shimogawa et al., 2015). Amygdala is one of the areas that are responsive to socially relevant stimuli (Newman, 1999; Sokolowski & Corbin, 2012) and highly involved in sexual behavior. Indeed, the high density of estrogen and androgen receptors implicates the MeA as a primary locus for the integration of sensory information (Canteras et al., 1995; Jennings & de Lecea, 2020; Simerly et al., 1990). Pheromonal information reaches the MeA throught the vomeronasal organ (VNO) and accessory olfactory bulb (AOB). On the other hand, olfactory/volatile information reaches the MeA from the main olfactory epithelium (MOE) and main olfactory bulb (MOB) (K. Hashikawa et al., 2016; Jennings & de Lecea, 2020). Major targets of the MeA include the MPOA and VMHvl (Canteras et al., 1995; Huijgens et al., 2021). The MeA olfactory information also reaches the PMv. Immediate early gene mapping showed that the PMv is strongly activated by the odor cues from conspecifics (Jose Donato et al., 2010; Y. Hashikawa et al., 2017; Kim et al., 2019; Motta, Carla, et al., 2013; Soden et al., 2016; Stagkourakis et al., 2018) and that is reciprocally connect with the VMHvl (Canteras et al., 1992; Judney Cley Cavalcante et al., 2014; Lo et al., 2019; Stagkourakis et al., 2018), suggesting that together form an interconnected circuit shown to be relevant in social interactions. However, its role in female behavior in general, and in sexual behavior, is mostly unknown.

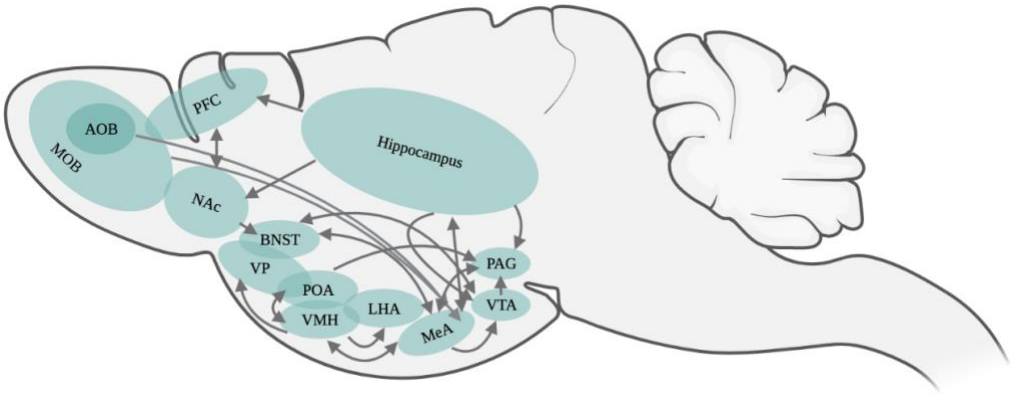

Figure 4. Important brain areas involved in female reproductive behavior. Arrows represent the connections between different brain regions. Adapted from: Snoeren *et al*, 2018.

2.1. PMv: a Particular Hypothalamic Nucleus

As previously mentioned, the ventral premammillary nucleus (PMv) is a group of neurons in the medial zone of the hypothalamus, located immediately caudal to the ventromedial nucleus of the hypothalamus and ventral to the dorsal premammillary nucleus (Canteras et al., 1992; Judney Cley Cavalcante et al., 2014; Jose Donato & Elias, 2011; Li & Dulac, 2018) (fig. 5).

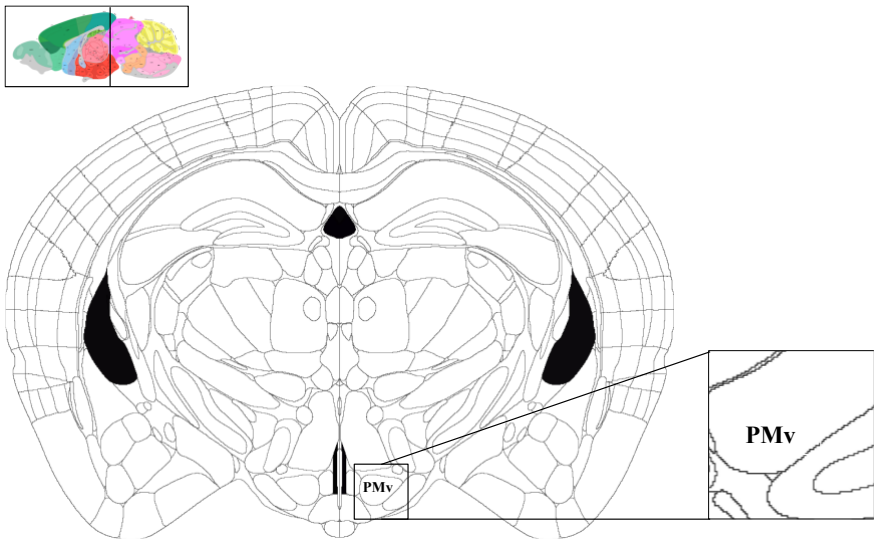

Figure 5. PMv location in the brain. Scheme of a sagittal and a coronal slice with location of PMv nucleus. Zoomed region shows the PMv nuclei in the right hemisphere along the third ventricle. Adapted from: Paxinos, G., & Franklin, K. B, 2008.

As shown in male rats and cats, the PMv is thought to receive dense inputs from the MeA (especially its posterodorsal part), the BNST, and the MPOA (particularly from the central and medial part) (Kevetter & Winans, 1981; Swanson & Cowan, 1979). Studies in rats also shown that PMv may also receive inputs from other nuclei of the involved in the circuitry involved in sexual behavior, including the VMHvl, ventral lateral septal nucleus (vLSN) and posterior nucleus of the amygdala (PA) (Canteras et al., 1992; Judney Cley Cavalcante et al., 2014). Interestingly all of these sources of afferents to the PMv listed are in a position to relay information from the olfactory system (Canteras et al., 1992), suggesting that the PMv may process olfactory information related to conspecific interactions (Canteras et al., 1992; Halpern & Martínez-Marcos, 2003). Accordingly, the PMv of rats expresses c-Fos immunoreactivity in response to opposite sex odor exposure and is involved in the expression of conspecific-directed behaviors (Judney C. Cavalcante et al., 2006; Jose Donato et al., 2010; Yokosuka et al., 1999). Because the PMv is not directly innervated by the AOB, odor-induced neuronal activation likely originates from the MeA, PA and/or principal nucleus of the bed nucleus of the stria terminalis (BNSTpr) projections (Canteras et al., 1992; Judney Cley Cavalcante et al., 2014; Kollack-Walker & Newman, 1995). Furthermore, the PMv expresses moderate density of sex steroids receptors (androgen, estrogen or progesterone). It was shown that the PMv has a large population of neurons with androgen receptors in the rat (Simerly et al., 1990; Yokosuka et al., 1997; Yokosuka & Hayashi, 1996) and the Syrian hamster (Wood &

Newman, 1995; Yokosuka et al., 1999). Therefore, PMv neurons may integrate external (odor) and internal (sex steroids) cues to modulate the downstream targets in behavioral responses (Judney Cley Cavalcante et al., 2014).

On the other hand, the PMv also expresses receptors for leptin, insulin and ghrelin, suggesting that it may contribute to metabolic regulation (Jose Donato & Elias, 2011). Is has been shown that hunger decreases reproductive capacity and delays puberty (Chan & Mantzoros, 2001). On the other hand, excess energy disrupts fertility (Blüher & Mantzoros, 2004; Chan & Mantzoros, 2001). It was also shown that endogenous re-expression of leptin receptors only in the PMv of mice otherwise null for leptin receptor induces puberty and improves fertility (Jose Donato et al., 2011). These findings indicate that the PMv plays a fundamental role in the integration of metabolism and reproduction (Judney Cley Cavalcante et al., 2014).

2.2. The Role of PMv in Social Behaviors

The PMv, amongst others hypothalamic nuclei, regulates social interactions (Canteras et al., 1992; Judney C. Cavalcante et al., 2006; J. Donato et al., 2013; Jose Donato & Elias, 2011; Motta, Guimarães, et al., 2013; Soden et al., 2016; Stagkourakis et al., 2018; Van Berg et al., 1983), but how PMv neurons transduce sex-related sensory signals emitted by conspecifics to trigger appropriate sexual behaviors is not fully understood.

Overall, the PMv is highly connected with the brain's social networks. Initial studies using electrolytic lesions of the premammillary area of rats suggested the involvement of the PMv in male conspecific aggression (Van Berg et al., 1983). The PMv of male rats and hamsters shows increased c-Fos expression after aggressive conspecific encounters, but notably also after sexual behavior (Kollack-Walker & Newman, 1995; Veening et al., 2005). Moreover, the exposure to female odors has been shown to be sufficient to consistently induce c-Fos in the PMv of male rats (Judney C. Cavalcante et al., 2006). Interestingly, c-Fos mapping showed that the PMv is predominantly activated by the presence of a male intruder in both sexes, and is only minimally activated by a female intruder in male subjects (Borelli et al., 2009; Judney C. Cavalcante et al., 2006; Jose Donato et al., 2010; Soden et al., 2016). Altogether, these studies suggest that PMv integrates information about socially relevant cues and may be involved in generating appropriate behavioral outcomes (Judney C. Cavalcante et al., 2006).

Previously, it was shown that neurons in the PMv express mRNA for the dopamine active transporter (DAT) (Meister & Elde, 1993). In males, PMv-DAT neurons only constitute approximately 25% of the total number of neurons of the PMv, suggesting that PMv-DAT neurons might not be the only population involved in social behaviors (Soden et al., 2016). Inhibition of PMv-DAT neurons, through conditional expression of the inhibitory DREADD receptor hM4Di

activated by the selective agonist clozapine-N-oxide (CNO), significantly reduced social exploration, while activation of these neurons, using the light-activated ion channel channelrhodopsin (ChR2), promotes social investigation of the cage-mate (Soden et al., 2016). More recently, Stagkourakis *et al.* investigate specifically the role of PMv-DAT neurons in male aggression (Stagkourakis et al., 2018). They found that optogenetic activation, using the light gated ion channel ChR2 (H. Wang et al., 2007; F. Zhang et al., 2006), of PMv-DAT neurons can elicit attack in spontaneously aggressive male mice, while optogenetic silencing of these neurons, using a light gated ion channel halorhodopsin (eNpHR3), interrupts attacks (Stagkourakis et al., 2018). This study identifies the PMv-DAT neuronal population as a critical component of the circuit that shapes aggressive behavior in males (fig. 6) (Soden et al., 2016; Stagkourakis et al., 2018).

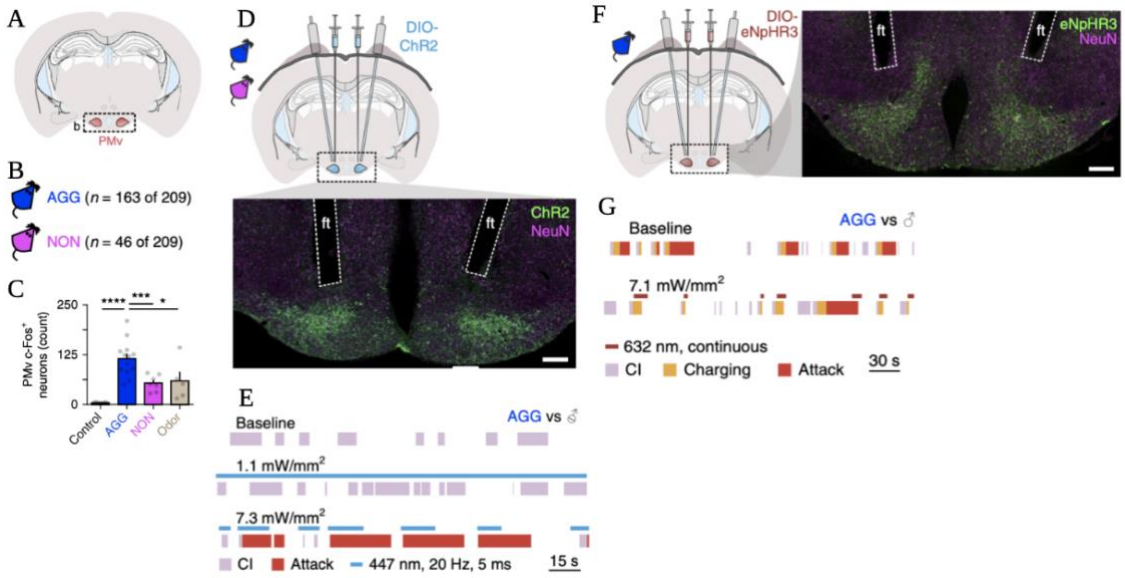

Figure 6. The activity of PMv-DAT$^+$ neurons is necessary for male mice aggression. (A) Schematic drawing of PMv at –2.46 mm from bregma in a coronal mouse brain section. (B) Groups of males in the study: aggressive and non-aggressive. (C) Number of c-Fos immunoreactive neurons in PMv with and without introduction of intruder and intruder bedding. (D) Schematic drawing of PMv viral transduction with ChR2 and fiber implants as performed in AGGs and NONs. Confocal micrograph (below) shows ChR2-expressing PMv-DAT$^+$ neurons and immunoreactivity for the neuronal marker NeuN, with optic fiber placement indicated. (E) Sample behavior raster plots of 0 (baseline), low-, and high-intensity ChR2 stimulation in an AGG. CI, close investigation. (F) Schematic drawing of PMv viral transduction with eNpHR3 and fiber implants as performed in AGGs. Confocal micrograph (right) shows eNpHR3$^+$ PMv-DAT$^+$ neurons and NeuN immunoreactivity, with optic fiber placement indicated. (G) Sample behavior raster plots with and without PMv-DAT$^+$ neuron silencing in AGGs. Adapted from: Stagkourakis *et al.*, 2018.

Recently, to record the activity of PMv-DAT neurons, Chen *et al.* injected adeno-associated virus (AAV) encoding Cre-inducible Ca^{2+} indicators GCaMP6s into the PMv of DAT-Cre male mice and implanted an optic fiber above the PMv (A. Chen et al., 2020). GCaMP6s fluorescence signals were found to increase when the animal actively investigated male urine. To test whether PMv-DAT neurons are required for recognition of male urine cues, they chemogenetically inhibited

PMv-DAT neurons by injecting AAVs encoding Cre-inducible hM4D-mCherry into the PMv of DAT-Cre males. Control mCherry-expressing males spent significantly more time investigating urine-spotted paper with clear preference for male cues, while the preference for male urine cues was completely abolished in hM4D males after CNO administration (A. Chen et al., 2020). Accordingly, authors proposed that upon encounter with odors, activation of PMv-DAT neurons promote investigatory behaviors, which serves the function to bring the animal into close contact with chemical cues (A. Chen et al., 2020). These results suggest that PMv-DAT neurons are required for behavioral recognition of conspecific male urine cues (A. Chen et al., 2020).

By the aforementioned studies, much is known about the influence of PMv in male social behaviors, namely in aggression. However, the PMv role in female social behaviors, especially in sexual behavior, remains to be determined. In females, what is known until now regards the maternal behavior in rats (Motta, Guimarães, et al., 2013; Soden et al., 2016).

2.3. Importance of the PMv for Maternal Behavior

In mothers, sexual behavior and infanticide are virtually abolished, whereas maternal behavior and aggression toward intruders increase dramatically, in order to protect their offspring (K. Hashikawa et al., 2018; Lonstein & Gammie, 2002; Wei et al., 2021). Dams not only show pup-directed maternal behavior, i.e. arched back posture, lactation, pup grooming and licking, but also attack conspecifics approaching the nest (Hao Wang, 2020). Maternal behavior seems to be dependent on olfactory stimuli. Pup-derived olfactory chemosignals or the perception of sensory cues from an intruder can promote aggressiveness in lactating females, and it is accepted that PMv is highly responsive to the male intruder (Motta, Guimarães, et al., 2013). Marín-Sánchez *et al* compared the aggressive response towards male intruders by lactating dams and virgin females. It was found that lactating females attacked males more than virgin females (Martín-sánchez et al., 2014). As the PMv is targeted by the MeA and because the MeA is critical for social recognition in rodents, it may exert a key role in processing olfactory information critical for detecting a male intruder (Martín-sánchez et al., 2014).

Motta *et al* performed PMv bilaterally lesions in rats, which were found to produce a reduction in maternal aggression towards intruder males, both in the number of attacks and in attack duration (Motta, Guimarães, et al., 2013) (fig. 6A). Moreover, c-Fos activity is much higher in a unlesioned dam exposed to a male intruder comparing to a lactating rat left undisturbed with her pups (fig. 6B and C). PMv lesions led to a reduction in c-Fos expression in PMv and in other hypothalamic nuclei related to maternal aggression, including the MPN, the VMHvl, and the ventral part of the BNST, which reveals that PMv modulates the network controlling maternal aggression (fig. 7) (Motta, Guimarães, et al., 2013).

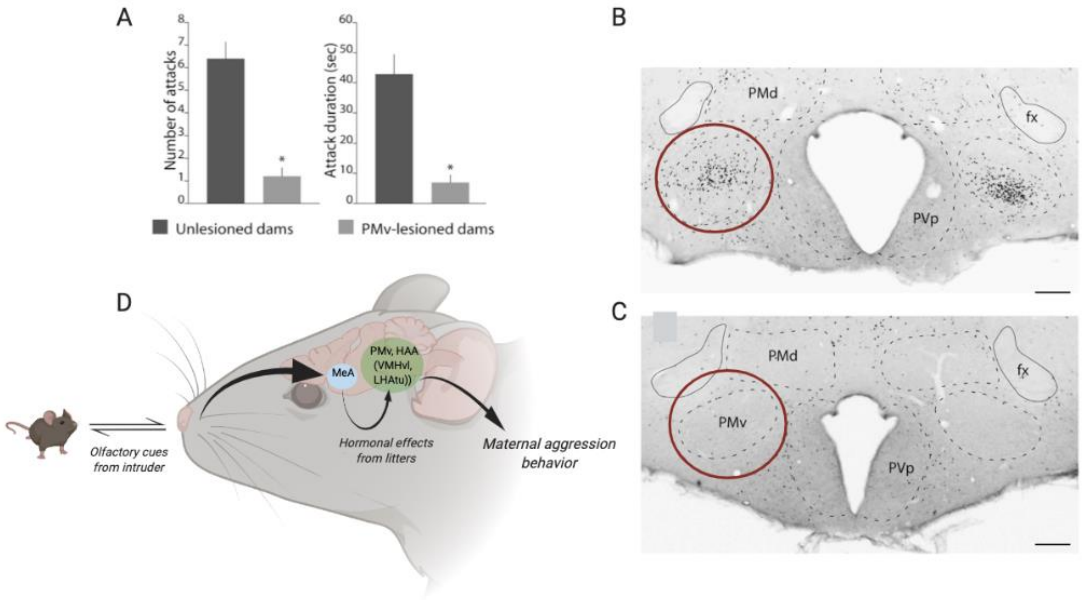

Figure 7. Role of PMv in Maternal Behavior. (A) Histograms of the behavior of unlesioned (n=5) and PMv-lesioned (n=5) dams tested for maternal aggression, showing number of attacks and total duration of attacks. (B and C) Photomicrographs of transverse sections containing Fos-immunoreactive cells at the level of the PMv from an unlesioned dam exposed to a male intruder (B) and a lactating rat left undisturbed with her pups (C). (D) Schematic diagram showing the putative brain network underlying maternal aggression. Adapted from: Motta *et al.*, 2013.

Until now, the knowledge regarding the role of PMv in female mice social behavior is still scarce. Our laboratory has been investigating the role of the VMHvl in female sexual behavior and more recently, since the VMHvl is reciprocally connected to the PMv, we have extended our studies into this other hypothalamic nucleus. Preliminary results from a PhD Student in the laboratory, António Dias, using fiber photometry with calcium indicators of neuronal activity, found that when a female interacts with a male, there is an increase in the emitted fluorescence, indicating an increase in the activity of PMv-DAT neurons; interestingly, relatively no change is observed when females interact with other females (unpublished data from Lima Lab) (fig. 8). This leads us to conclude that the PMv-DAT cell activation occurs in the presence of opposite sensory cues.

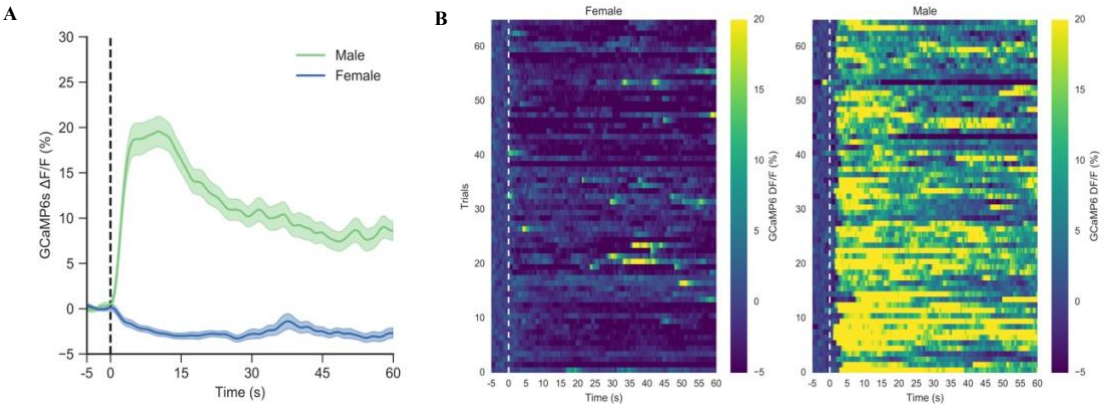

Figure 8. PMv-DAT$^+$ Activity in Female-Male and Female-Female Interactions. (A) Genetically encoded calcium indicator GCamP6s activity in PMv-DAT$^+$ neurons of DAT-Cre female mice recorded using fiber photometry. (B) Heat map representative of the GCamP6s activity in female PMv-DAT$^+$ neurons. Blue colors are associated with less GCamP6s activity. In both graphics, neuronal activity is much higher in female-male compared with female-female interactions. Unpublished data from Lima Lab, Champalimaud Foundation.

3. Objectives

Dopamine transporter expressing neurons of the premammillary nucleus of the hypothalamus (PMv-DAT) receive input from the olfactory system and are specifically activated by male cues in both female and male mice, suggesting that this hypothalamic region is important for male-directed behaviors in both sexes (Borelli et al., 2009; Judney C. Cavalcante et al., 2006; Jose Donato et al., 2010; Soden et al., 2016). This poses an interesting conundrum, since male-directed interactions can develop into quite disparate outcomes across sexes. While male-female interactions can develop into sex, male-male interactions are mostly antagonistic. This suggests that, while the olfactory pathways conveying information to PMv-DAT neurons maybe shared across the sexes, the projections of this population might impinge onto distinct brain regions involved in the execution of the appropriate, sex specific behavioral outputs. Recent studies have investigated the function of the PMv-DAT population in males, supporting a role in aggression, but the function of this population in females is mostly unknown. Thus, we decided to focus on the importance of PMv-DAT neurons for sexual behavior in female mice. To get insight into the PMv structure, the first goal of this project is to identify the female outputs of the PMv-DAT cells to understand how the PMv outputs may be involved in male directed behaviors. To specifically target the PMv-DAT population, we used a combination of Cre-expressing mice (DAT-Cre) together with a Cre-dependent viral vector expressing synaptophysin-GFP, which specifically labels the presynaptic terminals of this population. Afterwards, to understand the influence of this specific neuronal population of PMv on behavior, a genetic neuronal ablation technique was performed specifically for PMv-DAT cells, using the Diphtheria Toxin receptor and its ligand to induce neuronal death. Lastly, using the neuronal ablated females, a sexual behavioral study was carried out to clarify the role of PMv in the sexual context and in the regulation of male directed behaviors.

Materials and Methods

2. Materials and Methods

2.1. Animals

Animal care and experimental procedures were performed following European guidelines (Directive 2010/63/EU) on the protection of animals used for scientific purposes and approved by the Portuguese National Authority for Animal Health (Direcção Geral de Alimentação e Veterinária; DGAV) and the Commission for Experimentation and Animal Welfare of the Champalimaud Centre for the Unknown (Órgão para o Bem Estar Animal; ORBEA).

Animals were kept under controlled temperature of 23 ± 1 °C and photoperiod of reversed 12 h light/dark cycle (light available from 8p.m. to 8a.m.) conditions, housed in standard cages (1284L, Techniplast, 365 x 207 x 140 mm and 1145T, Techniplast, 369 x 165 x 132 mm). Food and water (Global Diet 2914, Mucedolas.r.l) were provided *ad libitum*. Cotton (cocoon cylinders, LBS) and paper houses (GLP Des Res Mice Dome Home, LBS) were provided for environmental enrichment. Cage maintenance was performed once per week to provide new bedding, food and water. Mice were weaned at 20-21 days of age and group housed with two to five animals.

All females used in this project are between 4 to 7 months old. Experiments were conducted using adult female mice from the transgenic lines DAT-IRES-Cre (B6.SJL-Slc6a3$^{tm1.1(cre)Bkmn}$/JAX stock #006660) and Ai9(RCL-tdTomato) (B6;129S6-Gt(ROSA)26Sor$^{tm9(CAG-tdTomato)Hze}$/JAX stock #007905). The DAT-IRES-Cre line expresses Cre recombinase in neurons where the dopamine active transporter (DAT) is active, which includes dopaminergic neurons, without disrupting the endogenous expression of DAT gene (Backman et al., 2006). In turn, the Ai9 is a Cre-dependent reporter line designed to have a loxP-flanked STOP cassette preventing transcription of a CAG promoter-driven red fluorescent protein variant (tdTomato). The females used in the sexual behavior study were the offspring of the cross between the DAT-Cre line and the Ai9, which have the STOP cassette deleted by the action of Cre recombinase specifically in cells expressing the DAT gene, resulting in the expression of the tdTomato protein.

Adult C57BL/6J male mice from different genetic backgrounds (Gal-Cre, Pr-Cre, Esr1-Cre and DAT-IRES-Cre) were used as stimuli in behavioral experiments. All male mice were sexually experienced and had at least 2 sexual training sessions with an ovariectomized female mouse prior to behavioral testing (Valente et al., 2021).

2.2. Viruses

The AAV1-CAG-floxed-SynGFPrev-WPRE (serotype 1, titer 1,12x10^{14} vg/mL) virus was purchased from the Molecular and Transgenic Tools Platform of the Champalimaud Foundation. The AAV2-CAG-DIO-tacaspase3-TEVp (serotype 2/5, titer 1.363x10^{13} vg/mL) was purchased from Taitool Bioscience Co, Shangai. The AAV2-FLEX-DTR-GFP (serotype 2, titer 8,9×10^{12} vg/mL) was purchased from Addgene (catalogue # 124364-AAV2). AAV8-FLEX-DTR-GFP and AAV9-FLEX-DTR-GFP were a kind offer from the Carey Lab (Neural Circuits and Behavior Lab) at Champalimaud Center for the Unknow. For testing DTR neuronal ablation efficiency, we have used 3 stereotypes (AAV2, 8 and 9). Since they all showed similar results, we pooled all the animals, and they are presented in this thesis as just AAV2. For sexual behavior experiments, we used only animals injected with AAV2.

2.3. *In vitro* Cell Death Assessment

In order to test the efficiency of the caspase-expressing virus *in vitro*, we infected a 293T Cre-dependent cell line (J. Zhang et al., 2016) with AAV2-CAG-DIO-taCaspase3-TEVp virus. We plated 50.000 with a MOI of 10^5 overnight. In each condition (virus or control), 3 wells were plated: one without Hoecsht, a cell death marker, and two duplicates with Hoecsht. As a control, we have used the same cell line without any virus (uninfected cells). On the next day, the medium was replaced, to remove the viral particles. Different timepoints were accessed by the Fluorescence-Activated Cell Sorting (FACS): 48h, 72h, 96h and one week. In the one-week timepoint, the medium was also changed after 5 days of infection. One the day of the sorting, cell medium was centrifugated and resuspended in 300 uL of PBS with 2% Fetal Bovine Serum Buffer. For cell death testing, we added 3 uL of Hoechst 3258 and waited 20 minutes on ice (2-8ºC) before the FACS. Cell sorting was performed using a BD LSRFortessa™ X-20 Flow Cytometer provided by the Flow Cutometer Platform of the Champalimaud Foundation.

2.4. Brain Surgeries

Brain surgery. Female mice were placed in a Kopf stereotaxic frame under deep anesthesia (3% isoflurane), hair was removed from the scalp, and the incision site was prepped with alcohol and betadine. Equipment was kept sterile throughout the procedure with 70% ethanol and a heated glass bead sterilizer. In all surgeries, mice were injected subcutaneously with 0.1 mL of Buprenorphine (Bupaq ®, for mice 0.5-1 mg/kg), at the beginning of the surgery, and a heating-pad was used to keep the animal warm during the procedure. During the procedure, the eyes are covered with eye lubricant ointment Vitaminoftalmina (5 g). The skull was exposed with a midline scalp incision, and aligned using visual landmarks, i.e., bregma and lambda. After the incision was made,

the skin was pulled aside and clamped with an eye retractor to ensure access to the surgical field on the top of the skull. The periosteum was removed using sterile cotton swabs dipped in 0.3% hydrogen peroxide. For viral injection, the following bregma coordinates, referenced by the Allen Mouse Brain Atlas and subsequently adjusted, were used to target the PMv: AP: - 1.70 mm, ML: ± 0.55 mm, DV: - 5.80 mm (A. Chen et al., 2020). A small burr hole was drilled into the skull using a board drill (at the above coordinates) to expose the brain. A 20 nm handmade capillary loaded with virus was aligned at bregma and slowly inserted through the hole until it penetrated into PMv (- 5.80 mm) and waited 5 minutes in the injection zone before virus delivery. All viral injections were performed using a Drummond Nanoject II™ Auto-Nanolitre Injector at a rate of 4.6 nL per 10 seconds. For **output tracing**, animals were injected with 25nL of AAV1-CAG-floxed-SynGFPrev-WPRE unilaterally. For **caspase neuronal ablation experiments**, 500 nL/1 µL of AAV2-CAG-DIO-tacaspase3-TEVp were injected bilaterally. For **neuronal ablation experiments using DTR strategy**, 200 nL of AAV2/8/9-FLEX-DTR-GFP, diluted in PBS (dilution of 1:1), were injected unilaterally. For **sexual behavior experiments,** 200 nL of AAV2-FLEX-DTR-GFP, diluted in PBS (dilution of 1:1), were injected bilaterally. As a control, animals received a bilateral craniotomy without any virus injection. After the virus injection, the capillary was left in place for an additional 10 minutes to allow for the diffusion of the virus. Mice skin was sutured, using Dafilon 6/0 (B. Braun, Dafilon Blue 6/0 (0,7) 45 cm DS9 Aesculap), and the animals were allowed to recover over a heating pad for 24 hours.

2.5. Histology and Immunostaining

For the **PMv output tracing**, 2 weeks after viral injection, mice were perfused transcardially with 0.01M PBS followed by 4% paraformaldehyde (PFA). Brains were extracted and post-fixed in 4% PFA for one day at 4°C followed by 72h in 30% sucrose with 0,1% of sodium azide. Coronal 45 mm thick sections were prepared using a microtome (Leica SM2000 R) and transferred to a 12-well plate with 0.01M PBS for storage. Brain slices were mounted on Microscope Slides (RS FRANCE ground edge 76x26 mm 90°, B/50), using Mowiol mounting medium (from Glass Wash and Media Preparation of Champalimaud Centre for the Unknown), and coverslipped for imaging on Slidescanner (Zeiss AxioScan Z1 microscope).

For **neuronal ablation using AAV2-CAG-DIO-tacaspase3-TEVp**, brain slices containing the PMv were divided in two series. One series was stained with Nissl and other with NeuN. Nissl (Molecular Probes, catalogue # N21480, NeuroTrace 500/525 Green Fluorescent Nissl Stain; dilution 1:100) staining is a standard histological method for visualizing neuron cell bodies. Briefly, the Nissl staining protocol starts with a 40-minute rehydratation step using 0.1M PBS, followed by a 10 minute permeabilization step with 0.1M PBS 0.1% Triton X-100. Slices were then washed twice in 0.1M PBS for 5 minutes and incubated with the NeuroTracer (1:100 in 0.1M PBS)

for 20 minutes. A final series of washes with 0.1M PBS in 0.1% Triton X-100 and 0.1M PBS were made. Finally, slides were washed in PB and coverslipped for imaging on the Zeiss AxioImager M2 microscope, using Mowiol mounting medium. In the other PMv series, an immunoassay with the primary antibody Mouse Anti-Neuronal Nuclei, NeuN (Millipore, catalogue # MAB377; dilution 1:1000) was performed. Goat Anti-Mouse 488 (Invitrogen, catalogue # A-11029; Polyclonal; IgG; Alexa Fluor 488; dilution 1:250) was used as a secondary antibody. Similar to Nissl, NeuN is a neuronal nuclear biomarker. The NeuN protocol starts with three 5 minute slice hydration steps with 0.01M PBS. Slices were washed during 10 minutes with 0.3% PBS-T and incubated overnight at room temperature with the NeuN primary antibody (1:500) diluted in 0.3% PBS-T with 5% goat serum. Slices go through a series of washes followed by a 2-hour incubation with the secondary antibody Goat Anti-Mouse 488, also room temperature. Finally, slices were washed in 0.3% PBS-T and PBS and coverslipped, using Mowiol mounting medium for imaging on the Zeiss AxioImager M2 microscope.

For the **neuronal ablation experiments using DTR**, 2 weeks after virus injection, 50 ng/g (0.1 mL/10 g) of DTx (diphtheria toxin) was injected in the animals intraperitoneally. One week after, females were exposed to a male and allowed to interact for 5 minutes. After 1h30min, mice were perfused transcardially with 0.01M PBS followed by 4% PFA. Brains were extracted, post-fixed in 4% PFA for one day at 4°C followed by 72h in 30% sucrose with 0,1% of sodium azide, sectioned in a coronal plane at 45 mm using a microtome (Leica SM2000 R) to collect the PMv sections and transferred to 0.01M PBS for storage. An immunoassay was made for the immediate early gene c-Fos and GFP, using a mix of two primary antibodies: Rabbit Anti c-Fos (Synaptic Systems, catalogue # 226003; polyclonal; dilution 1:2000) and Goat Anti-GFP (Abcam; catalogue # ab6673; polyclonal; dilution 1:500). For the correspondent secondary antibodies, we used Donkey Anti-Rabbit 647 (Abcam; catalogue # ab150075; polyclonal; Alexa Fluor 647; dilution 1:1000) and Donkey Anti-Goat 488 (Abcam, catalogue # ab150077; polyclonal; Alexa Fluor 488; dilution 1:1000), respectively. The protocol starts with 0.01M PBS washes for 10, 20 and 30 minutes, sequentially, and incubation in 10% BSA (bovine serum albumin) in 0.3% PBS-T for 1 hour. Then, an overnight incubation was done at room temperature with the primary antibodies diluted in 10% BSA, 0.1% sodium azide and 0.3% PBS-T (1:2000). The same PBS washes were done again and a 2-hour incubation with 10% BSA in 0.3% PBS-T. Subsequently, the secondary antibodies were incubated, at room temperature, diluted in 10% BSA, 0.1% sodium azide and 0.3% PBS-T (1:1000), for 2 hours. Finally, slices were washed in 0.1M PB for 10, 30 and 40 minutes, sequentially, and mounted on Microscope Slides (RS FRANCE ground edge 76x26 mm 90°, B/50), using Mowiol mounting medium, and coverslipped for imaging on the Zeiss AxioImager M2 microscope. For the **sexual behavior experiments after DTR neuronal ablation**, tissue processing and staining was done as previously described, both for experimental and control females.

2.6. Estrous Cycle Monitoring

Microscopic evaluation of the types of cells present in vaginal smears has long been used to evaluate sexual receptivity in female mice. The female's estrous cycle is divided into 4 stages (proestrus, estrus, metestrus, and diestrus) and repeats every 4 to 5 days unless interrupted by pregnancy, or pseudopregnancy. The stage of the estrous cycle is determined based on the presence or absence of different cell types, such as leukocytes, cornified epithelial and nucleated epithelial cells (Nelson et al., 1984). When the female is in proestrus (lasting an average of 24 hours), mostly nucleated and some cornified epithelial cells are present. Some leukocytes may be present if the female is in early proestrus. The proestrus-estrus phase is when the female is sexually receptive and is characterized by the presence of nucleated and cornified eipithelial cells, in roughly the same proportion, and an absence of leukocytes. Following proestrus-estrus, female's enter in estrus (duration ranges between 12 and 48 hours), where mostly cornified epithelial cells are present. Between estrous and diestrus, females will enter the metestrus phase. Metestrus is a brief stage when the uterine lining will begin to slough and cornified eipithelial cells and leukocytes are present. Diestrus is the longest of the stages lasting more than 2 days. Vaginal swabs during diestrus show primarily leukocytes and a few nucleated cells during late diestrus (Byers et al., 2012).

To assess the reproductive state of naturally cycling female mice, vaginal swabs were collected every morning for at least one entire cycle (four/five consecutive days), approximately at the same time of the day (9-11a.m.). This collection was done by vaginal lavage with a pipette, cut pipette tips (T-210-Y, AXYGEN) and 10µL of 0.01M PBS. The saline is gently flushed into the vagina and back out three or four times without touching the vaginal wall to avoid cervical stimulation and pseudopregnancy. The flush containing vaginal fluid was transferred to a glass slide and dried in a hot plate for 3 minutes (50º to 100º) (Caligioni, 2009). A papanicolaou staining was used to differentiate cells (Bio-Optica protocol using reagents 05-12011, 05-12013, 05-12019). The protocol includes: embedded the slides, 2 minutes, in ethanol 95º, 1 minute in distilled water, 2 minutes in the Papanicolau Ematossilina Haris dye, 2 minutes in tap water (repeated two times), 15 seconds in etanol 95º and then more 2 minutes in the Papanicolaou OG6 dye. After repeat the washes (2 times in ethanol 95º for 16 seconds), slides are embedded in the Papanicolaou EA50 dye for 5 minutes. Finally, wash 2 times in ethanol absolute for 30 seconds each. After allowing sample dry at room temperature, mount in a slide (Menzel-Glaser cover slips; 24x60 mm) using DPX mounting medium (Sigma-Aldrich; # 06522) and were observed under a Zeiss AxioScope A1 brightfield microscope with a 10X objective. The identification of the reproductive cycle phase was done based on the proportion of each cell type in the smear. Experiments were performed when females were in proestrus/estrus (sexually receptive) (Dias et al., 2021).

2.7. Behavioral Paradigm

To sexually train male mice, wildtype C57BL/6J OVX females were used as sexual partners. OVX females were allowed a 2-week recovery from surgery prior to subsequent experiments/hormone priming started. Females were hormonally primed following previously published protocols (Ring, 1944; Xu et al., 2005). Briefly, for the first hormone priming, it was administered, subcutaneously, β-Estradiol 3-benzoate on day −4 (0.1 mL; Sigma, 1,3,5(10)-Estratriene-3,17β-diol 3-benzoate minimum 97%, catalogue # E8515-1G), day -2 (0.1 mL) and progesterone (0.1 mL; Sigma, 4-Pregnene-3,20-dione minimum 99%, catalogue # P0130-25G) on the day of testing. On the next assays, the estradiol injection at day -4 was removed. The females were paired, for at least for 1 hour, with resident males 4 hours after receiving progesterone injection. After sexual training, females were rested for 7 days to allow hormone levels to subside to baseline levels prior to estrus induction for the next assay. Male mice were also rested for 7 days between the assays. Male mice were considered sexually experienced if they ejaculated at least 3 times when paired with an OVX female.

In behavioral experiments using the DTR ablation approach**,** the same procedure was done in control (just craniotomy) and experimental animals (with virus): after 2 weeks of the viral injection, 50 ng/g (0.1 mL/10 g) of DTx (diphtheria toxin) was injected in the animals intraperitoneally. One week after, the female's cycle started to be assessed and sexual behavior was performed during the receptive state (proestrus-estrus).

All female mice were singly housed for at least two weeks prior to behavioral tests and soiled male bedding was provided each week to promote hormonal cycling. Natural hormone cycling assessment was carried every day, approximately at least 1 hour after lights turn on. All experiments were performed under red light during the period in which mice are most active. Subject females (experimental or control) were habituated to the behavioral apparatus (32,5 cm x 12,5 cm x 19,5 cm; transparent acrylic) for 10 minutes. Once those 10 minutes had elapsed, the male was introduced, and the animals were allowed to interact freely. The experiment terminated when the male ejaculated or when 60 minutes had elapsed after the first mount. Males that did not performed any mount attempt (with or without intromissions) in the first 30 minutes were removed and a new male was placed inside. Males (n=8) were randomly allocated to the cages with females, and each male was used in more than one trial. The sessions were videotaped from the top and front-angles using two cameras (Flea3; Monochrome Point Grey, frame rate, 30 Hz per second) for offline analysis. Bonsai Software was used to record the session (Open Access Software) (Lopes et al., 2015). Females were perfused on the next day following behavioral testing and after 5 minutes exposure to a male, to access the expression of c-Fos protein. The brain was processed and stained as described above for neuronal ablation experiments using DTR. Data was analyzed from 5

experimental females (DTR transfection and DTx injection) and 4 controls (*sham* females with DTx injection). One of the experimental females died before behavioral experiments started.

2.8. Data Analysis

All data analysis was carried out blinded to the group or the treatment condition of the animals.

2.8.1. PMv Outputs Quantification

We injected 7 DAT-Cre TdTomato females with AAV, but only 5 of those injections were correctly targeted. The DAT gene is expressed in many other neuronal populations besides the PMv, particularly in the dopaminergic neurons of the ventral tegmental area (VTA), which is in close proximity to the PMv. Since VTA-DAT neurons project to the striatum (Beier et al., 2015), but PMv-DAT neurons do not, the presence of fibers in the striatum was used to exclude injected animals. Quick inspection of the brain slices revealed the presence of fluorescence in the striatum in 2 brains; therefore those 2 animals were discarded. Images from all brain slices were captured with 10x and 20x objectives using the Zeiss AxioImager M2 microscope.

We first started by the identification of all brain regions containing fluorescent fibers in each animal. For all brain regions present in at least 3 of the injected animals we quantified their fluorescence intensity; for each brain area, the fluorescence intensity was measured in 3 slices corresponding to three levels in the anterior posterior axis (anterior, medial and posterior). Slices, obtained with an 10x amplification, were overlapped with the correspondent section of the Allen Brain Atlas (coronal view). For quantification of outputs/terminals location, images were analyzed using Fiji/ImageJ Software (Bitplane, Oxford Instruments) and Abode Illustrator/Photoshop 2019 (Adobe Systems Incorporated).

For quantification of fluorescence intensity, the average pixel intensity in a target region containing presynaptic GFP punctae was calculated, in Fiji/Image J, and the background was subtracted to exclude autofluorescence of the tissue. The background consists in an adjacent unlabeled region, without any terminal marked with synaptophysin (Kohl et al., 2018). A survey with all areas with synaptic terminals was done, according with the percentage of animals with signal in each region. For the projection density quantification, the pixel intensity was normalized by the area of the region in each animal. Moreover, projection density of specific brain regions normalized by the injection site was plotted to all animals. Graphs were made using GraphPad Prism 8 Software.

2.8.2. PMv Neuronal Ablation Quantification

Caspase ablation assessment was made in 4 animals and 3 controls (*sham* females; without viral injection). tdTomato expression were captured with 10x and 20x objectives using the Zeiss AxioImager M2 microscope. One representative PMv slice from controls and injected animals were quantified. The slice was chosen in the same way for all animals to avoid ambiguous regarding more anterior/posterior regions of the PMv in different brains. Localization of the neurons in the brain atlas sections was performed in Adobe Illustrator CS6. The images of the slices, obtained with 10x magnification, were matched with the correspondent Allen Brain Atlas section (coronal view). tdTomato positive neurons were identified and counted by hand (blind to condition), using Adobe Photoshop 2019 and analyzed with a written MATLAB script. Graphs were made using GraphPad Prism 8 Software.

DTR ablation pilot assessment was performed using 5 animals and 2 controls (*sham* females; without DTR viral transfection). tdTomato, DTR and c-Fos fluorescence was captured with a 10x and 20x objectives using the Zeiss AxioImager M2 microscope. All the PMv slices from all the animals were quantified. Localization of the neurons in the brain atlas sections was performed in Adobe Illustrator CS6 (Adobe Systems Incorporated). The images of the slices, obtained with an 10x amplification, were overlapped with the correspondent section of the Allen Brain Atlas (coronal view) and with the maximum projection of the PMv stacks to locate the neurons specifically in this region. tdTomato, DTR and c-Fos-positive neurons were identified and counted by hand (blind to condition), using ImageJ software and Adobe Photoshop 2019. The different sets of neurons were then analyzed with a written MATLAB script and plotted after area normalization (cell density). Graphs were made using GraphPad Prism 8 Software.

2.8.3. Sexual Behavior Experiments Quantification

Injection of the AAV carrying the DTR gene and DTx injections were performed in 10 females, followed by behavior experiments. One of the females died 3 weeks after the injection before sexual behavior experiments, thus it was not counted in the quantification. tdTomato, DTR and c-Fos fluorescence was captured and analyzed according to what is describe above for PMv neuronal ablation quantification.

Behavioral annotation was performed using the Phyton Video Annotator program, developed by the Scientific Software and Development Platform of the Champalimaud Foundation (https://pythonvideoannotator.readthedocs.io/en/master/). The behaviors were analyzed from the female's perspective and divided into 5 categories: stimulus (male in, first contact between male and female, ejaculation and male out), investigation (nasal, body to body and anogenital), mount

attempts (without intromissions; divided in 3 types: male inability, female walk away and female rejection), successful mounts (with intromissions) and aggressive/rejection-related behaviors (kicking or boxing). Frequency, mean duration and latencies were calculated for each behavior, and normalized by the time of the session, using Microsoft Excel.

2.8.4. Statistical Analysis

Statistical analyses were performed using Microsoft Office Excel or GraphPad Prism 8 Software. Normality was tested with the D'Agostino-Pearson test and the homogeneity of variance was tested with Bartlett's test. In the normally distributed groups, for comparison between hemispheres of the same animal, a T Test for paired samples was used and, in comparisons between different animals, a T Test for two independent samples was used. When at least one group was not normally distributed, Mann-Whitney test was performed. Error bars represent mean ± SD. Significance was noted as $*p < 0.05$, $**p < 0.01$, $***p < 0.0005$.

Results

3. Results

To get insight into the function of the PMv-DAT population in female mice, we took a two-pronged approach: 1) we examined its projection targets to determine which brain regions receive its information and to compare it to the male; 2) we specifically ablated the female PMv-DAT population to examine its impact on female sexual behavior. Accordingly, this chapter is organized in two different sub chapters: first, the results regarding the identification of PMv outputs are presented; second, the results related to PMv-DAT neuronal ablation behavioral experiments will be introduced.

3.1. Outputs of Ventral Premammillary Nucleus

To reveal connectivity across different brain regions, neuronal tracing experiments are commonly used. Selected brain areas can be injected with compounds that enter neurons through their axonal terminals or somas and travel intracellularly with retrograde (towards the soma) or anterograde (towards the axonal terminals) movements revealing connectivity (Emin Oztas, 2003; Maday et al., 2014). More recently, viral vectors can have the ability to enter in a specific populations of neurons (Xiangmin Xu et al., 2020).

For the output tracing, we have used a Cre mouse model conjugated with Cre-dependent adeno-associated based virus. The Cre/loxP system is one of the most powerful tools developed for mouse genetics as it gives control over the location of gene expression (Duyne, 2001; McLellan et al., 2017; Yarmolinsky & Hoess, 2015). The system consists of an enzyme, Cre recombinase, that recombines a pair of short target sequences called the LoxP sequences (Yarmolinsky & Hoess, 2015). Placing Lox sequences appropriately between a DNA element allows the Cre recombinase enzyme to recombine it, which induces genes to be activated, repressed, or exchanged for other genes (Sengupta et al., 2017). For this project, we used a mouse model that utilizes the endogenous DAT promoter to express Cre recombinase in cells where the DAT gene is expressed (Backman et al., 2006; Lammel et al., 2015; Zhuang et al., 2005).

To specifically target the PMv-DAT population, we used a combination of the above described Cre-expressing mice, together with Cre-dependent viral vectors. In the first aim, where we investigate the output regions of the PMv-DAT population, we injected Cre-dependent AAV carrying the GFP gene fused to synaptophysin (Syn-GFP), which targets GFP to presynaptic terminals (Kwon & Chapman, 2011). After injection of the virus and allowing the appropriate amount of time for viral travelling and expression, we processed the whole brain to determine which brain regions receive input from the PMv-DAT population. Figure 9 shows representative images of the injection site and of brain regions where fluorescence was detected.

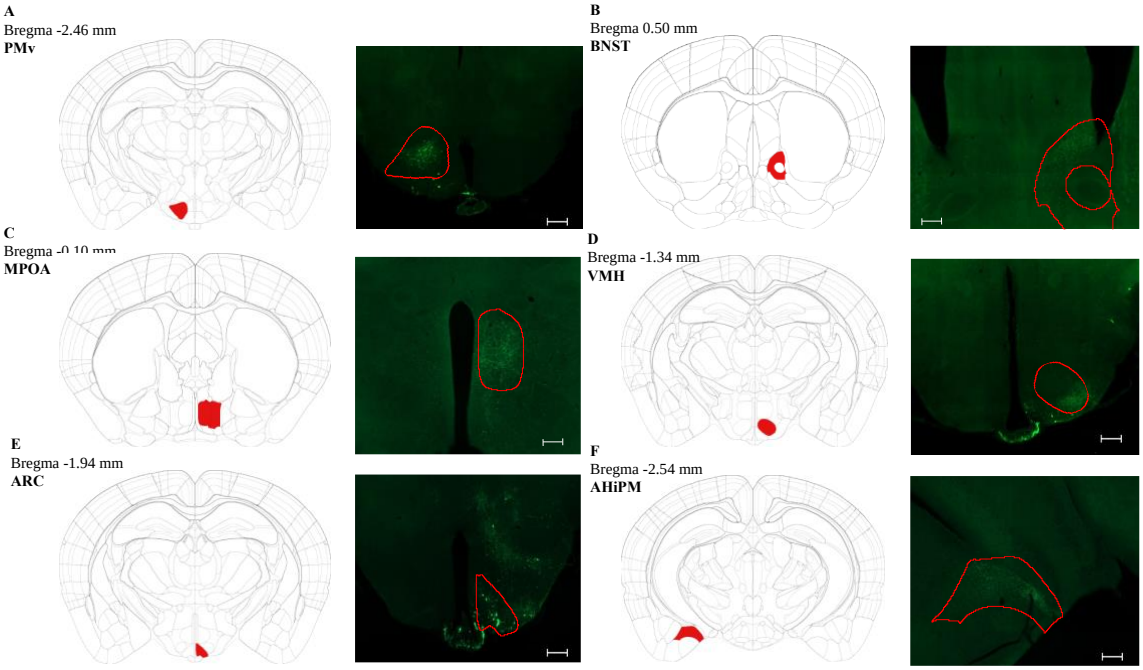

Figure 9. Representative images of the injection site and PMv outputs after 25nL injection of AAV1-CAG-floxed-SynGFPrev-WPRE. Atlas images show injected brain regions are color-coded and surrounded in red in the microscope image. (A) Ventral premammillary nucleus (PMv), injection site. (B) Bed nucleus of the stria terminalis (BNST). (C) Medial preoptic area (MPOA). (D) Ventromedial nucleus of the hypothalamus, ventrolateral region (VMHvl). (E) Arcuate nucleus (ARC). (F) Amygdalohippocampal posteromedial, posterior part (AHiPM). Median Eminence is another output area visible in (D) and (E). Bregma coordinates represented for each region, according to the classification from The Mouse Brain in Stereotaxic Coordinates 3rd Edition, by Franklin & Paxinos. Scale bar: 200 um.

The first approach was to investigate all the areas that exhibited fluorescence across the entire brain, meaning the ones that receive axons originating in the PMv-DAT population (n=5) (table 1; supplementary table 1). Table 1 depicts all brain areas where we observed GFP positive fibers. While some areas are present in all 5 animals included in the analysis, in other cases we observed labeled fibers only in a subset of those 5 animals. The highest levels of concordance across animals occurs within other hypothalamic areas such as the VMHvl, but also in pallidal structures such as the BNST or components of the olfactory pathway, such as the MeA (fig 9; table 1).

Table 1. Description of the PMv outputs after 25nL injection of AAV1-CAG-floxed-SynGFPrev-WPRE (n=5). Brain areas classification retrieved from: Paxinos, G., & Franklin, K. B, 2008.

PMv Outputs (n=5)		
Brain Regions	**Output Areas**	**% animals with synpatic terminals**
Cerebral Cortex	**AHiPM**	100
Cerebral Cortex	**M1**	40
Cerebral Cortex	**M2**	40
Striatum	**MePD**	100
Striatum	**MePV**	100
Striatum	**LSV**	100
Striatum	**ICj**	60
Striatum	**LSI**	20
Pallidum	**BNST**	100
Pallidum	**StA**	20
Pallidum	**VP**	20
Thalamus	**Rt**	20
Hypothalamus	**SHy**	100
Hypothalamus	**VMVvl**	100
Hypothalamus	**ME**	100
Hypothalamus	**MPOA**	100
Hypothalamus	**ARC**	100
Hypothalamus	**AHA**	80
Hypothalamus	**LA**	80
Hypothalamus	**RML**	80
Hypothalamus	**mt**	80
Hypothalamus	**AHC**	60
Hypothalamus	**AHP**	60
Hypothalamus	**RMM**	60
Hypothalamus	**PLH**	60
Hypothalamus	**PaV**	40
Hypothalamus	**PaMP**	40
Hypothalamus	**DM**	40
Hypothalamus	**VTM**	40
Hypothalamus	**StHy**	40
Hypothalamus	**PaAP**	20
Hypothalamus	**RCh**	20
Hypothalamus	**RChl**	20
Midbrain	**LPAG**	60
Midbrain	**VTA**	40
Midbrain	**SNR**	40
Midbrain	**VLPAG**	20
Fiber Tracts	**MFB**	100
Fiber Tracts	**IPACM**	20
Fiber Tracts	**IPACL**	20
Fiber Tracts	**LO**	20
Fiber Tracts	**SM**	20
Fiber Tracts	**Opt**	20

In order to perform population analysis and because there is variability in the area from the target structures where fluorescence was measured and in the number of starting DAT^+ cells in the PMv, we did a normalization to account for these differences. First, we measured the absolute intensity in each target region: projection intensity (total fluorescence pixels from labeled axons fibers in the target structure); then, the projection intensity was normalized by the area: projection density. We performed this analysis in all the areas that were present in at least 3 of 5 animals (fig. 10A, B and C). For quantification of fluorescence intensity/density, the average pixel intensity in a target region containing presynaptic GFP punctae was calculated and the background (near region without GFP signal) was subtracted (fig. 10).

Furthermore, we used the projection density of the injection site (PMv) to normalize outputs densities within each animal (fig. 10D, E). In figure 10D, it is possible to observe the variability across animals, i.e., animal represented in pink was a much higher density of projection in the VMHvl and ARC, meaning that the output to those regions are, in principle, stronger. Moreover, we reported a matrix with the projection densities normalized by the PMv, for all

animals, which corroborate the previous data in how different outputs are distributed across animals (fig. 10E). Across the 5 animals quantified, there is some variability in the projection densities in different areas. By looking to the data of all animals, ARC, VMHvl and ME are the regions that present more density of synaptic terminals, which suggest that these are the regions to which PMv projects more. Moreover, the BNST, AHiPM and MPOA have the lowest density of projections.

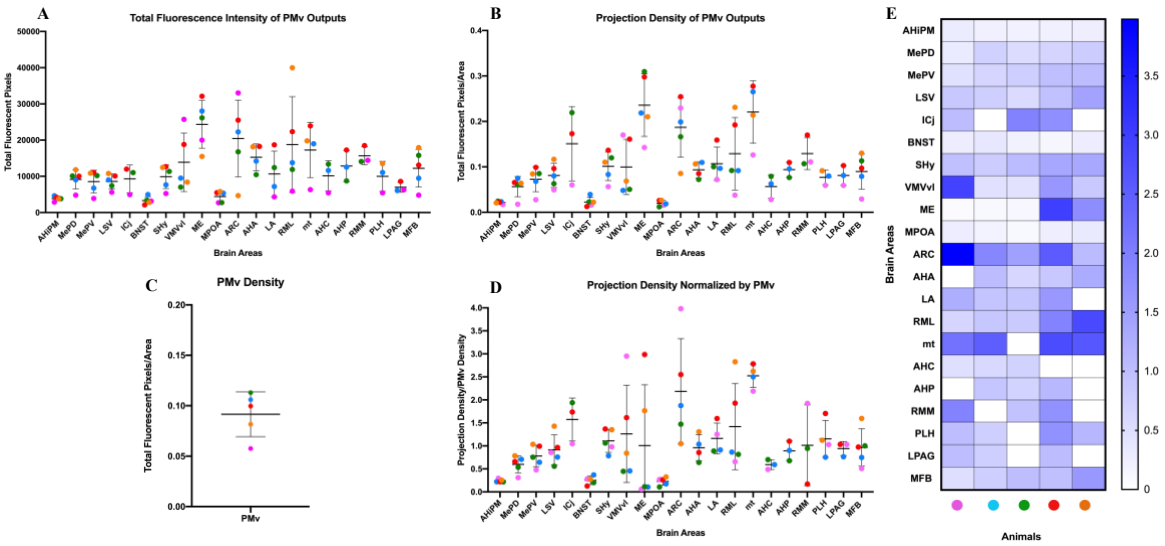

Figure 10. Quantification of PMv-DAT projection areas. (A) Total fluorescence pixels from labelled axons fibers in the target structure. (B) Fluorescence pixels normalized by the area (density) of each output region. (C) Density of the injection site (PMv) in all animals. (D) Density of each output area normalized by the density of the injection site. (E) Illustrative matrix of how different outputs are distributed across animals. Scale represents the fluorescence density of each brain area, normalized by the density of the injection site, across the quantified 5 animals. Different coulour points correspond to different animals.

3.2. PMv-DAT^{+} Neuronal Ablation

Lesion studies have been used throughout the years as a key technique to unravel the function of specific brain regions in different social behaviors (Glenn et al., 2005). Techniques used to ablate brain structures in rodents have undergone considerable evolution. Electrolytic lesions have been made using a stainless steel metal electrode that create a lesion by passing current (Al, 2003). Over the last years, the use of chemical lesion methods has become more common than the electrolytic lesion techniques. Two major chemicals have been used: kainic acid and ibotenic acid, analogues of neurotransmitter glutamate (Al, 2003). Moreover, it is possible to use pharmacological methods to lesion selected brain areas, for example using tetrodotoxin (TTX), which specifically block voltage-gated sodium channels on the surface of neuronal membranes (Al, 2003; Glenn et al., 2005). Nowadays, genetic ablation, a DNA modification to disrupt the production of a specific gene, can be performed in combination with transgenic technology, which allows lesions to be specific (Palmiter et al., 1987). For instance, genetic ablation studies can be performed using a

transgene that encodes a toxin's receptor, such as the diphtheria toxin receptor (Saito et al., 2001). This receptor is toxic to neurons only when diphtheria toxin is present. Neurons that do not express the receptor will not be sensitive to the toxin (Saito et al., 2001). Ultimately, this allows a scientist to ablate neurons at any time point during an animal's lifespan.

Therefore, to study the function of PMv-DAT^{+} cells, we have accessed two different neuronal ablation strategies:

1. A genetic ablation using caspase-3;
2. A genetic ablation using diphtheria toxin.

To achieve that, we used a tdTomato mouse reporter line crossed with the DAT-Cre previously used line (Ai9 (RCL-tdTomato) DAT-IRES-Cre flox/wt cre/wt) (fig. 11). The resulting offspring will express tdTomato fluorescence following Cre-mediated recombination, resulting in DAT cells that express red fluorescence.

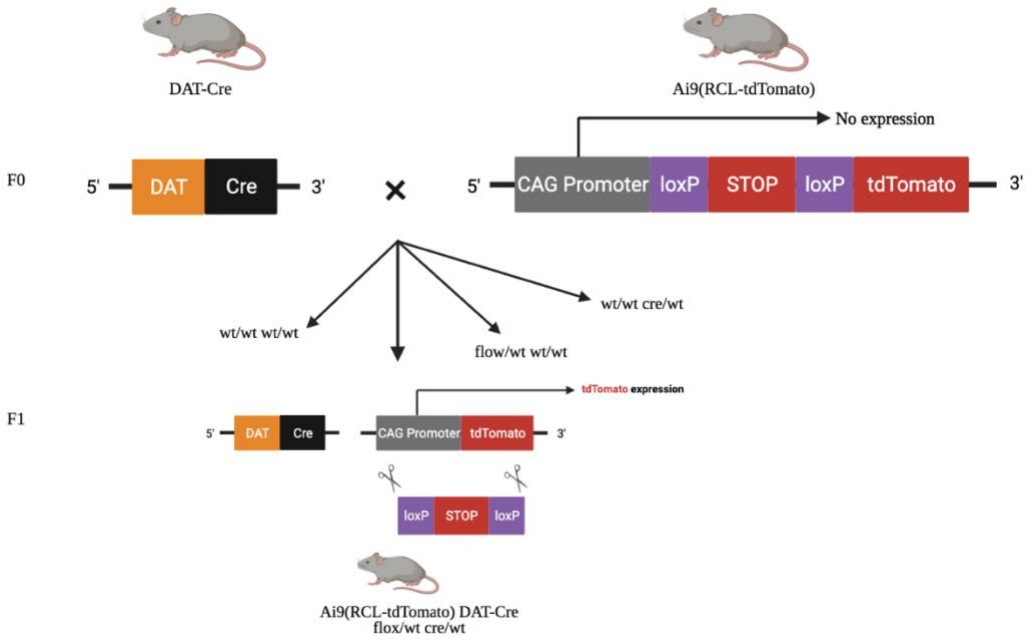

Figure 11. Mouse Model for PMv-DAT^{+} Neuronal Ablation. Illustration of a Ai9 (RCL-tdTomato) mouse reporter line crossed with DAT-IRES-Cre, containing the Cre recombinase, which is expressed simultaneously with endogenous DAT gene. Ai9 is a Cre reporter strain designed to have a loxP-flanked STOP cassette preventing transcription of a CAG promoter-driven red fluorescent protein variant. Ai9(RCL-tdTomato) DAT-Cre flox/wt cre/wt resulting offspring will have the STOP cassette deleted by the action of Cre recombinase specifically in cells expressing DAT, which results in tdTomato expression. Adapted from: L. R. Lee *et al.*, 2019.

3.2.1. PMv-DAT^{+} Neuronal Ablation with Caspase-3

Using this mouse model, we designed a pilot experiment where we employed a genetically engineered caspase 3, whose activation commits a cell to apoptosis, to eliminate PMv-DAT^{+} neurons. Consequently, the expected outcome is a complete neuronal ablation of the PMv-DAT^{+} cells and, consequently, less, or even absence, of tdTomato fluorescence expression.

Caspases are a family of proteases that are highly conserved and mediate apoptosis, which are dependent on caspase-3 (Creagh & Martin, 2001; Gray et al., 2010; Hyman & Yuan, 2012). Apoptosis is a type of cell death characterized by nuclear and cytoplasmic condensation and cell fragmentation (Kerr J. F. R., Wyllie A. H., 1972; Lossi et al., 2018). Usually, apoptotic signals activate upstream caspases that cleave procaspase 3 into its active form. Our strategy was to use a procaspase 3 that lacks the cleavage site for upstream caspases and encodes a cleavage site for the heterologous enzyme tobacco etch virus protease (TEVp), which activates pro-taCasp3 into the functional taCasp3 (fig. 12A). For that, we used an AAV to drive the expression of both pro-taCasp3 and TEVp in a Cre-dependent manner, that ultimately will commit PMv-DAT^{+} neurons to apoptosis (Atasoy et al., 2008; D'Amelio et al., 2010; Gray et al., 2010). DAT-tdTomato mice were injected in the PMv with AAV2-CAG-DIO-taCaspase3-TEV and perfused after 3 weeks (n=4) (supplementary fig. 1). Control animals are sham females (without any viral injection) (n=3). To access for the differences observed in the number of DAT^{+} at PMv (tdTomato labelled cells), one representative PMv slice of each animal was counted (fig. 12B). The difference between control and viral condition is significant ($p < 0.05$) (fig. 12B).

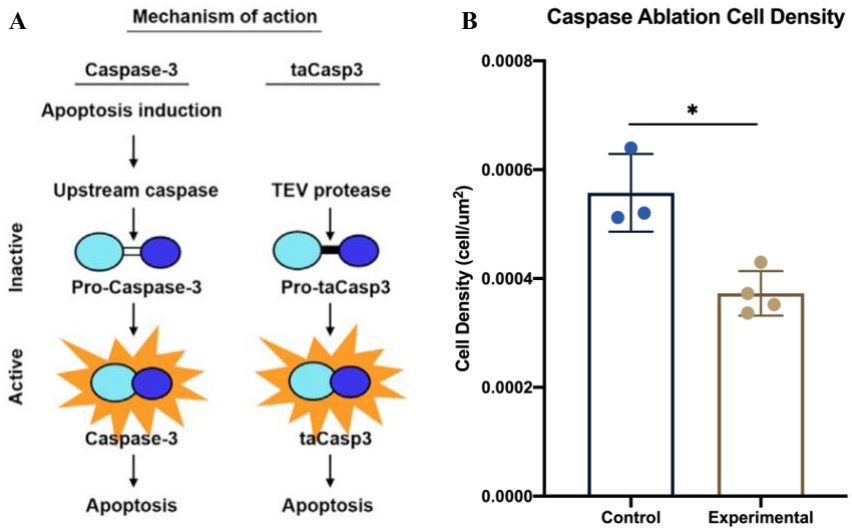

Figure 12. Caspase as a genetic technique to ablate PMv-DAT$^+$ neurons. (A) Genetic strategy to ablate neurons in a Cre-Dependent manner. The cleavage of endogenous procaspase 3 by upstream caspases activates caspase 3, which induces apoptosis. This cleavage site has been replaced by a TEV-linker domain (black bar) in inactive taCasp3 (pro-taCasp3) such that only TEV protease activates taCasp3, which then induces apoptosis. Adapted from: Yang *et al*., 2013. (B) Cell density after viral transfection with AAV-CAG-DIO-taCaspase3-TEVp bilaterally and in *sham* females. One representative PMv slice (n=4 in caspase and n=3 in control condition) of each animal was quantified. Normality was tested in all groups. T-Test for two independent sample was used to access statistical significance. Error bars represent mean ± SD. Significance was noted as *p < 0.05, **p < 0.01, ***p < 0.0005.

Nevertheless, as we expected to see an absence of tdTomato cells after the ablation, we move forward to test the virus's capacity to cause cell death *in vitro*. To test the virus's ability to induce neuronal death *in vitro*, we transduced it in a 293T Cre-dependent cell line (J. Zhang et al., 2016). As a cell death marker, we use Hoechst 3258 dye, a nucleic acid binding dye. By incorporation of the dye into the cell, it is possible to count the percentage of death cell in the given sample. As a control, we have used the same cell line without any virus (uninfected cells). The results of the Fluorescence-Activated Cell Sorting (FACS) shown that, after one week, cells infected with the caspase virus were about 66% dead. In addition, the uninfected cells were also 66% dead (supplementary fig. 2). By this, we can hypothesize that the cells, *in vitro*, are no longer dying from being infected with these AAVs conjugated with caspase-3.

As mentioned previously, we performed other ablation technique, using the genetically encoded toxin receptor in combination with their ligand, Diphtheria Toxin. This second strategy seemed to be more effective, so we choose them to use in the following behavior experiments with the ablated animals.

3.2.2. PMv-DAT$^+$ Neuronal Ablation with Diphtheria Toxin

A genetic method to achieve cell ablation is through expression of the receptors of toxins in combination with introduction of the toxin in the organism. One widely used example for this approach were the dendrotoxins (DTx), which are isolated from mamba (*Dendroaspis*) snakes (Buch et al., 2005), which block voltage-dependent potassium channels in neurons (A. Harvey & Robertson, 2012). Specifically, diphtheria toxin is a 535 amino acid polyprotein that is cleaved into two fragments, A and B. The A fragment is the amino terminal containing the catalytically active toxin domain, whereas the B fragment contains the domain interacting with the cell surface receptor for DTx. Mice are not normally sensitive to DTx since the Epithelial Growth Factor Receptor in mice does not bind DTx as it does in other species (Buch et al., 2005). In susceptible hosts, B fragment binding to the receptor causes the internalization and cleavage of A fragment (Buch et al.,

2005). The A fragment, upon entry into the cytoplasm, binds to protein synthesis machinery, inhibiting protein synthesis leading to cell death via apoptotic pathway (Buch et al., 2005; A. L. Harvey & Karlsson, 1982; A. Harvey & Robertson, 2012). DTx-mediated cell ablation model can be generated by expression of the DT-receptor (DTR) in the targeted cell population coupled with injection of DTx to the animal (fig. 13A) (Brockschnieder et al., 2004; Ivanova et al., 2005; F. Liu et al., 2019).

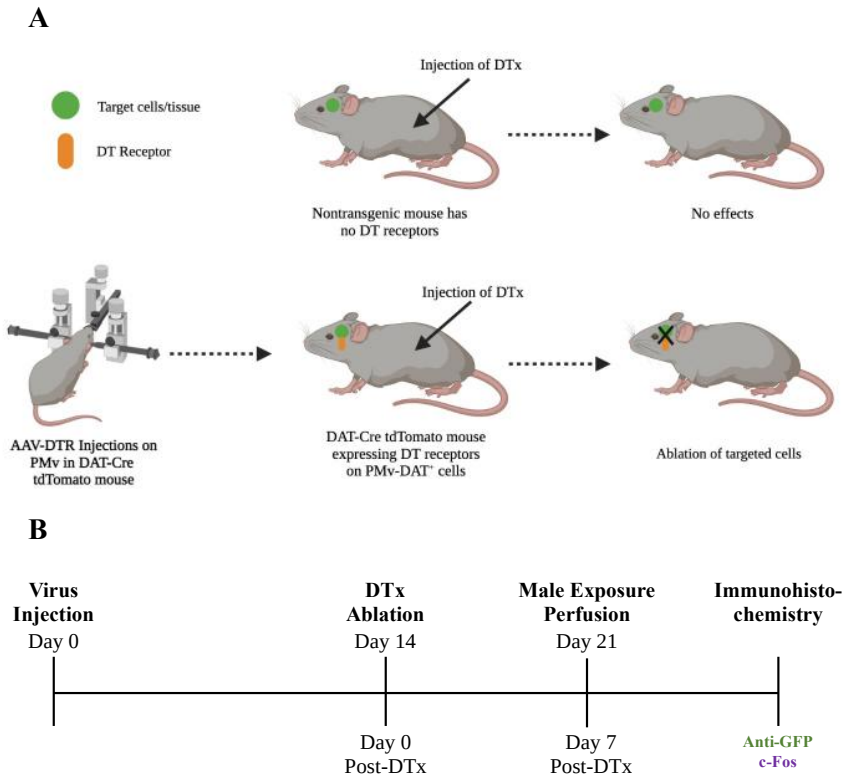

Figure 13. DTR Neuronal Ablation Experimental Design. (A) Diphtheria toxin receptor-mediated PMv-DAT$^+$ neuronal ablation. Because mice do not express Diphtheria toxin receptors (DTR), injection of DTx caused no abnormalities in wild-type mice (Pappenheimer et al., 1982). We used the DAT-Cre mouse injected with the DT receptor and examined the effects of DTx administration. Adapted from: Saito *et al*., 2001. (B) Timeline of the experimental protocols. For immunohistochemical analysis of the efficacy of DTx-induced PMv-DAT$^+$ cells ablation, mice were transfected with virus on day 0, followed by DTx treatment on day 14. Seven days after the DTx injection, female mice were exposed to a male for 5 minutes and perfused 1h30min afterwards. Tissue was stained and processed for antibody labeling of c-Fos and GFP.

To approach the efficiency of Diphtheria toxin-induced cell death, unilaterally injections were performed using AAV2-CBA-FLEX-DTR-GFP in DAT-Cre tdTomato females, which carries a floxed version of the diphtheria toxin receptor gene (fig. 13B). When the virus enters DAT expressing neurons, the Cre recombinase will recombine the loxP sites, allowing for the correct orientation of the DTR gene (Ruedl & Jung, 2018). By injecting diphtheria toxin, intraperitoneal and two weeks after the viral injection, it will bind the receptor and lead to cell death by apoptosis. After 3 weeks (time for viral expression and ligand ligation), we assessed infection/cell death in three ways: by the reduction in the number of the DAT$^+$ (tdTomato expressing cells) cells on the injected site, by the number of DTR$^+$ cells in the injected site and, since females were exposed to

male stimuli 90 minutes before being sacrificed, by the number of c-Fos$^+$ neurons (on both sides). We used c-Fos immediate early gene as proxy for neuronal activation. Immediate early genes (IEGs) are a set of genes, whose activation occurs in response to a wide variety of stimuli (Bahrami & Drabløs, 2016; Chung, 2015; Fowler et al., 2011; Lanahan & Worley, 1998). They are activated firstly at the transcription level, before any new proteins are synthesized (Bahrami & Drabløs, 2016; Chung, 2015). Generally, the kinetics of the c-Fos response to stimuli is transient, with a peak of c-Fos protein between 90–120 minutes (Chung, 2015; Kovács, 2008). Since we injected the virus in a single hemisphere and we know that the PMv-DAT$^+$ population does not send projection to the contralateral hemisphere (as we did not observe any fluorescence in the Syn-GFP experiments from the previous chapter), we used the contralateral (non-injected) hemisphere as control to evaluate the extent of the manipulation. In all animals, we have confirmed that the receptor is located in the PMv and that the virus did not spread around other brain areas (data not shown). In females injected with AAV2-FLEX-DTR-GFP, the diphtheria toxin receptors appear represented in green (by the association with GFP) in the ipsilateral (injected) hemisphere (fig. 14A and B).

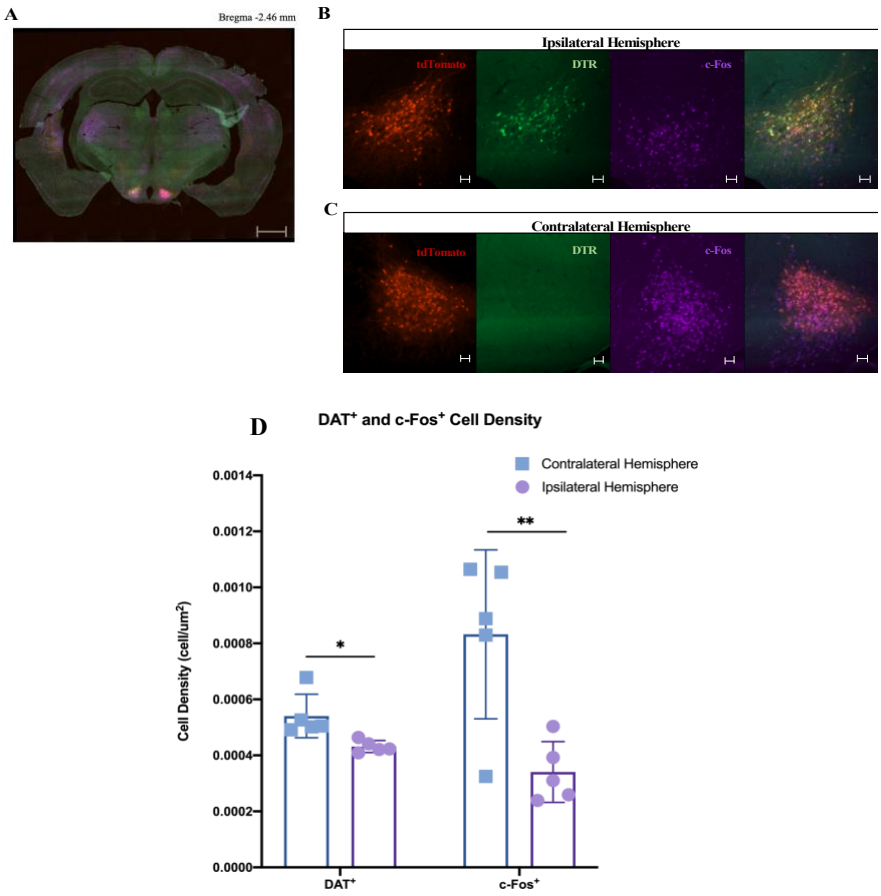

Figure 14. Comparison between DAT$^+$ and c-Fos$^+$ cells after unilateral injection of 200 nL of AAV2-FLEX-DTR-GFP between ipsi and contralateral hemispheres. Animals were injected unilaterally on the ipsilateral hemisphere. (A) Representation of a brain slice (bregma: -2.46 mm), with 10X magnification and viral injection on the left side; scale bar: 1000 um. (B) Representative ROI images of the PMv, with 20X magnification, in the ipsilateral hemisphere; scale bar: 50 um. (C) Representative ROI images of the PMv, with 20X magnification, in the contralateral hemisphere; scale bar: 50 um. DAT$^+$ are represented in red by

the fluorophore tdTomato. In green (Alexa 488) are the Diphtheria Toxin Receptor (DTR) positive cells and, in purple (Alexa 647), are represented the c-Fos positive cells. Females were exposed 5 minutes to a male mouse before perfusion, resulting in the activation of the DAT^+ cells in the PMv. Lee c-Fos activation is reported in the injected hemisphere. Images were acquired using a Zeiss AxioImager M2 microscope. (D) Comparison of cell density of DAT^+ and $c\text{-}Fos^+$ in ipsi and contralateral hemisphere (n=5). Each point type represents a different animal. Mann-Whitney test for two independent samples was used for statistical significance. Error bars represent mean ± SD. Significance was noted as *p < 0.05, **p < 0.01, ***p < 0.0005.

We performed the image analysis separately for the two hemispheres: contralateral (cont; non-injected) and ipsilateral hemisphere (ipsi; injected). The first question we asked was if there is any difference in the density of DAT^+ and $c\text{-}Fos^+$ cells across hemispheres. We observed a significant reduction in the density of the DAT^+ population in the ipsi hemisphere ($p < 0,05$) (fig. 14D). Regarding $c\text{-}Fos^+$ density, we also observed a decrease in the ipsi hemisphere ($p < 0,01$) (fig. 14D). This suggests that the injection of the diphtheria toxin is ablating DAT^+ neurons and, consequently, less DAT^+ cells will respond to the male cues and, therefore there is less $c\text{-}Fos^+$ in the ipsi hemisphere. By visual inspection, we noticed that a large percentage of the $c\text{-}Fos^+$ cells were not DAT^+ positive. Therefore, we wondered if the reduction in the $c\text{-}Fos^+$ population was indeed due to a decrease in the $DAT^+/c\text{-}Fos^+$ or/and in the $DAT^-/cFos^+$ cells. For that, we first calculated the proportion of each population and compared their density across hemispheres (fig. 15). This analysis revealed that both populations, $DAT^+/c\text{-}Fos^+$ and $DAT^-/cFos^+$, were reduced in the ipsi hemisphere (fig. 15).

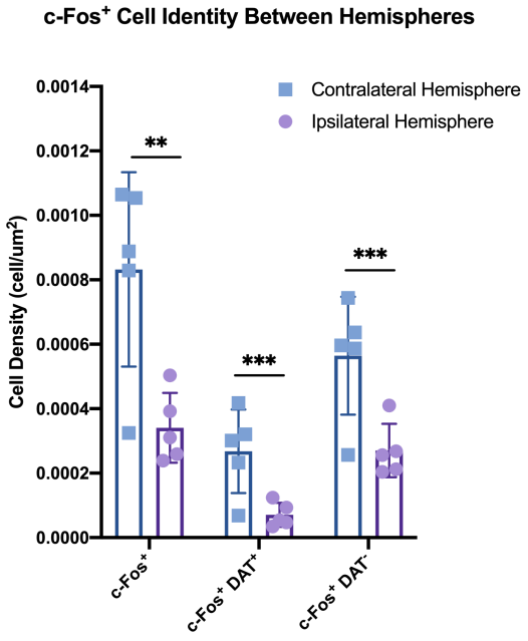

Figure 15. $c\text{-}Fos^+$ cell identity across hemispheres in injected animals. Mann-Whitney test for two independent samples was used for statistical significance. Error bars represent mean ± SD. Significance was noted as *p < 0.05, **p < 0.01, ***p < 0.0005.

Since the DTR is supposed to only be expressed in DAT^+ (which contain the Cre recombinase), the reduction in the number of $DAT^-/cFos^+$ may be the result of two phenomena: 1) the DAT^+ population is interconnected with the DAT^- and, consequently, a reduction in the number

of DAT$^+$ cells could lead to a reduction in the number of DAT$^-$ that are activated by male cues (which are c-Fos$^+$); 2) if there is any leakiness in the virus, this is, if the DTR is also expressed in the DAT$^-$ population, the reduction in DAT$^-$/c-Fos$^+$ neurons could have been a direct consequence of the DTR expression. To calculate the percentage of DAT$^-$ cells that expressed the DTR gene, we should have determined the number of DTR$^+$ cells in animals before injection of the DTx. Because we did not do that, and because we observed DTR expression even after the injection of the toxin, as an approximation for viral leakiness, we determined the number of DAT$^+$/DTR$^+$ and DTA$^-$ /DTR$^+$. Therefore, we assessed the leakiness of the virus, which is plotted in figure 16. To our surprise, there is a considerable percentage of DAT$^-$ cells that also express the DTR gene, suggesting that the FLEX cassette is not fully preventing the transcription of the DTR gene (Abdallah et al., 2018; Fischer et al., 2019; Sjulson et al., 2016).

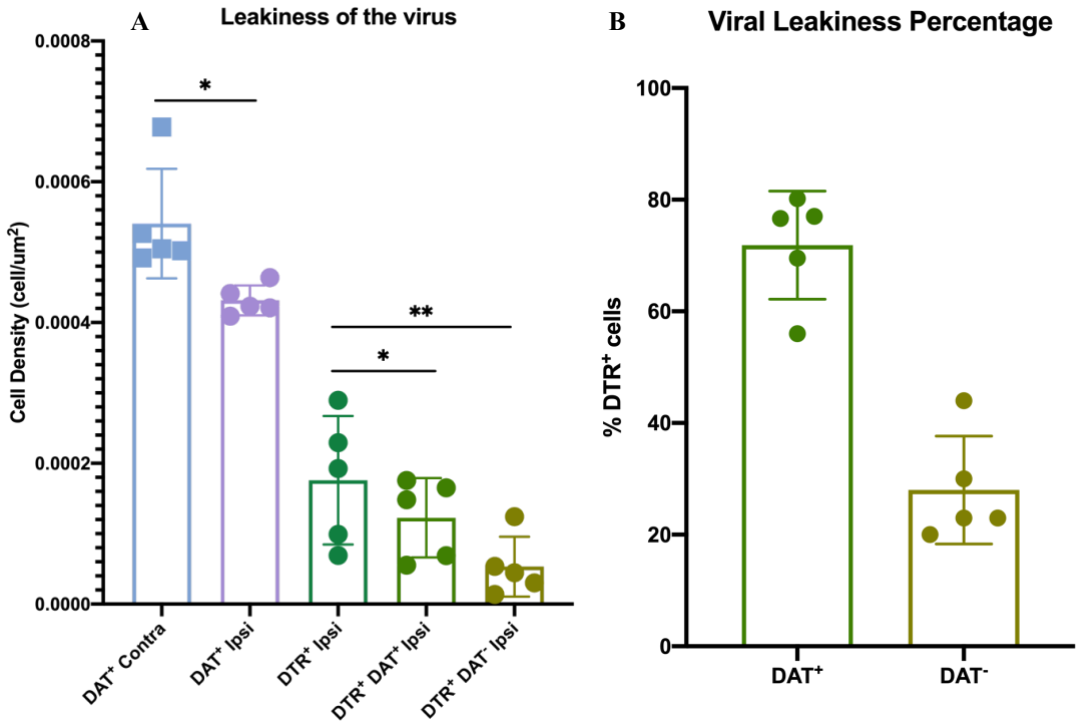

Figure 16. Viral leakiness of AAV2-DTR-GFP in the ipsilateral hemisphere. (A) Cell density (number of positive cells per area) for DAT$^+$, DTR$^+$ and co-localization between DAT$^+$ and DTR$^+$. (B) Percentage of cells contain the diphtheria toxin receptor that also express or not DAT. 100% was defined for the total DTR$^+$ cell density. Circles represent the ipsilateral and squares represent the contralateral hemisphere. Normality was tested in all groups (n=5). T-Test for two independent sample was used for access statistical significance. Error bars represent mean ± SD. Significance was noted as *p < 0.05, **p < 0.01, ***p < 0.0005.

3.3. Sexual Behavior Effects in PMv-DAT^{+} Ablated Cells

As a last step, we aim to test what is the behavioral effect of the neuronal ablation in sexual behavior. For this, six Ai9(RCL-tdTomato) DAT-Cre (*flox/wt cre/wt*) females were injected bilaterally with AAV2-FLEX-DTR-GFP and, two weeks after, administrated with diphtheria toxin. We have started the behavioral experiments after 3 weeks of the injections (fig. 17A). As a control, we used Ai9(RCL-tdTomato) DAT-Cre *sham* females, without any viral injection (just craniotomy) and injected with diphtheria toxin (fig. 17B). The behavioral experiments were conducted in the receptive female (proestrus-estrus of the estrous cycle). During this stage, a sexually trained male is introduced in the experimental cage with the female and allowed them to sexually interact freely.

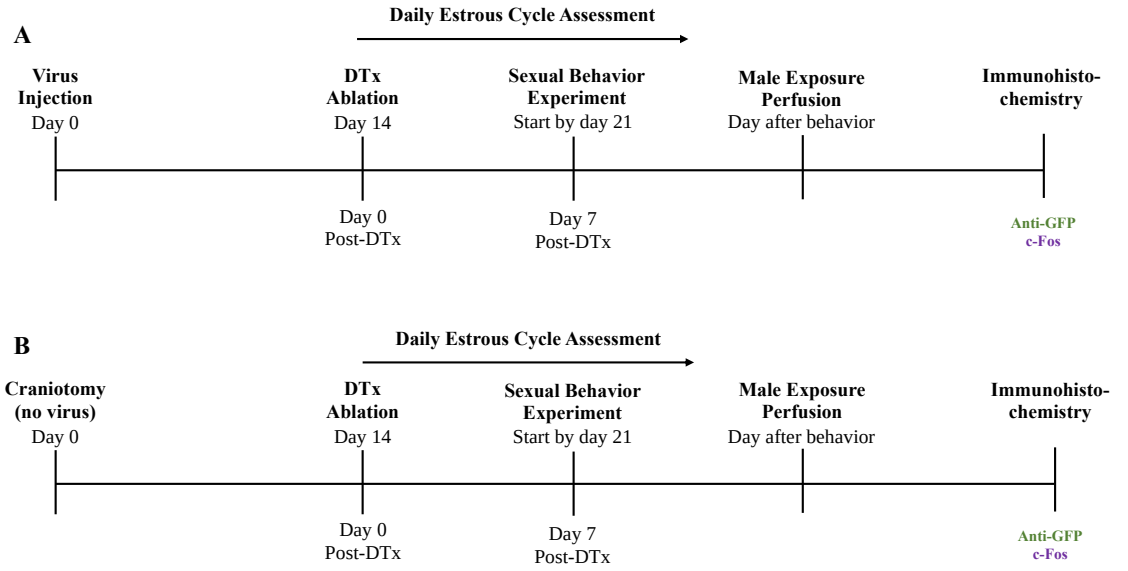

Figure 17. Sexual behavior experimental design. (A) Timeline of the experimental behavior. For analysis of the efficacy of DTx-induced PMv-DAT cells ablation, mice were transfected with virus on day 0, followed by DTx treatment on day 14. Daily estrous cycle evaluation has started, to access the receptive stage of the females. After 3 weeks from the injection day, sexual experiments have started using receptive females and a previously sexually trained male. On the day after the behavior performance, female mice were exposed to a male for 5 minutes and perfused 1h30min afterwards. Brain tissue was stained and processed for antibody labelling of c-Fos and GFP. (B) Timeline of the control behavior protocols. For immunohistochemical analysis, mice were submitted to a craniotomy on day 0 (without virus injection), followed by DTx treatment on day 14. After 3 weeks from the injection day, cycle assessment, behaviors experiments, and tissue processing were performed as previously described for experimental animals.

We performed similar analysis to what was shown before for the pilot experiment using DTR for PMv-DAT^{+} ablation (supplementary fig. 3). However, in this case, we have both hemispheres manipulated. Since each hemisphere received an independent injection of AAV2-DTR, we started by analyzing if there are difference in the cell numbers between hemispheres. No significant differences were reported between hemispheres in experimental females (fig. 18A). This supports that the injections were concordant in the two hemispheres across animals. Consequently, the subsequent analyses will represent a pool of both hemispheres. Moreover, we have done the

same for control animals, that received just the toxin injection and we did not find any difference between hemispheres, which suggests that the toxin itself does not present an effect in cell number (fig. 18B).

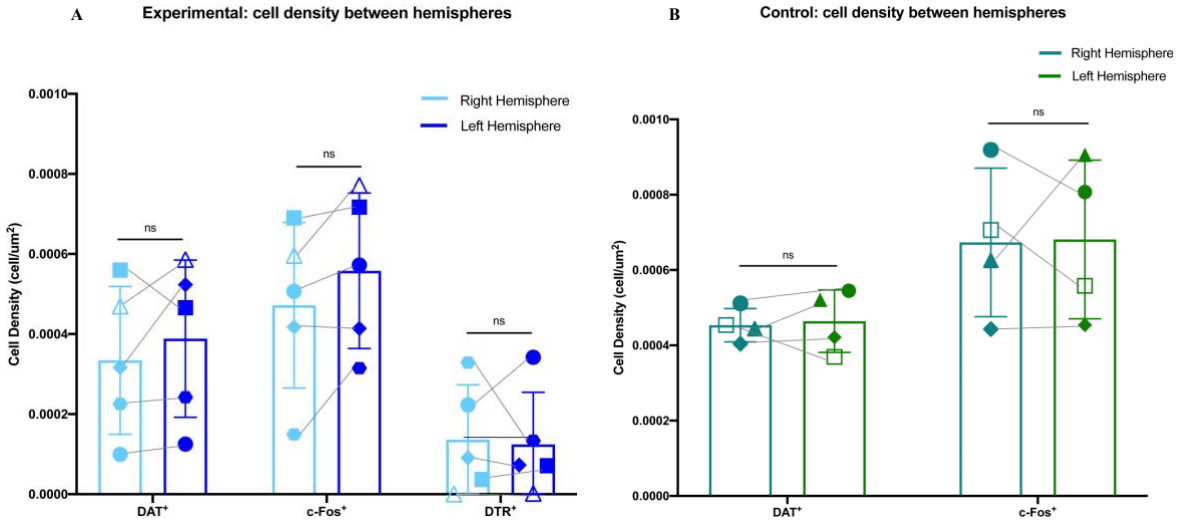

Figure 18. DAT$^+$, c-Fos$^+$ and DTR$^+$ cell density variability across hemispheres. (A) Cell number per area in different hemispheres both with injection of 200 nL of AAV2-DTR-GFP (n=5). (B) Cell number per area in both hemispheres in *sham* females (without DTR, but with DTx injection) (n=4). Each point type represents a different animal. Open symbols represent animals that were not counted in the behavioral analysis as they did not perform a complete sexual behavior session (triangle in experimental group and square in control group). Normality was tested in all groups. T-Test for two dependent samples was used for access statistical significance. Error bars represent mean ± SD. Significance was noted as *p < 0.05, **p < 0.01, ***p < 0.0005.

After pooling both hemispheres, we have made comparisons between the experimental and the control animals to access the extent of the ablation, similar with the previous pilot experiment. However, we did not saw a significant difference in DAT$^+$ and c-Fos$^+$ cell number in the experimental females comparing with the control ones (fig. 19).

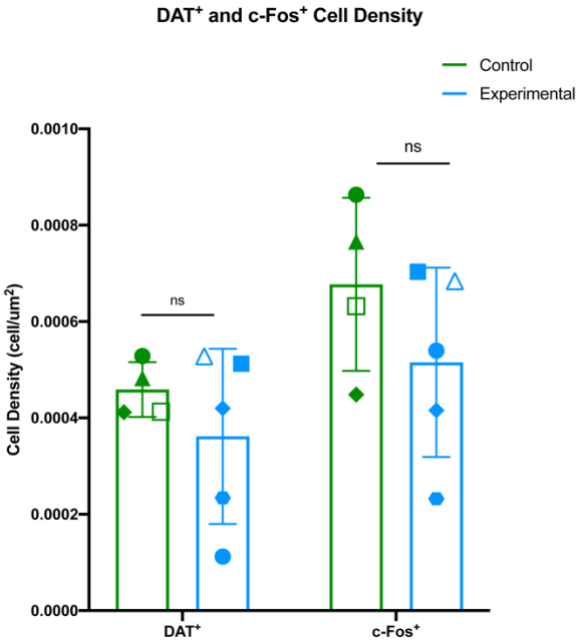

Figure 19. DAT$^+$ and c-Fos$^+$ cell density in experimental and control conditions. Cell number per area in control (just craniotomy) (n=4) and experimental females (injection of 200 nL of AAV2-DTR-GFP bilaterally) (n=5). Each point type represents a different animal. Open symbols represent animals that were not counted in the behavioral analysis as they did not perform a complete sexual behavior session (triangle in experimental group and square in control group). Normality was tested in all groups. Mann-Whitney test or T-test for two independent samples were used for statistical significance. Error bars represent mean ± SD. Significance was noted as *p < 0.05, **p < 0.01, ***p < 0.0005.

Within c-Fos quantification, we accessed the identity of the c-Fos$^+$ cells: DAT$^+$ and DAT$^-$ (supplementary fig. 4). Previously, in the pilot experiment, we proposed that the reduction in the overall c-Fos$^+$ also affects c-Fos activity in DAT$^-$. Here there is also a significant difference in c-Fos active cells for DAT$^-$ subpopulation in experimental females compared to the control group (supplementary fig. 4). As we have done before, to approach the viral leakiness, we quantify the co-localization between DTR$^+$ and DAT$^+$, and we noticed that there are DAT$^-$ cells infected with the virus, as in the pilot experiment (supplementary fig. 5).

Furthermore, since the behavior was done in different days, depending on the estrous cycle state of the females, an interesting question is to see if there are differences in the cell number of the populations across time (fig. 20). Consequently, we plot the time passed since the injection until the sexual behavior performance across the density of DAT$^+$, c-Fos$^+$ and DTR$^+$ cells. The results suggest a decrease in the number of c-Fos$^+$ cells over time, although with a low correlation coefficient (fig. 20B). As seems not to occur a correlation between DAT$^+$ cell density with time (fig. 20A), the decrease in c-Fos cells may then be because the DTR virus is infecting other cells (DAT$^-$). These results corroborate the hypothesis of virus leakiness.

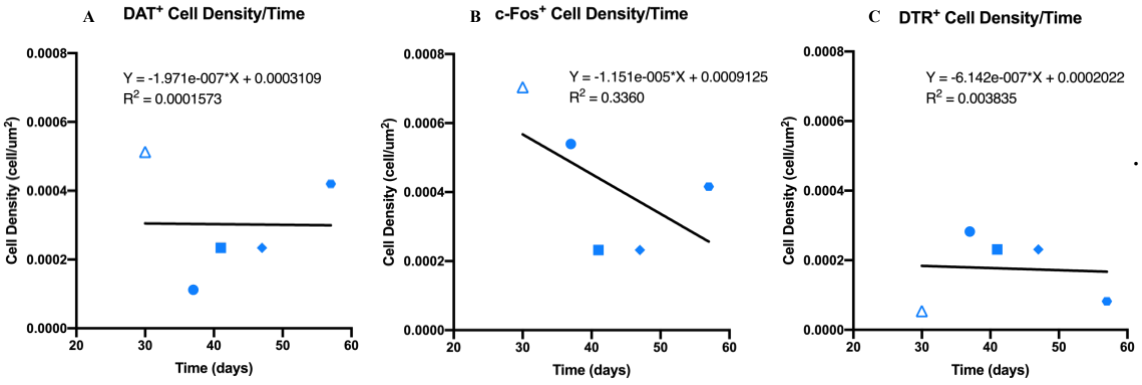

Figure 20. DAT$^+$, c-Fos$^+$ and DTR$^+$ cell density in experimental females according to the time between viral transfection and perfusion. (A-C) Cell density of experimental females (n=5) correlated with the time of the end of the experiment (days). Each point type represents a different animal. Open symbols represent animals that were not counted in the behavioral analysis as they did not perform sexual behavior (triangle in experimental group).

Even not having statistical confidence that the PMv-DAT$^+$ neurons are ablated (fig. 19), we analyzed the sexual behavior of females. Regarding the behavioral session, we questioned if there are differences in the sexual performance of the females with PMv-DAT$^+$ cells ablated in comparison with the control ones. The behaviors performed during the sexual sessions were

analyzed from a female perspective, meaning when the female has the initiative (investigations and kicking), except for mounts and mount attempts. We divided them into 5 categories: stimulus (male in, first contact between male and female, ejaculation and male out), investigation (nasal, body to body and anogenital), mount attempts (without intromissions), successful mounts (with intromissions) and aggressive-related behaviors (kicking or boxing). The experiment was finished when the male ejaculated.

For the analysis of behavior, the first question we answered was whether females, both in the control group and those with the ablated PMv, perform sexual behavior in the presence of a male. All the females have done sex, except one of the experimental females that, after 3 session attempts in their receptive state, does not allow the male to mount (not included in the next analysis). We reported also other outlier: a control female performed sexual behavior during around 3 hours with the male (having successful mounts with intromissions), but the male did not reach the ejaculation point (not included in the follow analysis). Beginning by the overall duration of the behavioral session, starting from the entry of the male until ejaculation, there is no significant difference between the experimental and the control groups (fig. 21).

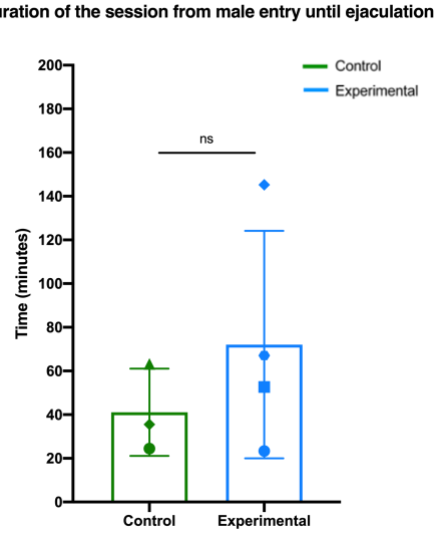

Figure 21. Overall duration of the sexual behavior session. Duration of a complete sexual behavior session, from the entry of the male in the experimental cage to the ejaculation in both conditions: controls (n=3) and experimental (n=4) animals. Each point type represents a different animal. Normality was tested in all groups. T-Test for two independent sample was used for access statistical significance. Error bars represent mean ± SD. Significance was noted as *p < 0.05, **p < 0.01, ***p < 0.0005.

As mentioned in the introduction, sexual behavior is divided into 3 main phases: appetitive, consummatory and post consummatory. Since female sexual receptivity can significantly affect aspects of the male's sexual performance, including latency to mount and ejaculation rate (Dewsbury, 1990; Theodore Landau & Madden, 1983), the behavioral analysis done was divided according to each phase and the latencies and structure of the behaviors were analyzed. Regarding the structure of the behaviors, we have reported the rate (number of behaviors divided by the duration of the session) of each behavior (fig. 22 A-D). Behaviors such as investigations or kicking

are present during all the phases do sexual performance. Although the rate of each behavior seems to be higher in control females, the difference within groups is not statistically significant ($p>0,05$) (fig. 22 A-D).

The first phase is the appetitive and is characterized by investigations between the female and the male: nose to nose, body to body or anogenital. Within this phase, we investigated the latency since the entry of the male in the experimental box to the first mount attempt, which did not present a significant difference between groups (fig. 22E). This suggests that there is no difference in the male capacity to initiate sexual behavior. Since we are manipulating females, one behavioral effect of the PMv-DAT$^+$ ablation might be an increase in the time for the female to become sexually aroused and allow a successful mount. Based on this, we access the time from the first mount attempt to the first successful mount, which also has no significant different between the control and experimental group (fig. 22F). Consequently, we did not report any change in the female arousal state. Moreover, we accessed the rate of investigations, just from male in until first mount attempt or successful mount, which did not show significant differences between groups (fig. 22G).

Within the consummatory phase, we plotted the rate of mount attempts from the first mount attempt until first successful mount. Control animals present a higher rate of mount attempts compared with the experimental ones ($p < 0.05$) (fig. 22H). We classified the mount attempts in 3 types, as already mentioned: male inability (when the male, for an internal reason, is not able to make intromissions), female walk away (when the female runs away as the male try to approach her) and female rejection (when the female performs aggressive behaviors towards the male to reject the mount). To understand which type of mount attempt is more common in control and experimental females, we quantified each mount type. We saw that, despite a decrease in mount attempts in the experimental animals, they are mainly due male inability, which are not related with the female performance (fig. 22I). In addition, from first successful mount until ejaculation, we observed the rate of mount attempts, rate of successful mounts and successful mount ratio (number of successful mounts divided by total number of mounts). In none of these parameters, we observed a significant difference between experimental and control groups (fig. 22J, K and L). Last, we accessed if the latency to ejaculate, starting from the first mount with intromissions, is somehow affected when the PMv-DAT$^+$ population is ablated. From the results presented, there is no significant difference between both groups (fig. 22M).

Behaviors During All Session

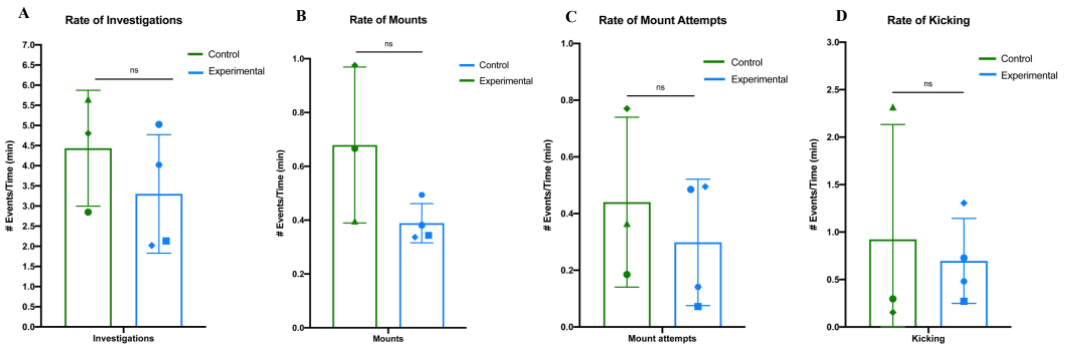

Behaviors During Appetitive Phase

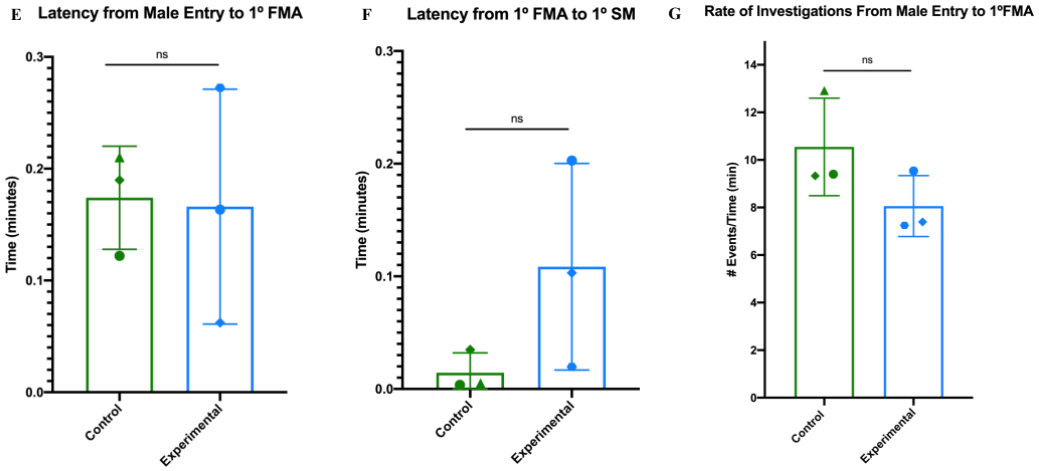

Behaviors During Consummatory Phase

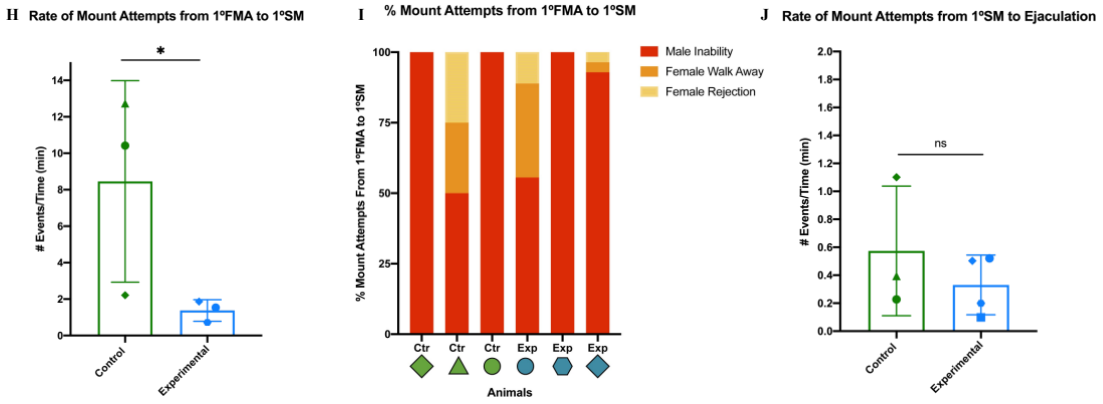

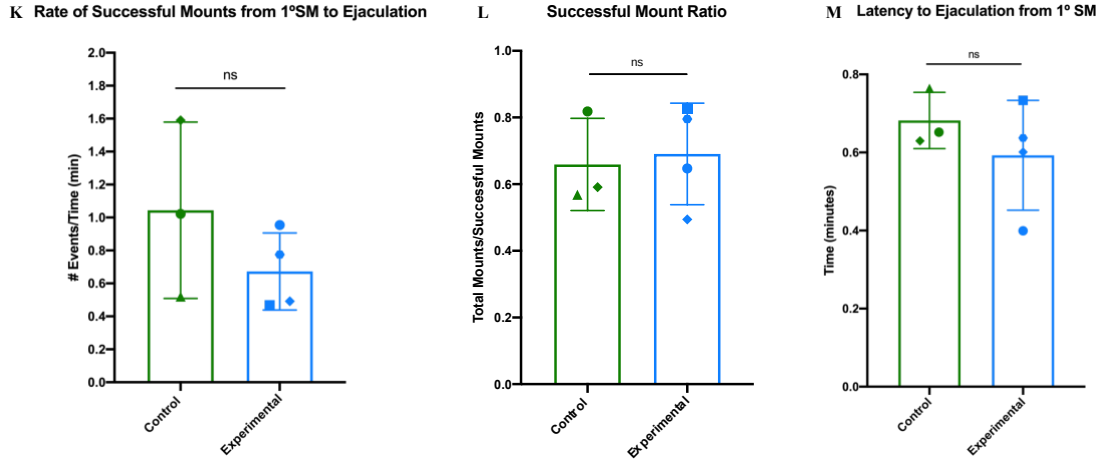

Figure 22.

Panel 1. Relative values of the sexual microbehaviors during the session. (A) Number of investigations divided by the duration of the behavioral session. (B) Number of mounts divided by the duration of the behavioral session. (C) Number of mount attempts divided by the duration of the behavioral session. (D) Number of kicking behaviors divided by the duration of the behavioral session.

Panel 2. Latencies and rate of behaviors during appetitive phase. (E) Latency since the entry of the male in the experimental box to the first failed mount attempt, in minutes. (F) Latency from the first mount attempt to the first successful mount, in minutes. (G) Number of investigations from male entry in the experimental box to the first mount attempt, normalized by the time of the approach in minutes (since the male entry in the box until the first failed mount attempt). Exceptionally, control and experimental groups are composed by 3 animals. One of the experimental animals were excluded from the representation because her consummatory phase started with a successful mount (with intromissions) and not by a mount attempt.

Panel 3. Latencies and rate of behaviors during consummatory phase. (H) Number of mount attempts from the first mount attempt until first successful mount, normalized by the time of the approach. (I) Percentage of the 3 types of mount attempts (female rejection, female walk away and male inability) from the first failed mount attempt to the first successful mount. Exceptionally, control and experimental groups are composed by 3 animals. One of the experimental animals were excluded from the representation because her consummatory phase started with a successful mount (with intromissions) and not by a mount attempt. (J) Number of mount attempts from the first successful mount until male ejaculation, normalized by the time of the approach. (K) Number of successful attempts from the first successful mount until male ejaculation, normalized by the time of the approach. (L) Number of successful mounts per number of total mounts. (M) Graphical representation of the time, in minutes, from the first mount with intromissions (successful mount) until male ejaculation, in control (n=3) and experimental (n=4) groups. Control is composed by 3 animals and experimental group by 4 animals. Each point type represents a different animal. Normality was tested in all groups. T-Test for two independent sample was used for access statistical significance. Error bars represent mean ± SD. Significance was noted as $*p < 0.05$, $**p < 0.01$, $***p < 0.0005$.

Finally, to access if the genetic ablation as some effect on the behaviors, we performed analysis where the extent of ablation is correlated with behaviors. As we verify the cell death both by the number of DAT^+ cells and the number of c-Fos^+ cells, we correlate the two groups with each sexual microbehaviors defined in the session (investigations, failed mount attempts, successful mounts and kicking) (fig. 23). As the n number is relatively low, we observe a huge variability between the animal's behavior. Accordingly, we have lower significance in the linear regression lines, and we were unable to make any effective statement about the data. Nevertheless, regarding the DAT^+ cell density and the number of investigations, we saw a high significance value (R^2 = 0.9425) in the correlation, which suggests that, when there are more DAT^+ cells, we observe fewer investigations (fig. 23B). In control females, the same analysis was done (supplementary fig. 6). The correlation of failed mount attempts with DAT^+/c-Fos^+ cell density suggests that, when the cell density is higher, the number of failed mount attempts is lower (supplementary fig. 6).

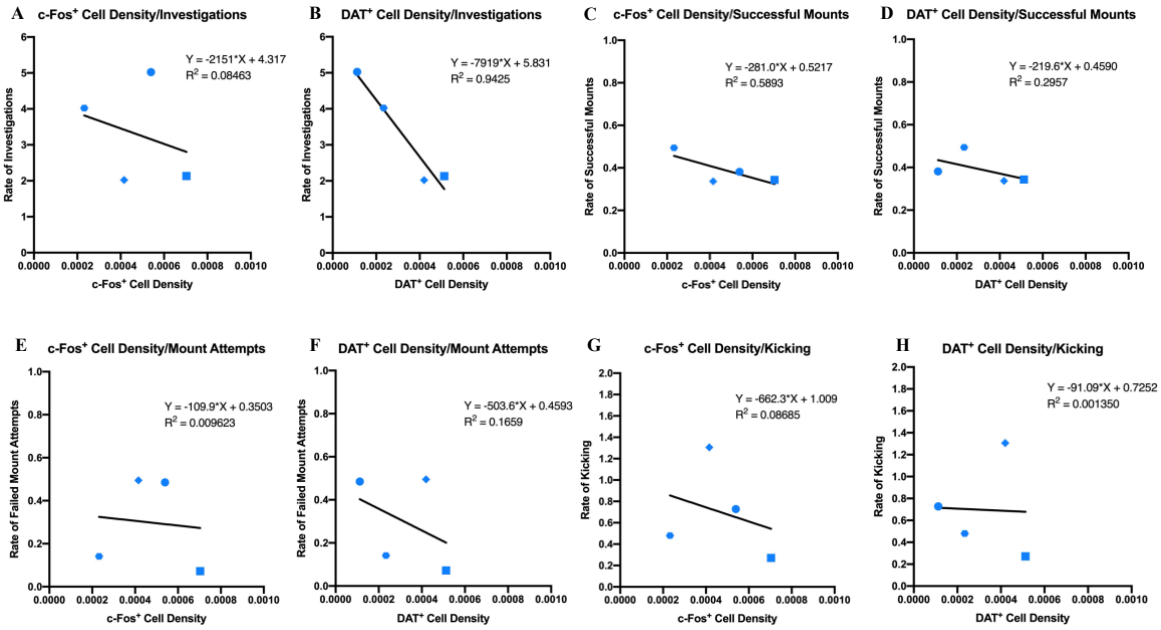

Figure 23. Correlation between c-Fos$^+$ and DAT$^+$ cell density with sexual microbehaviors in experimental females (n=4). (A) Rate of investigations during all session correlated with c-Fos$^+$ cell density. (B) Rate of investigations during all session correlated with DAT$^+$ cell density. (C) Rate of successful mounts during all session correlated with c-Fos$^+$ cell density. (D) Rate of successful mounts during all session correlate with DAT$^+$ cell density. (E) Rate of failed mount attempts during all session correlate with c-Fos$^+$ cell density. (F) Rate of failed mount attempts during all session correlate with DAT$^+$ cell density. (G) Rate of kicking during all session correlate with c-Fos$^+$ cell density. (H) Rate of kicking during all session correlate with DAT$^+$ cell density. Each point represents a different animal.

Discussion

4. Discussion

In this chapter, the results obtained throughout this project will be discussed. In the first part, the results regarding the identification of PMv outputs will be compared and examined regarding the previous literature. Posteriorly, some possible results explanations will be introduced regarding the PMv-DAT^{+} neuronal ablation and their effects on female sexual behavior.

4.1. Outputs of Ventral Premammillary Nucleus

To systematically map the outputs of PMv-DAT neurons, we used DAT-Cre mice, together with Cre-dependent AAV-based anterograde virus (Guselnikova & Korzhevskiy, 2015) that labels the synaptic terminals in the output targets, represented by the green fluorescence protein. Our results suggest that in principle, the putative impact of the PMv-DAT population is correlated to the amount of fluorescence, this is, areas with higher fluorescence should receive more input. From the results presented, we infer that the outputs occur mainly to other nuclei in the hypothalamus (table 1; fig. 24). Within the hypothalamus, there are concordant areas with synaptic terminals from the PMv, such as VMHvl, ME, MPOA, BNST, ARC or AHIPM (fig. 10).

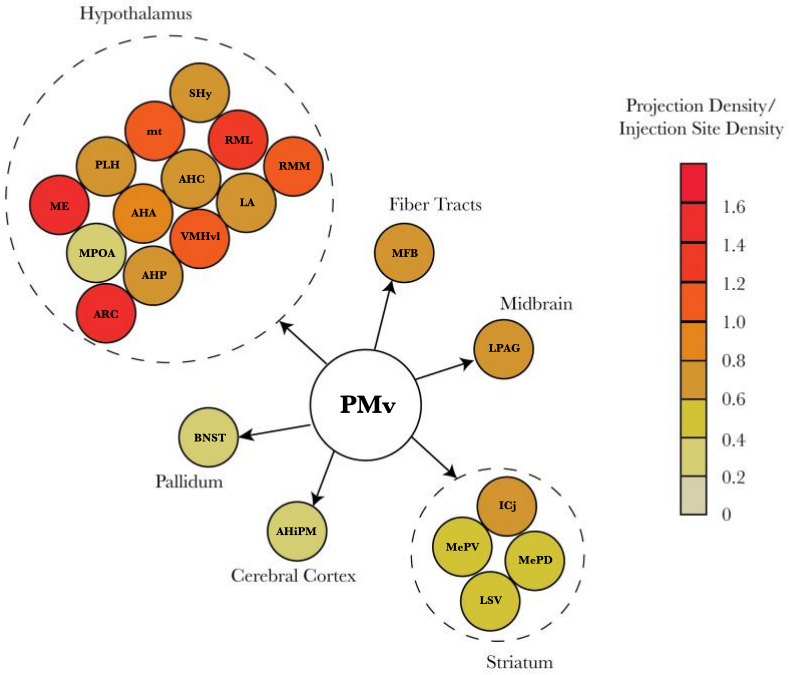

Figure 24. Representation of the PMv-DAT outputs in females. Brain areas are organized by regions. Scale bar represents the projection density of each brain area (total fluorescence intensity divided by the area) normalized with the animal PMv (injection site) density.

In addition to the outputs described above that are concordant between all animals, other areas also have terminals from PMv, however they appear less frequently (table 1). Example of that is the anterior hypothalamic area (AHA), island of Calleja (ICj) or peduncular lateral hypothalamic nuclei (PLH) (table 1; fig. 24). Another interesting projection found in a small percentage of the analyzed brains is the optic tract (Opt), which agrees with the previous findings that present PMv as a region were the information from the sensory neurons converge (Lin et al., 2011; Soden et al., 2016; Yang et al., 2013). As PMv is already known to integrate olfactory cues from conspecifics (Jose Donato et al., 2010; Hashikawa et al., 2017; Kim et al., 2019; Motta et al., 2013; Soden et al., 2016; Stagkourakis et al., 2018), it can serve as a receiving point in the hypothalamus of these cues, transmits them onto other hypothalamic nuclei responsible for controlling several social behaviors, including mating. Few axon terminals were also found in the primary and secondary motor cortex, suggesting that the PMv provide inputs to motor related regions (table 1). Interestingly, as we have done unilaterally injections of Syn-GFP to target PMv-DAT output regions, we noticed that there are no contralateral projections between hemispheres. This constitutes evidence that allow us to make effective comparisons between hemispheres in the following experiments (namely in the pilot experiment for DTR neuronal ablation).

Prior studies regarding the mapping of the PMv circuit were conducted in adult male/female rats (Canteras et al., 1992b; Cavalcante et al., 2014). They have shown innervation in the periventricular zone and through the medial zone of the hypothalamus, namely in the VMHvl (fig. 25). Moreover, labeled fibers were seen in MPN, BNST and AHiPM (fig. 25). In addition, Cavalcante *et al*, by a comparative analysis of labeled neurons following Cholera Toxin B (CTb) injection into the PMv of male and female rats, confirm that the PA, the MPN and the VMHvl present synaptic projections from PMv, which goes in agreement in our findings regarding the projections from the PMv-DAT neurons. In addition, our results support the view that the PMv seems to be an area where there is feedback/forward, that is, the same areas that send inputs also receive outputs, i.e., reciprocally connectivity with the VMHvl (Canteras et al., 1992b; Cavalcante et al., 2014; Lo et al., 2019; Stagkourakis et al., 2018). Furthermore, PA and BNST display reciprocal connections with the PMv (Canteras et al., 1992b, 1992a; Simerly et al., 1990), being able to modulate projections to the PMv (Canteras et al., 1992b).

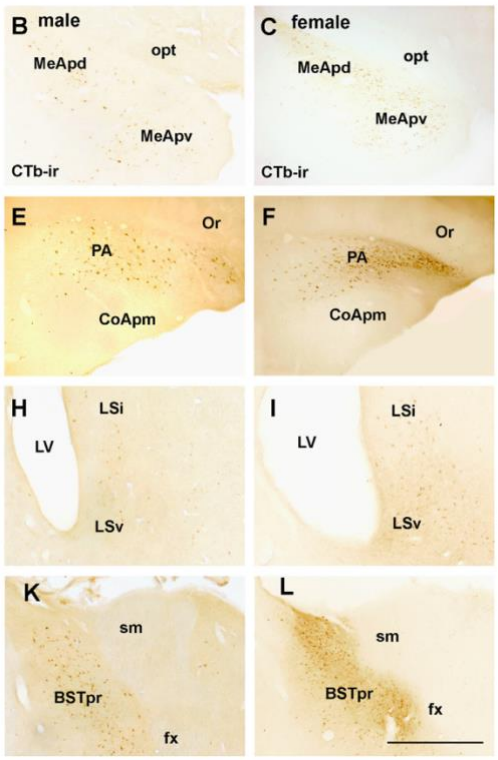

Figure 25. Projections of PMv in adult male and female rat. B and C Brightfield images showing Cholera Toxin b immunoreactive neurons (CTb-ir) in the posterodorsal and posteroventral subdivisions of the medial nucleus of the amygdala (MeApd and MeApv, respectively) of male (B) and female (C) rats. E and F Brightfield images showing CTB-ir neurons in the posterior nucleus of the amygdala (PA) of male (E) and female (F) rats. H and I Brightfield images showing CTb-ir neurons in the lateral septum ventral (LSv) and lateral septum intermediate (LSi) of male (H) and female (I) rats. K and L Brightfield images showing CTb-ir neurons in the principal subdivision of the bed nucleus of the stria terminalis (BSTpr) of male (K) and female (L) rats. Scale bar: 300 μm. Retrieved from: Cavalcante *et al.*, 2014.

Besides getting information about brain regions that receive information from the PMv-DAT$^+$ in the female brain, since the similar data exists for the same neuronal population in the male (Male et al., 2016), we decided to compare the two sexes. Soden *et al* characterized PMv-DAT neurons in male mice (Soden et al., 2016). They revealed axonal projections to the VMHvl, MPO, BNSTpd, BNSTpv, AHN and PAG, which are targets involved in the regulation of social behavior (fig. 26) (Soden et al., 2016). As mentioned above, PMv neurons are activated by opposite sex cues and as such, we hypothesize that the PMv may be involved in male directed behaviors. Within this framework, PMv-DAT$^+$ neurons should target brain areas that are involved in the control of male directed behaviors, such as sexual behavior. Since the male PMv is also activated in the presence of male cues, but the behavioral outcomes of male-male interactions are quite disparate from female-male interactions, there might be sexual dimorphism in the output logic of the PMv-DAT$^+$ population. There are two main ways in which the dimorphism could be manifested: a) in a more extreme form, where the regions receiving information from the PMv-DAT population might be different; b) more likely to be the case, we may encounter difference in the relative density of projections to each brain region, even if the regions are the same between males and females. The available paper for male mice (Soden et al., 2016) based its quantification in data from just one

animal and they do not report a full list of output projections (fig. 26). Consequently, we cannot make comparisons about the full output spectrum in males and females. What is possible to say is that the regions reported for the males are also concordant between female animals, with slightly differences in the projection density. These results supports the previous idea that no clear difference was noticed in the innervation pattern comparing both sexes (Cavalcante et al., 2014).

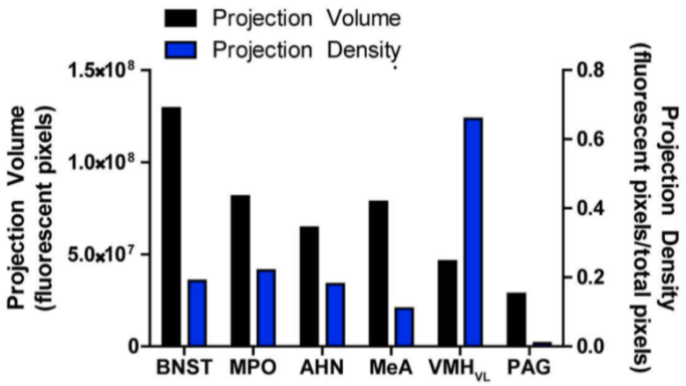

Figure 26. Male mice projections of PMv-DAT neurons revealed by expression of synaptophysin-EGFP in axon terminals. Quantification of PMv-DAT projections utilizing data from the Allen Brain Institute Connectivity Atlas. Projection Volume = total fluorescent pixels from labeled axon fibers in the indicated target structure. Projection Density = fluorescent pixels normalized to the total number of pixels in the target structure. Retrieved from: Male *et al*., 2016.

4.2. PMv-DAT$^+$ Neuronal Ablation

To test the function of the PMv-DAT$^+$ neurons on sexual behavior, we performed two types of genetic ablation: (1) using caspase-3; (2) using the diphtheria toxin receptor method. As for the first genetic ablation technique, using viral transfection of caspase-3, we notice a significant difference in the number of tdTomato positive cells, meaning that there are less DAT$^+$ neurons after ablation. Nevertheless, no complete neuronal death is observed, as expected. One plausible explanation may be the fact that tdTomato is still expressed, after caspase injection and cell death, due to the degradation of tdTomato protein in the neuronal death process. So, it could be that the cells take a long time to stop the tdTomato protein expression, and the time between the injection and the perfusion (3 weeks) were not enough to see a dramatic effect in cell reduction number. Furthermore, the proper analysis of the brain slices of animals injected with caspase was not possible to be carried out in the whole brain, since the histology of several animals suffered damages, which did not allow a correct quantification of the results. For the caspase experiment to be properly done, we should quantify all the PMv slides from all the animals and verify the variability across animals. Instead, we took representative examples of the same PMv slice, in all controls and in injected animals, and quantified. When testing the virus in a cell line, the results show that the percentage of cell death is equal in the virus-treated cells and in cells without the virus. There could be several reasons why the virus does not have an effect *in vitro*. The most

obvious will be directly the fact that could happen some mistake in the order/processing of the virus until it reaches the laboratory. To depict this hypothesis, we should test if the caspase-3 is expressed in the cell culture containing the viral particles. One way to do this is to incubate the cells with the caspase-3 virus and then, using PCR technique, confirm whether there is caspase-3 RNA expression in the viral infected cells.

For the second genetic ablation technique, we transfected the DTR to the PMv coupled with an injection of DTx. Our hypothesis undertakes that, after ablation of DAT^+ cells, they should stop responding to male cues, hence presenting a decrease in DAT^+ cells and c-Fos expression. Our results corroborated the hypothesis, showing a significant decrease in the number of DAT^+ neurons and in the c-Fos^+ cells actively responding to male cues (fig. 15). Moreover, we saw that the reduction in c-Fos activity occurs both in the DAT^+ and DAT^- population (fig. 16), which can be cause by viral leakiness (when DTR is also expressed in DAT^- cells) or by an interconnectivity between DAT^+ and DAT^- subpopulations (the reduction of the former leads to a reduction in DAT^- population). In other words, the stimuli received in the DAT^+ subpopulation is passed onto other subpopulations of neurons in the PMv, revealing a connectivity between DAT^+ and DAT^-.

Surprisingly, there is a considerable percentage of DAT^- cells that also express the DTR gene. This suggests that the FLEX cassette, in the AAV2-DTR virus, is not fully preventing the transcription of the DTR gene. LoxP sites in FLEX constructs are known to recombine during DNA amplification and viral vector production, which may result in a small percentage of Cre-activated viral vectors. This can lead to a small number of cells exhibiting Cre-independent transgene expression (Fischer et al., 2019). To address this, we should titrate the virus to find the optimal concentration required for Cre-dependent transgene expression *in vivo*. If the virus used as a higher concentration, this increases the risk of having recombined viral particles infecting Cre-negative cells and express the transgene in an off-target population. As we observed viral leakiness, we can not role out if the reduction in DAT^- cells are also due to an interconnection with DAT^+ cells.

Nevertheless, the type of quantification done was a tricky aspect since if we are expecting the cells to die and if they if fact stop to express tdTomato (DAT^+), it is supposed that the cells also stop to express DTR. However, we saw DTR expression, even in a small quantity. From this, we can speculate that the DTR can have a specific time window for their expression (Abdallah et al., 2018). To understand the exact timescale in which the diphtheria toxin receptors act, a previous control study should have been carried out in which animals with DTR are injected without injecting the toxin and another group where there is toxin injection. Subsequently, they should be perfused at different timepoints, i.e., 2, 3 and 4 weeks, to understand the best experimental timeline to optimize the effect of receptors expression DAT^+ cells.

An important caveat, however, is that there are examples in which neuronal activation occurs without induction of c-Fos, so the absence of neuronal c-Fos expression cannot be interpreted as a lack of influence on neuronal activity (Bepari et al., 2012; Kovács, 2008). Despite the limitation, the visualization of c-Fos as proxy for neuronal activation continue to be an extremely powerful tool. As PMv-DAT$^+$ have a low level of spontaneous activity in females (fiber photometry shows that calcium signal is very low when there is no male stimulus; *unpublished data*), in the presence of a male stimulus, the cells activate abruptly, which makes the c-Fos a good read out.

4.3. Sexual Behavior Effects in PMv-DAT$^+$ Ablated Cells

For sexual behavior experiments, we did not report any difference extension of the two lesions in different hemispheres (fig. 19), supporting the idea that bilaterally injections were concordant in the two hemispheres across animals. Regarding the analyze of the structure of the behaviors and the latencies to mount/ejaculate, the difference within groups was not statistically significant (fig. 22). Only within the consummatory phase, from the first mount attempt until first successful mount, control animals present a higher rate of mount attempts compared with the experimental ones (fig. 22). We saw that, these failed mount attempts are mainly due male inability, which are not related with the female performance (fig. 22). Furthermore, a missing animal group that we should have used in the behavioral experiment was the virus control, by giving viral injection of DTR and intraperitoneal injection of saline.

Regarding the correlation between cell density and the different types of behaviors, if we compare the DAT$^+$ cell density related to the number of investigations, we saw a high significance value ($R^2 = 0.9425$) in the correlation, which suggests that when there are more DAT$^+$ cells, we observe fewer investigations (fig. 23). We proposed an explanation in which the female needs a larger number of cells to reach a threshold and make the behavioral decision of approaching the male (Bitzer et al., 2014). In this case, as DAT$^+$ cells respond to male cues, if there are more investigations when the animal presents fewer cells, it could mean that the female needs to approach the male more often to integrate the sensory input of the male cues and perform a behavioral outcome.

Previous studies have demonstrated that bilateral excitotoxic neuronal lesions of the PMv, using N-methyl-D-aspartate (NMDA), in female rats significantly decreased female sexual behavior (J. Donato et al., 2013). Using a similar paradigm as described in this study, Donato *et al* evaluated the sexual proceptivity (occurrence of stereotypic behaviors including darting, hopping

and ear wiggling) and receptivity (occurrence of lordosis behavior following 10 attempts to mount) of each female (lesioned and non-lesioned) in the presence of a sexually experienced male (J. Donato et al., 2013). They observed that lesions of the PMv caused no major changes in proceptive behaviors. On the other hand, 50% of PMv-lesioned rats were non-receptive (no lordosis behavior in the first 10 attempts to mount), whereas only 18% of control rats failed to show lordosis (J. Donato et al., 2013). As reported in our results, they also did not observe a significant difference in the latency to mount between the PMv lesioned and PMv non-lesioned groups (J. Donato et al., 2013). By correlating this study in rats with ours, the results reveal similarities, since there are no differences in behaviors within sexual session between ablated and non-ablated females. Although they reported a decrease in lordosis posture in females with injured PMv, their injury destroys the entire PMv neurons, while our injury is specific to the DAT population. Since PMv-DAT neurons only constitute approximately 25% of the total neurons of the PMv (Soden et al., 2016), and numerous c-Fos positive PMv neurons are not DAT positive, PMv-DAT neurons likely are not the only population involved in female sexual behavior. Thus, lesioning of the entire PMv may disrupt multiple cell types that when collectively destroyed lead to different behavioral effects. As a future experiment, it will be interesting to also analyze the occurrence of lordosis behavior in the PMv-DAT ablated females and compared the results with the control group.

Regarding female behaviors, Motta *et al*, using the same lesion method as Donato *et al*, showed that PMv lesioned female rats exhibit significantly reduced maternal aggression, without affecting maternal care (Motta et al., 2013). As a context, postpartum rats have the function of protecting their offspring from harm and, consequently, are highly aggressive toward other males that enter the vicinity of their pups. The lesions did, however, produce a clear reduction in maternal aggression both in the number and the total duration of the attacks towards male intruders (Motta et al., 2013). Moreover, they saw a reduction in PMv projections to other hypothalamic sites, such as BNST, MPN and VMHvl, which reduced c-Fos expression after PMv lesions. A future interesting question to address is if the DAT population is responsible for this behavior or if there are other subpopulations in PMv that are responsible to regulate maternal aggression behaviors.

Conclusion and Future Perspectives

5. Conclusion and Future Perspectives

The neural circuits underlying social behaviors, such as mating, are responsible for animals basic needs and continuity of the species. Understanding the structure of the circuits will then help identify how specific neurons in different brain regions can further modulate the behavior function (Serrano-saiz & Isogai, 2021). Until now the knowledge of the how PMv integrates these circuits and regulates female behavior is undetermined. To investigate the anatomical output logic of the PMv nucleus in female mice, we have carried out systematic mapping of PMv-DAT neurons using a viral tracing system: anterograde terminals labelling using synaptophysin-GFP virus. This tracing technique has afforded a brain-wide overview of the PMv-DAT neuronal projections, revealing its hypothalamic projections to other parts of the brain. Inside this topic of understanding the PMv structure in female mice, there are other issues that should be clarified. The first is if there are different subpopulations of DAT cells that project to different targets - collaterals. There are two possible configurations: one-to-many and one-to-one model (Betley et al., 2013). For a one-to-many arrangement, groups of neurons project collateralized axons to subsets of output regions. Alternatively, in a one-to-one model, each projection field is a separate and do not send collateral projections to other brain areas (Betley et al., 2013). This can be accessed by injecting a retrograde AAV synaptophysin-GFP virus in the different known outputs of the PMv-DAT population, which will label DAT cell bodies that project to that nucleus. Afterwards, we can access if there are only terminals in the region where the retrograde AAVs was injected (one-to-one option) or if we also find labelled terminals in other output nuclei (one-to-many option). Furthermore, to better understand the PMv structure, specifically in DAT neurons, a further step will be to characterize the input regions of this population. For this, we can map its monosynaptic inputs, using a rabies-based approach. Briefly, a rabies virus (EnvA-SADΔG-GFP) is injected in the PMv, in combination with two helper viruses that express an avian receptor TVA (AAV-FLEX-TVA-mCherry) and an envelope glycoprotein RG (AAV-FLEX-RG). The first is responsible for the specificity since the rabies will only be present in cells that express avian tumor virus receptor A (TVA). For the second helper virus, the glycoprotein gene, that mediate transsynaptic viral transmission, have been deleted and replaced by fluorescent proteins. As a consequence, the virus cannot spread beyond the initially infected cells (Wickersham et al., 2007; Xu et al., 2020), preventing further viral proliferation (Liu et al., 2020), and as a result only monosynaptic inputs are mapped (Xiangmin Xu et al., 2020).

A promising field nowadays is the study of the functional neurobiology of sexual behavior. In broad terms, the brain integrates sensory stimuli with the internal state (Georgiadis et al., 2012) that will drive a particular behavior type: male or female directed. To unravel some of the mechanisms in this field, our second objective was to unravel the role of DAT^{+} neurons in controlling male-directed behaviors, particularly the sexual behavior, by performing a genetic ablation specifically on this subpopulation. Overall, sexual behavior seems not be significantly

affected by the PMv-DAT$^+$ ablation, however our number of animals was very reduced to allow a conclusive extrapolation. In the future, we must increase the experimental n to achieve more significance in the results and be able to draw more significant conclusions.

To characterize the role of PMv-DAT$^+$ cells in different male-directed behaviors, in the future, it would be interesting to access the effects in maternal aggression. For this, the procedure can be similar to the one previous described: injection of females with DTR when they are already pregnant and injection of the DTx after the pups are born. For the behavioral test itself, a male intruder (other than the father of the pups) must be placed inside the same cage with the mother and pups. The objective will be to record the differences between the behavior of females with PMv-DAT$^+$ ablated neurons with the control females without ablation (either with DTR expression or DTx injection only). It would also be exciting comparing the pattern of c-Fos expression in unlesioned and PMv-DAT$^+$ lesioned mother exposed to a male intruder, in order to, outline a network likely to underlie maternal aggression and study how the PMv modulates activation of this network (Motta et al., 2013).

Ultimately, this project identified the PMv-DAT output targets and have tested the function of these neurons in female sexual behavior.

Bibliography

Abdallah, K., Nadeau, F., Bergeron, F., Blouin, S., Blais, V., Bradbury, K. M., Lavoie, C. L., Parent, J. L., & Gendron, L. (2018). Adeno-associated virus 2/9 delivery of Cre recombinase in mouse primary afferents. *Scientific Reports*, *8*(1), 2–9. https://doi.org/10.1038/s41598-018-25626-y;

Al, D. G. L. et. (2003). Lesion Tecnhiques for Behavioral Experiments. *Handbook of Classical Conditioning*;

Atasoy, D., Aponte, Y., Su, H. H., & Sternson, S. M. (2008). A FLEX switch targets channelrhodopsin-2 to multiple cell types for imaging and long-range circuit mapping. *Journal of Neuroscience*, *28*(28), 7025–7030. https://doi.org/10.1523/JNEUROSCI.1954-08.2008;

Backman, C. M., Malik, N., Zhang, Y., Shan, L., Grinberg, A., Hoffer, B. J., Westphal, H., & Tomac, A. C. (2006). Characterization of a Mouse Strain Expressing Cre Recombinase From the 30 Untranslated Region of the Dopamine Transporter Locus. *Genesis*, *44*, 383–390. https://doi.org/10.1002/dvg;

Bahrami, S., & Drabløs, F. (2016). Gene regulation in the immediate-early response process. *Advances in Biological Regulation*, *62*(7491), 37–49. https://doi.org/10.1016/j.jbior.2016.05.001;

Baum, M. J., & Cherry, J. A. (2015). Processing by the main olfactory system of chemosignals that facilitate mammalian reproduction. *Hormones and Behavior*, *68*, 53–64. https://doi.org/10.1016/j.yhbeh.2014.06.003;

Beier, K. T., Steinberg, E. E., Deloach, K. E., Xie, S., Miyamichi, K., Schwarz, L., Gao, X. J., Kremer, E. J., Malenka, R. C., & Luo, L. (2015). Circuit Architecture of VTA Dopamine Neurons Revealed by Systematic Input-Output Mapping. *Cell*, *162*(3), 622–634. https://doi.org/10.1016/j.cell.2015.07.015;

Belluscio, L., Koentges, G., Axel, R., & Dulac, C. (1999). A map of pheromone receptor activation in the mammalian brain. *Cell*, *97*(2), 209–220. https://doi.org/10.1016/S0092-8674(00)80731-X;

Bepari, A. K., Sano, H., Tamamaki, N., Nambu, A., Tanaka, K. F., & Takebayashi, H. (2012). Identification of Optogenetically Activated Striatal Medium Spiny Neurons by Npas4 Expression. *PLoS ONE*, *7*(12), 1–8. https://doi.org/10.1371/journal.pone.0052783;

Berglund, K., Tung, J. K., Higashikubo, B., Gross, R. E., Moore, C. I., & Hochgeschwender, U. (2016). Combined optogenetic and chemogenetic control of neurons. *Methods in Molecular Biology*, *1408*, 207–225. https://doi.org/10.1007/978-1-4939-3512-3_14;

Betley, J. N., Cao, Z. F. H., Ritola, K. D., & Sternson, S. M. (2013). Parallel, redundant circuit organization for homeostatic control of feeding behavior. *Cell*, *155*(6), 1337–1350. https://doi.org/10.1016/j.cell.2013.11.002;

Bitzer, S., Park, H., Blankenburg, F., & Kiebel, S. J. (2014). Perceptual decision making: Drift-diffusion model is equivalent to a Bayesian model. *Frontiers in Human Neuroscience*, *8*(1 FEB), 1–17. https://doi.org/10.3389/fnhum.2014.00102;

Blaustein, J. D. (2008). Neuroendocrine regulation of feminine sexual behavior: Lessons from rodent models and thoughts about humans. *Annual Review of Psychology*, *59*, 93–118. https://doi.org/10.1146/annurev.psych.59.103006.093556;

Blüher, S., & Mantzoros, C. S. (2004). The role of leptin in regulating neuroendocrine function in humans. *Journal of Nutrition*, *134*(9). https://doi.org/10.1093/jn/134.9.2469s;

Borelli, K. G., Blanchard, D. C., Javier, L. K., Defensor, E. B., Brandão, M. L., & Blanchard, R. J. (2009). Neural correlates of scent marking behavior in C57BL/6J mice: detection and recognition of a social stimulus. *Neuroscience*, *162*(4), 914–923. https://doi.org/10.1016/j.neuroscience.2009.05.047;

Brockschnieder, D., Lappe-Siefke, C., Goebbels, S., Boesl, M. R., Nave, K.-A., & Riethmacher, D. (2004). Cell Depletion Due to Diphtheria Toxin Fragment A after Cre-Mediated Recombination. *Molecular and Cellular Biology*, *24*(17), 7636–7642. https://doi.org/10.1128/mcb.24.17.7636-7642.2004;

Buch, T., Heppner, F. L., Tertilt, C., Heinen, T. J. A. J., Kremer, M., Wunderlich, F. T., Jung, S., & Waisman, A. (2005). A Cre-inducible diphtheria toxin receptor mediates cell lineage ablation after toxin administration. *Nature Methods*, *2*(6), 419–426. https://doi.org/10.1038/nmeth762;

Burns-Cusato, M., Scordalakes, E. M., & Rissman, E. F. (2004). Of mice and missing data: What we know (and need to learn) about male sexual behavior. *Physiology and Behavior*, *83*(2), 217–232. https://doi.org/10.1016/j.physbeh.2004.08.015;

Butcher, R. L., Collins, W. E., & Fugo, N. W. (1974). Plasma concentration of LH, FSH, prolactin, progesterone and estradiol-17beta throughout the 4-day estrous cycle of the rat. *Endocrinology*, *94*(6), 1704–1708. https://doi.org/10.1210/endo-94-6-1704;

Byers, S. L., Wiles, M. V., Dunn, S. L., & Taft, R. A. (2012). Mouse estrous cycle identification tool and images. *PLoS ONE*, *7*(4), 2–6. https://doi.org/10.1371/journal.pone.0035538

Caligioni, C. S. (2009). Assessing reproductive status/stages in mice. *Current Protocols in Neuroscience*, *SUPPL. 48*, 1–8. https://doi.org/10.1002/0471142301.nsa04is48;

Canteras, N. S., Simerly, R. B., & Swanson, L. W. (1992a). Connections of the posterior nucleus of the amygdala. *Journal of Comparative Neurology*, *324*(2), 143–179. https://doi.org/10.1002/cne.903240203;

Canteras, N. S., Simerly, R. B., & Swanson, L. W. (1992b). Projections of the ventral premammillary nucleus. *Journal of Comparative Neurology*, *324*(2), 195–212. https://doi.org/10.1002/cne.903240205;

Canteras, N. S., Simerly, R. B., & Swanson, L. W. (1994). Organization of projections from the ventromedial nucleus of the hypothalamus: A Phaseolus vulgaris-Leucoagglutinin study in the rat. *Journal of Comparative Neurology*, *348*(1), 41–79. https://doi.org/10.1002/cne.903480103;

Canteras, N. S., Simerly, R. B., & Swanson, L. W. (1995). Organization of projections from the medial nucleus of the amygdala: A PHAL study in the rat. *Journal of Comparative Neurology*, *360*(2), 213–245. https://doi.org/10.1002/cne.903600203;

Cavalcante, Judney C., Bittencourt, J. C., & Elias, C. F. (2006). Female odors stimulate CART neurons in the ventral premammillary nucleus of male rats. *Physiology and Behavior*, *88*(1–2), 160–166. https://doi.org/10.1016/j.physbeh.2006.03.032;

Cavalcante, Judney Cley, Bittencourt, J. C., & Elias, C. F. (2014). Distribution of the neuronal inputs to the ventral premammillary nucleus of male and female rats. *Brain Research*, *1582*, 77–90. https://doi.org/10.1016/j.brainres.2014.07.034;

Chan, J. L., & Mantzoros, C. S. (2001). Leptin and the hypothalamic-pituitary regulation of the gonadotropin-gonadal axis. *Pituitary*, *4*(1–2), 87–92. https://doi.org/10.1023/A:1012947113197;

Chen, A., Yan, J., Zhang, W., Wang, L., Yu, Z., Ding, X., Wang, D., Zhang, M., Zhang, Y., Song, N., Jiao, Z., Xu, C., Zhu, S., & Xu, X. (2020). Specific Hypothalamic Neurons Required for Sensing Conspecific Male Cues Relevant to Inter-male Aggression. *Neuron*, 1–12. https://doi.org/10.1016/j.neuron.2020.08.025;

Chen, P., & Hong, W. (2018). Neural Circuit Mechanisms of Social Behavior. *Neuron*, *98*(1), 16–30. https://doi.org/10.1016/j.neuron.2018.02.026;

Chung, L. (2015). A Brief Introduction to the Transduction of Neural Activity into Fos Signal. *Development & Reproduction*, *19*(2), 61–67. https://doi.org/10.12717/dr.2015.19.2.061;

Cohen, R. S., & Pfaff, D. W. (1992). Ventromedial hypothalamic neurons in the mediation of long-lasting effects of estrogen on lordosis behavior. *Progress in Neurobiology*, *38*(5), 423–453. https://doi.org/10.1016/0301-0082(92)90045-G;

Coolen, L. M., Peters, H. J. P. W., & Veening, J. G. (1996). Fos immunoreactivity in the rat brain following consummatory elements of sexual behavior: A sex comparison. *Brain Research*, *738*(1), 67–82. https://doi.org/10.1016/0006-8993(96)00763-9

Creagh, E. M., & Martin, S. J. (2001). Caspases: Cellular demolition experts. *Biochemical Society Transactions*, *29*(6), 696–702. https://doi.org/10.1042/bst0290696;

D'Amelio, M., Cavallucci, V., & Cecconi, F. (2010). Neuronal caspase-3 signaling: Not only cell death. *Cell Death and Differentiation*, *17*(7), 1104–1114. https://doi.org/10.1038/cdd.2009.180;

Dias, I. C., Gutierrez-Castellanos, N., Ferreira, L., & Lima, S. Q. (2021). The structural and electrophysiological properties of progesterone receptor expressing neurons vary along the anterior-posterior axis of the ventromedial hypothalamus and undergo local changes across the reproductive cycle. *BioRxiv*, 2–5;

Donato, J., Lee, C., Ratra, D. V., Franci, C. R., Canteras, N. S., & Elias, C. F. (2013). Lesions of the ventral premammillary nucleus disrupt the dynamic changes in Kiss1 and GnRH expression characteristic of the proestrus-estrus transition. *Neuroscience*, *241*, 67–79. https://doi.org/10.1016/j.neuroscience.2013.03.013;

Donato, Jose, Cavalcante, J. C., Silva, R. J., Teixeira, A. S., Bittencourt, J. C., & Elias, C. F.

(2010). Male and female odors induce Fos expression in chemically defined neuronal population. *Physiology and Behavior*, *99*(1), 67–77. https://doi.org/10.1016/j.physbeh.2009.10.012;

Donato, Jose, Cravo, R. M., Frazão, R., Gautron, L., Scott, M. M., Lachey, J., Castro, I. A., Margatho, L. O., Lee, S., Lee, C., Richardson, J. A., Friedman, J., Chua, S., Coppari, R., Zigman, J. M., Elmquist, J. K., & Elias, C. F. (2011). Leptin's effect on puberty in mice is relayed by the ventral premammillary nucleus and does not require signaling in Kiss1 neurons. *Journal of Clinical Investigation*, *121*(1), 355–368. https://doi.org/10.1172/JCI45106;

Donato, Jose, & Elias, C. F. (2011). The ventral premammillary nucleus links metabolic cues and reproduction. *Frontiers in Endocrinology*, *2*(OCT), 1–10. https://doi.org/10.3389/fendo.2011.00057;

Dulac, C., & Torello, A. T. (2003). Molecular detection of pheromone signals in mammals: From genes to behaviour. *Nature Reviews Neuroscience*, *4*(7), 551–562. https://doi.org/10.1038/nrn1140;

Duyne, G. D. Van. (2001). A structural view of Cre-loxP site specific recombination. *Annual Review of Biophysical and Biomolecular Structure*, *1*(58), 87–104;

Emin Oztas. (2003). Neuronal tracing. *Neuroanatomy*, *2*, 2–5;

Erskine, M. S. (1993). Mating-induced increases in FOS protein in preoptic area and medial amygdala of cycling female rats. *Brain Research Bulletin*, *32*(5), 447–451. https://doi.org/10.1016/0361-9230(93)90289-N;

Eugene Millhouse, O. (1973). The organization of the ventromedial hypothalamic nucleus. *Brain Research*, *55*(1), 71–87. https://doi.org/10.1016/0006-8993(73)90489-7;

Falkner, A. L., Dollar, P., Perona, P., Anderson, D. J., & Lin, D. (2014). Decoding ventromedial hypothalamic neural activity during male mouse aggression. *Journal of Neuroscience*, *34*(17), 5971–5984. https://doi.org/10.1523/JNEUROSCI.5109-13.2014;

Falkner, A. L., Grosenick, L., Davidson, T. J., Deisseroth, K., & Lin, D. (2016). Hypothalamic control of male aggression-seeking behavior. *Nature Neuroscience*, *19*(4), 596–604. https://doi.org/10.1038/nn.4264;

Falkner, A. L., Wei, D., Song, A., Watsek, L. W., Chen, I., Chen, P., Feng, J. E., & Lin, D. (2020). Hierarchical Representations of Aggression in a Hypothalamic-Midbrain Circuit. *Neuron*, *106*(4), 637-648.e6. https://doi.org/10.1016/j.neuron.2020.02.014;

Fischer, K. B., Collins, H. K., & Callaway, E. M. (2019). Sources of off-target expression from recombinasedependent AAV vectors and mitigation with cross-over insensitive ATG-out vectors. *Proceedings of the National Academy of Sciences of the United States of America*, *116*(52), 27001–27010. https://doi.org/10.1073/pnas.1915974116;

Flanagan-Cato, L. M. (2011). Sex differences in the neural circuit that mediates female sexual receptivity. *Frontiers in Neuroendocrinology*, *32*(2), 124–136. https://doi.org/10.1016/j.yfrne.2011.02.008;

Fowler, T., Sen, R., & Roy, A. L. (2011). Regulation of primary response genes. *Molecular Cell*, *44*(3), 348–360. https://doi.org/10.1016/j.molcel.2011.09.014;

Georgiadis, J. R., Kringelbach, M. L., & Pfaus, J. G. (2012). Sex for fun: A synthesis of human and animal neurobiology. *Nature Reviews Urology*, *9*(9), 486–498. https://doi.org/10.1038/nrurol.2012.151;

Glenn, M. J., Lehmann, H., Mumby, D. G., & Woodside, B. (2005). Differential Fos expression following aspiration, electrolytic, or excitotoxic lesions of the perirhinal cortex in rats. *Behavioral Neuroscience*, *119*(3), 806–813. https://doi.org/10.1037/0735-7044.119.3.806;

Golden, S. A., Heshmati, M., Flanigan, M., Christoffel, D. J., Guise, K., Pfau, M. L., Aleyasin, H., Menard, C., Zhang, H., Hodes, G. E., Bregman, D., Khibnik, L., Tai, J., Rebusi, N., Krawitz, B., Chaudhury, D., Walsh, J. J., Han, M. H., Shapiro, M. L., & Russo, S. J. (2016). Basal forebrain projections to the lateral habenula modulate aggression reward. *Nature*, *534*(7609), 688–692. https://doi.org/10.1038/nature18601;

Gray, D. C., Mahrus, S., & Wells, J. A. (2010). Activation of specific apoptotic caspases with an engineered small-molecule-activated protease. *Cell*, *142*(4), 637–646. https://doi.org/10.1016/j.cell.2010.07.014;

Gu, G., Cornea, A., & Simerly, R. B. (2003). Sexual differentiation of projections from the principal nucleus of the bed nuclei of the stria terminalis. *Journal of Comparative Neurology*, *460*(4), 542–562. https://doi.org/10.1002/cne.10677;

Gusel'nikova, V. V., & Korzhevskiy, D. E. (2015). NeuN as a neuronal nuclear antigen and neuron differentiation marker. *Acta Naturae*, *7*(2), 42–47. https://doi.org/10.32607/20758251-2015-7-2-42-47;

Halpern, M., & Martínez-Marcos, A. (2003). Structure and function of the vomeronasal system: An update. *Progress in Neurobiology*, *70*(3), 245–318. https://doi.org/10.1016/S0301-0082(03)00103-5;

Harvey, A. L., & Karlsson, E. (1982). Protease Inhibitor Homologues From Mamba Venoms: Facilitation of Acetylcholine Release and Interactions With Prejunctional Blocking Toxins. *British Journal of Pharmacology*, *77*(1), 153–161. https://doi.org/10.1111/j.1476-5381.1982.tb09281.x;

Harvey, A., & Robertson, B. (2012). Dendrotoxins: Structure-Activity Relationships and Effects on Potassium Ion Channels. *Current Medicinal Chemistry*, *11*(23), 3065–3072. https://doi.org/10.2174/0929867043363820;

Hashikawa, K., Hashikawa, Y., Falkner, A., & Lin, D. (2016). ScienceDirect The neural circuits of mating and fighting in male mice. *Current Opinion in Neurobiology*, *38*, 27–37. https://doi.org/10.1016/j.conb.2016.01.006;

Hashikawa, K., Hashikawa, Y., Lischinsky, J., & Lin, D. (2018). The Neural Mechanisms of Sexually Dimorphic Aggressive Behaviors. *Trends in Genetics*, 1–22. https://doi.org/10.1016/j.tig.2018.07.001;

Hashikawa, K., Hashikawa, Y., Tremblay, R., Zhang, J., Feng, J. E., Sabol, A., Piper, W. T., Lee, H., Rudy, B., & Lin, D. (2017). *Esr1 + cells in the ventromedial hypothalamus control female aggression*. *20*(11). https://doi.org/10.1038/nn.4644;

Hashikawa, Y., Hashikawa, K., Falkner, A. L., & Lin, D. (2017). Ventromedial Hypothalamus and the Generation of Aggression. *Frontiers in Systems Neuroscience*, *11*(December), 1–13. https://doi.org/10.3389/fnsys.2017.00094;

Hudson, A. E. (2018). Genetic Reporters of Neuronal Activity: c-Fos and G-CaMP6. In *Methods in Enzymology* (1st ed., Vol. 603). Elsevier Inc. https://doi.org/10.1016/bs.mie.2018.01.023;

Huijgens, P. T., Heijkoop, R., & Snoeren, E. M. S. (2021). *Silencing and stimulating the medial amygdala impairs ejaculation but not sexual incentive motivation in male rats*;

Hull, E. M., & Dominguez, J. M. (2007). Sexual behavior in male rodents. *Hormones and Behavior*, *52*(1), 45–55. https://doi.org/10.1016/j.yhbeh.2007.03.030;

Hulla, E. M., & Dominguez, J. M. (2007). *Sexual behavior in male rodents*;

Hyman, B. T., & Yuan, J. (2012). Apoptotic and non-apoptotic roles of caspases in neuronal physiology and pathophysiology. *Nature Reviews Neuroscience*, *13*(6), 395–406. https://doi.org/10.1038/nrn3228;

Inoue, S., Yang, R., Tantry, A., Davis, C. ha, Yang, T., Knoedler, J. R., Wei, Y., Adams, E. L., Thombare, S., Golf, S. R., Neve, R. L., Tessier-Lavigne, M., Ding, J. B., & Shah, N. M. (2019). Periodic Remodeling in a Neural Circuit Governs Timing of Female Sexual Behavior. *Cell*, *179*(6), 1393-1408.e16. https://doi.org/10.1016/j.cell.2019.10.025;

Ivanova, A., Signore, M., Caro, N., Greene, N. D. E., Copp, A. J., & Martinez-Barbera, J. P. (2005). In vivo genetic ablation by Cre-mediated expression of diphtheria toxin fragment A. *Genesis*, *43*(3), 129–135. https://doi.org/10.1002/gene.20162;

Jänig, S., Weiß, B. M., & Widdig, A. (2018). Comparing the sniffing behavior of great apes. *American Journal of Primatology*, *80*(6), 1–7. https://doi.org/10.1002/ajp.22872;

Jennings, K. J., & de Lecea, L. (2020). Neural and hormonal control of sexual behavior. *Endocrinology (United States)*, *161*(10), 1–13. https://doi.org/10.1210/endocr/bqaa150;

Johansen, J. A., Clemens, L. G., & Nunez, A. A. (2008). Characterization of copulatory behavior in female mice: Evidence for paced mating. *Physiology and Behavior*, *95*(3), 425–429. https://doi.org/10.1016/j.physbeh.2008.07.004;

Karigo, T., Kennedy, A., Yang, B., Liu, M., Tai, D., Wahle, I. A., & Anderson, D. J. (2020). Distinct hypothalamic control of same- and opposite-sex mounting behaviour in mice. *Nature, December 2019*. https://doi.org/10.1038/s41586-020-2995-0;

Kerr J. F. R., Wyllie A. H., C. a. R. (1972). Apoptosis : a Basic Biological Phenomenon With Wide-. *Br. J. Cancer*, *26*, 239–257;

Kevetter, G. A., & Winans, S. S. (1981). Connections of the corticomedial amygdala in the golden hamster. II. Efferents of the "olfactory amygdala." *Journal of Comparative Neurology*,

197(1), 99–111. https://doi.org/10.1002/cne.901970108;

Kim, D. W., Yao, Z., Graybuck, L. T., Kim, T. K., Nguyen, T. N., Smith, K. A., Fong, O., Yi, L., Koulena, N., Pierson, N., Shah, S., Lo, L., Pool, A. H., Oka, Y., Pachter, L., Cai, L., Tasic, B., Zeng, H., & Anderson, D. J. (2019). Multimodal Analysis of Cell Types in a Hypothalamic Node Controlling Social Behavior. *Cell*, *179*(3), 713-728.e17. https://doi.org/10.1016/j.cell.2019.09.020;

Kohl, J., Babayan, B. M., Rubinstein, N. D., Autry, A. E., Marin-Rodriguez, B., Kapoor, V., Miyamishi, K., Zweifel, L. S., Luo, L., Uchida, N., & Dulac, C. (2018). Functional circuit architecture underlying parental behaviour. *Nature*, *556*(7701), 326–331. https://doi.org/10.1038/s41586-018-0027-0;

Kollack-Walker, S., & Newman, S. W. (1995). Mating and agonistic behavior produce different patterns of Fos immunolabeling in the male Syrian hamster brain. *Neuroscience*, *66*(3), 721–736. https://doi.org/10.1016/0306-4522(94)00563-K;

Kovács, K. J. (2008). Measurement of immediate-early gene activation- c-fos and beyond. *Journal of Neuroendocrinology*, *20*(6), 665–672. https://doi.org/10.1111/j.1365-2826.2008.01734.x;

Kudwa, A. E., Dominguez-Salazar, E., Cabrera, D. M., Sibley, D. R., & Rissman, E. F. (2005). Dopamine D5 receptor modulates male and female sexual behavior in mice. *Psychopharmacology*, *180*(2), 206–214. https://doi.org/10.1007/s00213-005-2150-5;

Kurnikova, A., Moore, J. D., Liao, S. M., Deschênes, M., & Kleinfeld, D. (2017). Coordination of Orofacial Motor Actions into Exploratory Behavior by Rat. In *Current Biology* (Vol. 27, Issue 5, pp. 688–696). https://doi.org/10.1016/j.cub.2017.01.013;

Kwon, S. E., & Chapman, E. R. (2011). Synaptophysin Regulates the Kinetics of Synaptic Vesicle Endocytosis in Central Neurons. In *Neuron* (Vol. 70, Issue 5, pp. 847–854). https://doi.org/10.1016/j.neuron.2011.04.001;

Lammel, S., Steinberg, E. E., Földy, C., Wall, N. R., Beier, K., Luo, L., & Malenka, R. C. (2015). Diversity of transgenic mouse models for selective targeting of midbrain dopamine neurons. *Neuron*, *85*(2), 429–438. https://doi.org/10.1016/j.neuron.2014.12.036;

Lanahan, A., & Worley, P. (1998). Immediate-early genes and synaptic function. *Neurobiology of Learning and Memory*, *70*(1–2), 37–43. https://doi.org/10.1006/nlme.1998.3836;

Lee, H., Kim, D. W., Remedios, R., Anthony, T. E., Chang, A., Madisen, L., Zeng, H., & Anderson, D. J. (2014). Scalable control of mounting and attack by Esr1+ neurons in the ventromedial hypothalamus. *Nature*, *509*(7502), 627–632. https://doi.org/10.1038/nature13169;

Levine, J. E., Bauer-Dantoin, A. C., Besecke, L. M., Conaghan, L. A., Legan, S. J., Meredith, J. M., Strobl, F. J., Urban, J. H., Vogelsong, K. M., & Wolfe, A. M. (1992). Neuroendocrine regulation of the luteinizing hormone-releasing hormone pulse generator in the rat. *Recent Progress in Hormone Research*, *47*(1), 97–151. https://doi.org/10.1016/b978-0-12-571147-0.50008-1;

Li, Y., & Dulac, C. (2018). Neural coding of sex-specific social information in the mouse brain. *Current Opinion in Neurobiology*, *53*, 120–130. https://doi.org/10.1016/j.conb.2018.07.005;

Liberles, S. D. (2014). Mammalian pheromones. *Annual Review of Physiology*, *76*, 151–175. https://doi.org/10.1146/annurev-physiol-021113-170334;

Lin, D., Boyle, M. P., Dollar, P., Lee, H., Lein, E. S., Perona, P., & Anderson, D. J. (2011). Functional identification of an aggression locus in the mouse hypothalamus. *Nature*, *470*(7333), 221–226. https://doi.org/10.1038/nature09736;

Liu, F., Dai, S., Feng, D., Peng, X., Qin, Z., Kearns, A. C., Huang, W., Chen, Y., Ergün, S., Wang, H., Rappaport, J., Bryda, E. C., Chandrasekhar, A., Aktas, B., Hu, H., Chang, S. L., Gao, B., & Qin, X. (2019). Versatile cell ablation tools and their applications to study loss of cell functions. *Cellular and Molecular Life Sciences*, *76*(23), 4725–4743. https://doi.org/10.1007/s00018-019-03243-w;

Liu, Y., Hegarty, S., Winter, C., Wang, F., & He, Z. (2020). Viral vectors for neuronal cell type-specific visualization and manipulations. *Current Opinion in Neurobiology*, *63*, 67–76. https://doi.org/10.1016/j.conb.2020.03.011;

Lo, L., Yao, S., Kim, D. W., Cetin, A., Harris, J., Zeng, H., Anderson, D. J., & Weissbourd, B. (2019). Connectional architecture of a mouse hypothalamic circuit node controlling social behavior. *Proceedings of the National Academy of Sciences of the United States of America*, *116*(15), 7503–7512. https://doi.org/10.1073/pnas.1817503116;

Lonstein, J. S., & Gammie, S. C. (2002). Sensory, hormonal, and neural control of maternal

aggression in laboratory rodents. *Neuroscience and Biobehavioral Reviews*, *26*(8), 869–888. https://doi.org/10.1016/S0149-7634(02)00087-8;

Lopes, G., Bonacchi, N., Frazão, J., Neto, J. P., Atallah, B. V., Soares, S., Moreira, L., Matias, S., Itskov, P. M., Correia, P. A., Medina, R. E., Calcaterra, L., Dreosti, E., Paton, J. J., & Kampff, A. R. (2015). Bonsai: An event-based framework for processing and controlling data streams. *Frontiers in Neuroinformatics*, *9*(APR), 1–14. https://doi.org/10.3389/fninf.2015.00007;

Lossi, L., Castagna, C., & Merighi, A. (2018). Caspase-3 mediated cell death in the normal development of the mammalian cerebellum. *International Journal of Molecular Sciences*, *19*(12), 1–23. https://doi.org/10.3390/ijms19123999;

Maday, S., Twelvetrees, A. E., Moughamian, A. J., & Holzbaur, E. L. F. (2014). Axonal Transport: Cargo-Specific Mechanisms of Motility and Regulation. *Neuron*, *84*(2), 292–309. https://doi.org/10.1016/j.neuron.2014.10.019;

Martel, K. L., & Baum, M. J. (2009). A centrifugal pathway to the mouse accessory olfactory bulb from the medial amygdala conveys gender-specific volatile pheromonal signals. *European Journal of Neuroscience*, *29*(2), 368–376. https://doi.org/10.1111/j.1460-9568.2008.06564.x;

Martín-sánchez, A., Mclean, L., Beynon, R. J., Hurst, J. L., Ayala, G., Lanuza, E., & Martínez-garcia, F. (2014). Hormones and Behavior From sexual attraction to maternal aggression : When pheromones change their behavioural signi fi cance. *Hormones and Behavior*. https://doi.org/10.1016/j.yhbeh.2014.08.007;

McGill, T. E., & Coughlin, R. C. (1970). Ejaculatory reflex and luteal activity induction in Mus musculus. *Journal of Reproduction and Fertility*, *21*(2), 215–220. https://doi.org/10.1530/jrf.0.0210215;

McGill, Thomas E. (1961). Sexual Behavior in three inbred strains of mice. *Behaviour*, *19*, 341–350;

McLellan, M. A., Rosenthal, N. A., & Pinto, A. R. (2017). Cre-loxP-Mediated Recombination: General Principles and Experimental Considerations. *Current Protocols in Mouse Biology*, *7*(1), 1–12. https://doi.org/10.1002/cpmo.22;

Meister, B., & Elde, R. (1993). Dopamine Transporter mRNA in Neurons of the Rat Hypothalamus. *Neuroendocrinology*. https://doi.org/10.1159/000126568;

Miller, B. H., & Takahashi, J. S. (2014). Central circadian control of female reproductive function. *Frontiers in Endocrinology*, *5*(JAN), 1–9. https://doi.org/10.3389/fendo.2013.00195;

Motta, S. C., Carla, C., Clivatti, I., Harumi, M., Baldo, M. V. C., Lonstein, J. S., & Canteras, N. S. (2013). *Ventral premammillary nucleus as a critical sensory relay to the maternal aggression network*. https://doi.org/10.1073/pnas.1305581110/-/DCSupplemental.www.pnas.org/cgi/doi/10.1073/pnas.1305581110;

Motta, S. C., Guimarães, C. C., Furigo, I. C., Sukikara, M. H., Baldo, M. V. C., Lonstein, J. S., & Canteras, N. S. (2013). Ventral premammillary nucleus as a critical sensory relay to the maternal aggression network. *Proceedings of the National Academy of Sciences of the United States of America*, *110*(35), 14438–14443. https://doi.org/10.1073/pnas.1305581110;

Nectow, A. R., & Nestler, E. J. (2020). Viral tools for neuroscience. *Nature Reviews Neuroscience*. https://doi.org/10.1038/s41583-020-00382-z;

Nelson, F., Cessation, I. I., Felicio, S., Finch, E., & Lilly, E. (1984). Longitudinal Studies of Estrous of Cyclicity Vaginal Cyclicity and the in Aging Duration of Persistent Mice. *Biol Reprod*, *453*(31), 446–453;

Newman, S. (1999). The medial extended amygdala in male reproductive behavior. *Ann NY Acad Sci*, *877*, 242–257. https://doi.org/10.1111/j.1749-6632.1999.tb09271.x;

Nomoto, K., & Lima, S. Q. (2015). Enhanced male-evoked responses in the ventromedial hypothalamus of sexually receptive female mice. *Current Biology*, *25*(5), 589–594. https://doi.org/10.1016/j.cub.2014.12.048;

Palmiter, R. D., Behringer, R. R., Quaife, C. J., Maxwell, F., Maxwell, I. H., & Brinster, R. L. (1987). Cell lineage ablation in transgenic mice by cell-specific expression of a toxin gene. *Cell*, *50*(3), 435–443. https://doi.org/10.1016/0092-8674(87)90497-1;

Pappenheimer, A. M., Harper, A. A., Moynihan, M., & Brockes, J. P. (1982). Diphtheria toxin and related proteins: Effect of route of injection on toxicity and the determination of cytotoxicity for various cultured cells. *Journal of Infectious Diseases*, *145*(1), 94–102. https://doi.org/10.1093/infdis/145.1.94;

Pfaff, D. W., & Sakuma, Y. (1979a). Deficit in the lordosis reflex of female rats caused by lesions in the ventromedial nucleus of the hypothalamus. *The Journal of Physiology*, *288*(1), 203–210. https://doi.org/10.1113/jphysiol.1979.sp012691;

Pfaff, D. W., & Sakuma, Y. (1979b). Facilitation of the lordosis reflex of female rats from the ventromedial nucleus of the hypothalamus. *The Journal of Physiology*, *288*, 189–202. https://doi.org/10.1113/jphysiol.1979.sp012691;

Pfaus, J. G., Kleopoulos, S. P., Mobbs, C. V., Gibbs, R. B., & Pfaff, D. W. (1993). Sexual stimulation activates c-fos within estrogen-concentrating regions of the female rat forebrain. *Brain Research*, *624*(1–2), 253–267. https://doi.org/10.1016/0006-8993(93)90085-2;

Pfaus, James G. (1999). Neurobiology of sexual behavior. *Current Opinion in Neurobiology*, *9*(6), 751–758. https://doi.org/10.1016/S0959-4388(99)00034-3;

Pfaus, James G., Scardochio, T., Parada, M., Gerson, C., Quintana, G. R., & Coria-Avila, G. A. (2016). Do rats have orgasms? *Socioaffective Neuroscience & Psychology*, *6*(1), 31883. https://doi.org/10.3402/snp.v6.31883;

Polston, K. E., & Erskine, S. M. (1995). Patterns of Induction of the Immeadiate-Early Genes c-fos and egr-1 in the Female Rat Brain following Differential Amounts of Mating Stimulation. *Behavioral Neuroendocrinology*, *62*, 370–384;

Quadros, P. S., Schlueter, L. J., & Wagner, C. K. (2008). Distribution of progesterone receptor immunoreactivity in the midbrain and hindbrain of postnatal rats. *Developmental Neurobiology*, *68*(12), 1378–1390. https://doi.org/10.1002/dneu.20664;

Ring, J. R. (1944). Tthe estrogen-progesterone induction of sexual receptivity in the spayed female mouse. *Endocrinology*, *34*(4), 269–275. https://doi.org/10.1210/endo-34-4-269;

Rowe, D. W., & Erskine, M. S. (1993). c-Fos proto-oncogene activity induced by mating in the preoptic area, hypothalamus and amygdala in the female rat: role of afferent input via the pelvic nerve. *Brain Research*, *621*(1), 25–34. https://doi.org/10.1016/0006-8993(93)90294-W;

Ruedl, C., & Jung, S. (2018). DTR-mediated conditional cell ablation—Progress and challenges. *European Journal of Immunology*, *48*(7), 1114–1119. https://doi.org/10.1002/eji.201847527;

Saito, M., Iwawaki, T., Taya, C., Yonekawa, H., Noda, M., Inui, Y., Mekada, E., Kimata, Y., Tsuru, A., & Kohno, K. (2001). Diphtheria toxin receptor-mediated conditional and targeted cell ablation in transgenic mice. *Nature Biotechnology*, *19*(8), 746–750. https://doi.org/10.1038/90795;

Sarkar, D. K., Chiappa, S. A., Fink, G., & Sherwood, N. M. (1976). Gonadotropin-releasing hormone surge in pro-oestrous rats. *Nature*, *264*(5585), 461–463. https://doi.org/10.1038/264461a0;

Sengupta, R., Mendenhall, A., Sarkar, N., Mukherjee, C., Afshari, A., Huang, J., & Lu, B. (2017). Viral Cre-LoxP tools aid genome engineering in mammalian cells. *Journal of Biological Engineering*, *11*(1), 1–9. https://doi.org/10.1186/s13036-017-0087-y;

Serrano-saiz, E., & Isogai, Y. (2021). Single-cell molecular and developmental perspectives of sexually dimorphic circuits underlying innate social behaviors. *Current Opinion in Neurobiology*, *68*, 159–166. https://doi.org/10.1016/j.conb.2021.03.010;

Shimogawa, Y., Sakuma, Y., & Yamanouchi, K. (2015). Efferent and afferent connections of the ventromedial hypothalamic nucleus determined by neural tracer analysis: Implications for lordosis regulation in female rats. *Neuroscience Research*, *91*, 19–33. https://doi.org/10.1016/j.neures.2014.10.016;

Simerly, R. B., Swanson, L. W., Chang, C., & Muramatsu, M. (1990). Distribution of androgen and estrogen receptor mRNA-containing cells in the rat brain: An in situ hybridization study. *Journal of Comparative Neurology*, *294*(1), 76–95. https://doi.org/10.1002/cne.902940107;

Simonian, S. X., Spratt, D. P., & Herbison, A. E. (1999). Identification and characterization of estrogen receptor α-containing neurons projecting to the vicinity of the gonadotropin-releasing hormone perikarya in the rostral preoptic area of the rat. *Journal of Comparative Neurology*, *411*(2), 346–358. https://doi.org/10.1002/(SICI)1096-9861(19990823)411:2<346::AID-CNE13>3.0.CO;2-S;

Sjulson, L., Cassataro, D., Dasgupta, S., & Miesenböck, G. (2016). Cell-Specific Targeting of Genetically Encoded Tools for Neuroscience. *Annual Review of Genetics*, *50*, 571–594. https://doi.org/10.1146/annurev-genet-120215-035011;

Snoeren, E. M. S. (2018). Female Reproductive Behavior. *Curr Topics Behav Neuroscience*.

https://doi.org/10.1007/7854;

Soden, M. E., Miller, S. M., Burgeno, M., Phillips, P. E. M., Thomas, S., & Zweifel, L. S. (2016). Genetic Isolation of Hypothalamic Neurons that Report Genetic Isolation of Hypothalamic Neurons that Regulate Context-Specific Male Social Behavior. *CellReports*, *16*(2), 304–313. https://doi.org/10.1016/j.celrep.2016.05.067;

Sokolowski, K., & Corbin, J. G. (2012). Wired for behaviors: From development to function of innate limbic system circuitry. *Frontiers in Molecular Neuroscience*, *5*(APRIL), 1–15. https://doi.org/10.3389/fnmol.2012.00055;

Song, C., & Knöpfel, T. (2016). Optogenetics enlightens neuroscience drug discovery. *Nature Reviews Drug Discovery*, *15*(2), 97–109. https://doi.org/10.1038/nrd.2015.15;

Spehr, M., Spehr, J., Ukhanov, K., Kelliher, K. R., Leinders-Zufall, T., & Zufall, F. (2006). Parallel processing of social signals by the mammalian main and accessory olfactory systems. *Cellular and Molecular Life Sciences*, *63*(13), 1476–1484. https://doi.org/10.1007/s00018-006-6109-4;

Stagkourakis, S., Spigolon, G., Williams, P., Protzmann, J., Fisone, G., & Broberger, C. (2018). A neural network for intermale aggression to establish social hierarchy. *Nature Neuroscience*, *21*(6), 834–842. https://doi.org/10.1038/s41593-018-0153-x;

Swanson, L. W., & Cowan, W. M. (1979). The connections of the septal region in the rat. *Journal of Comparative Neurology*, *186*(4), 621–655. https://doi.org/10.1002/cne.901860408;

Tetel, M. J., Getzinger, M. J., & Blaustein, J. D. (1993). Fos Expression in the Rat Brain Following Vaginal-Cervical Stimulation by Mating and Manual Probing. *Journal of Neuroendocrinology*, *5*(4), 397–404. https://doi.org/10.1111/j.1365-2826.1993.tb00500.x;

Tian, L., Andrew Hires, S., & Looger, L. L. (2012). Imaging neuronal activity with genetically encoded calcium indicators. *Cold Spring Harbor Protocols*, *7*(6), 647–656. https://doi.org/10.1101/pdb.top069609;

Tian, L., Hires, S. A., Mao, T., Huber, D., Chiappe, M. E., Chalasani, S. H., Petreanu, L., Akerboom, J., McKinney, S. A., Schreiter, E. R., Bargmann, C. I., Jayaraman, V., Svoboda, K., & Looger, L. L. (2009). Imaging neural activity in worms, flies and mice with improved GCaMP calcium indicators. *Nature Methods*, *6*(12), 875–881. https://doi.org/10.1038/nmeth.1398;

Trezza, V., Campolongo, P., & Vanderschuren, L. J. M. J. (2011). Evaluating the rewarding nature of social interactions in laboratory animals. In *Developmental Cognitive Neuroscience* (Vol. 1, Issue 4, pp. 444–458). https://doi.org/10.1016/j.dcn.2011.05.007;

Valente, S., Marques, T., & Lima, S. Q. (2021). No evidence for prolactin's involvement in the post-ejaculatory refractory period. *Communications Biology*, *4*(1), 2–11. https://doi.org/10.1038/s42003-020-01570-4;

Van Berg, M. J. D., Horst, G. J. T., & Koolhaas, J. M. (1983). The nucleus premammillaris ventralis (pmv) and aggressive behavior in the rat. *Aggressive Behavior*, *9*(1), 41–47. https://doi.org/10.1002/1098-2337(1983)9:1<41::AID-AB2480090106>3.0.CO;2-9;

Veening, J. G., Coolen, L. M., De Jong, T. R., Joosten, H. W., De Boer, S. F., Koolhaas, J. M., & Olivier, B. (2005). Do similar neural systems subserve aggressive and sexual behaviour in male rats? Insights from c-Fos and pharmacological studies. *European Journal of Pharmacology*, *526*(1–3), 226–239. https://doi.org/10.1016/j.ejphar.2005.09.041;

Walmer, D. K., Wrona, M. A., Hughes, C., & Nelson, K. G. (1992). Lactoferrin Tract during the Natural Estrous Cycle: Correlation with Circulating Estradiol and Progesterone. *Endocrinology*.

Wang, H., Peca, J., Matsuzaki, M., Matsuzaki, K., Noguchi, J., Qiu, L., Wang, D., Zhang, F., Boyden, E., Deisseroth, K., Kasai, H., Hall, W. C., Feng, G., & Augustine, G. J. (2007). High-speed mapping of synaptic connectivity using photostimulation in Channelrhodopsin-2 transgenic mice. *Proceedings of the National Academy of Sciences of the United States of America*, *104*(19), 8143–8148. https://doi.org/10.1073/pnas.0700384104;

Wang, Hao. (2020). *Neural Circuits of Innate Behaviors*;

Wei, D., Talwar, V., & Lin, D. (2021). Neural circuits of social behaviors: innate yet flexible. *Neuron*, 1–21. https://doi.org/10.1016/j.neuron.2021.02.012;

Wickersham, I. R., Lyon, D. C., Barnard, R. J. O., Mori, T., Finke, S., Conzelmann, K. K., Young, J. A. T., & Callaway, E. M. (2007). Monosynaptic Restriction of Transsynaptic Tracing from Single, Genetically Targeted Neurons. *Neuron*, *53*(5), 639–647. https://doi.org/10.1016/j.neuron.2007.01.033;

Wood, R. I., & Newman, S. W. (1995). Androgen and estrogen receptors coexist within individual neurons in the brain of the Syrian hamster. *Neuroendocrinology*, *62*(5), 487–497. https://doi.org/10.1159/000127039;

Xu, Xiangmin, Holmes, T. C., Luo, M.-H., Beier, K. T., Horwitz, G. D., Zhao, F., Zeng, W., Hui, M., Semler, B. L., & Sandri-Goldin, R. M. (2020a). Viral Vectors for Neural Circuit Mapping and Recent Advances in Trans-synaptic Anterograde Tracers. *Neuron*, 1–19. https://doi.org/10.1016/j.neuron.2020.07.010;

Xu, Xiangmin, Holmes, T. C., Luo, M. H., Beier, K. T., Horwitz, G. D., Zhao, F., Zeng, W., Hui, M., Semler, B. L., & Sandri-Goldin, R. M. (2020b). Viral Vectors for Neural Circuit Mapping and Recent Advances in Trans-synaptic Anterograde Tracers. *Neuron*, *107*(6), 1029–1047. https://doi.org/10.1016/j.neuron.2020.07.010;

Xu, Xiaohong, Coats, J. K., Yang, C. F., Wang, A., Ahmed, O. M., Alvarado, M., Izumi, T., & Shah, N. M. (2005). Modular genetic control of sexually dimorphic behaviors. *Cell*, *148*(3), 596–607. https://doi.org/10.1016/j.cell.2011.12.018;

Yang, C. F., Chiang, M. C., Gray, D. C., Prabhakaran, M., Alvarado, M., Juntti, S. A., Unger, E. K., Wells, J. A., & Shah, N. M. (2013). Sexually dimorphic neurons in the ventromedial hypothalamus govern mating in both sexes and aggression in males. *Cell*, *153*(4), 896–909. https://doi.org/10.1016/j.cell.2013.04.017;

Yarmolinsky, M., & Hoess, R. (2015). The Legacy of Nat Sternberg: The Genesis of Cre-lox Technology. *Annual Review of Virology*, *2*, 25–40. https://doi.org/10.1146/annurev-virology-100114-054930;

Yokosuka, M., & Hayashi, S. (1996). Colocalization of neuronal nitric oxide synthase and androgen receptor immunoreactivity in the premammillary nucleus in rats. *Neuroscience Research*, *26*(3), 309–314. https://doi.org/10.1016/S0168-0102(96)01109-1;

Yokosuka, M., Matsuoka, M., Ohtani-Kaneko, R., Iigo, M., Hara, M., Hirata, K., & Ichikawa, M. (1999). Female-soiled bedding induced Fos immunoreactivity in the ventral part of the premammillary nucleus (PMv) of the male mouse. *Physiology and Behavior*, *68*(1–2), 257–261. https://doi.org/10.1016/S0031-9384(99)00160-2;

Yokosuka, M., Prins, G. S., & Hayashi, S. (1997). Co-localization of androgen receptor and nitric oxide synthase in the ventral premamillary nucleus of the newborn rat: An immunohistochemical study. *Developmental Brain Research*, *99*(2), 226–233. https://doi.org/10.1016/S0165-3806(96)00217-9;

Zha, X., Wang, L., Jiao, Z. L., Yang, R. R., Xu, C., & Xu, X. H. (2020). VMHvl-Projecting Vglut1+ Neurons in the Posterior Amygdala Gate Territorial Aggression. *Cell Reports*, *31*(3), 107517. https://doi.org/10.1016/j.celrep.2020.03.081;

Zhang, F., Wang, L. P., Boyden, E. S., & Deisseroth, K. (2006). Channelrhodopsin-2 and optical control of excitable cells. *Nature Methods*, *3*(10), 785–792. https://doi.org/10.1038/nmeth936;

Zhang, J., Zhang, Y., Liu, X., Xiang, J., & Zhang, C. (2016). Establishment of a HEK293T cell line able to site-specifically integrate and stably express GDNF by rAAV-2 vector. *Electronic Journal of Biotechnology*, *22*, 75–80. https://doi.org/10.1016/j.ejbt.2016.05.001;

Zhuang, X., Masson, J., Gingrich, J. A., Rayport, S., & Hen, R. (2005). Targeted gene expression in dopamine and serotonin neurons of the mouse brain. *Journal of Neuroscience Methods*, *143*(1), 27–32. https://doi.org/10.1016/j.jneumeth.2004.09.020;

Zilkha, N., Sofer, Y., Kashash, Y., & Kimchi, T. (2021). The social network: Neural control of sex differences in reproductive behaviors, motivation, and response to social isolation. *Current Opinion in Neurobiology*, *68*, 137–151. https://doi.org/10.1016/j.conb.2021.03.005.

Annexes

Supplementary Table 1. PMv-DAT$^+$ outputs distribution across animals. SQL-number correspond to the animal denomination (n=5).

PMv Outputs Distribution Across Animals (n=5)						
Brain Regions	**Output Areas**	**SQL-04235**	**SQL-04236**	**SQL-04500**	**SQL-01296**	**SQL-03711**
Cerebral Cortex	AHiPM (Amygdalohippocampal area, posteromedial part)	X	X	X	X	X
Cerebral Cortex	M1 (Primary Motor Cortex)				X	X
Cerebral Cortex	M2 (Secondary Motor Cortex)				X	X
Striatum	MePD (Medial Amygdala Nucleus, posterodorsal)	X	X	X	X	X
Striatum	MePV (Medial Amydala Nucleus, posteroventral)	X	X	X	X	X
Striatum	ICj (island of Calleja)	X	X		X	
Striatum	LSV (lateral septal nucleus, ventral part)	X	X	X	X	X
Striatum	LSI (Lateral Spetal Nucleus, intermediate part)	X				
Pallidum	BNST (Bed Nucleus of the Stria Terminalis, medial/lateral division)	X	X	X	X	X
Pallidum	VP (Ventral Pallidum)					X
Pallidum	StA (Strial Part Preoptic Area)	X				
Thalamus	Rt (Reticular Thalamic Nucleus)	X				
Hypothalamus	VMVvl (Ventromedial Hypothalamic Nucleus, ventrolateral part)	X	X	X	X	X
Hypothalamus	ME (Median Emience)	X	X	X	X	X
Hypothalamus	MPOA (Medial Preoptic Area, lateral/medial part)	X	X	X	X	X
Hypothalamus	ARC (Arcuate Nucleus, medial/dorsal/lateral posterior)	X	X	X	X	X
Hypothalamus	SHy (Septohypothalamic Nuclei)	X	X	X	X	X
Hypothalamus	AHA (Anterior Hypothalamic Area, anterior)	X	X	X		X
Hypothalamus	AHC (Anterior Hypothalamic Area, central)	X			X	X
Hypothalamus	AHP (Anterior Hypothalamic Area, posterior)	X	X			X
Hypothalamus	LA (Lateroanterior Hypothalamic Nucleus)	X	X		X	X
Hypothalamus	RMM (Retromammilary Nucleus, medial)	X	X		X	
Hypothalamus	RML (Retromammilary Nucleus, lateral)	X	X	X	X	X
Hypothalamus	mt (mammillothalamic tract)		X	X	X	X
Hypothalamus	PLH (Peduncular Hupothalamic Nuclei, lateral part)			X	X	X
Hypothalamus	PaV (Paraventricular Hypothalamic Nuclei, ventral part)	X		X		
Hypothalamus	PaAP (Paraventricular Hypothalamic, anterior parvicell)				X	
Hypothalamus	PaMP (Paraventricular Hypothalamic, medial parvicell)	X	X			
Hypothalamus	RCh (Retrochiasmatic Area)		X			
Hypothalamus	RChl (Retrochiasmatic Area, lateral part)				X	
Hypothalamus	DM (Dorsomedial Hypothalamic Nucleus)	X				X
Hypothalamus	VTM (Ventral Tuberomammilary Nucleus)	X	X			
Hypothalamus	StHy (Striohypothalamic Nuclei)			X	X	
Midbrain	VTA (Ventral Tegmental Area)		X			X
Midbrain	SNR (Substantia Nigra Reticular)		X		X	
Midbrain	LPAG (Lateral Periadeductal Grey)		X		X	X
Midbrain	VLPAG (Ventrolateral Periaqueductal Grey)				X	
Fiber Tracts	MFB (Medial Forebrain Bundle)	X	X	X	X	X
Fiber Tracts	IPACM (IPAC medial)					X
Fiber Tracts	IPACL (IPAC lateral)					X
Fiber Tracts	LO (Lateral Olfactory Tract)				X	
Fiber Tracts	SM (Nucleus Stria Medullaris)	X				
Fiber Tracts	Opt (Optic tract)	X		X		

500 nL AAV-CAG-DIO-taCaspase3-TEVp

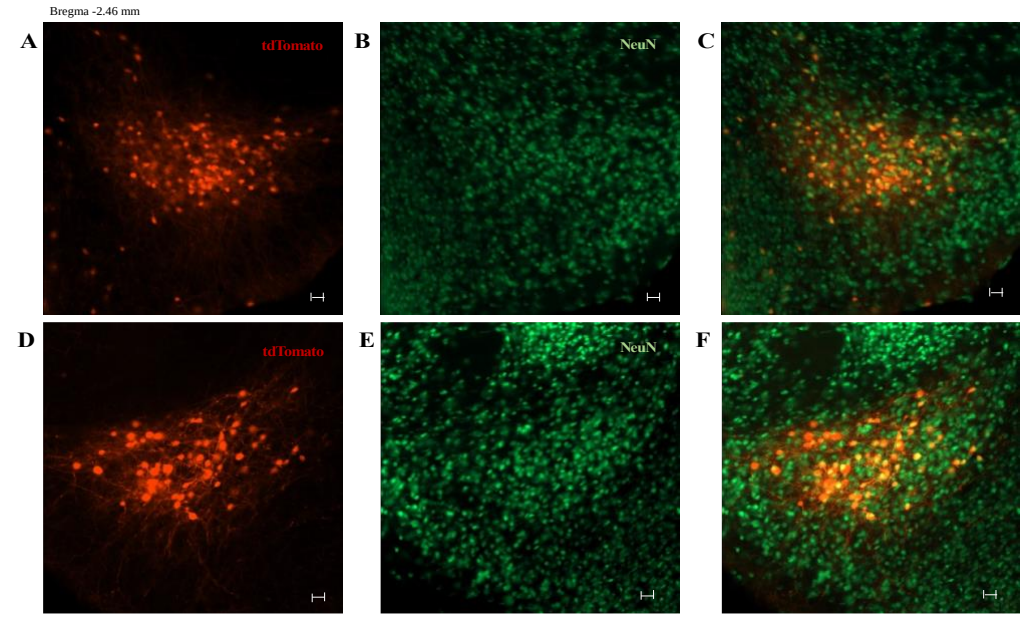

1 uL AAV-CAG-DIO-taCaspase3-TEVp

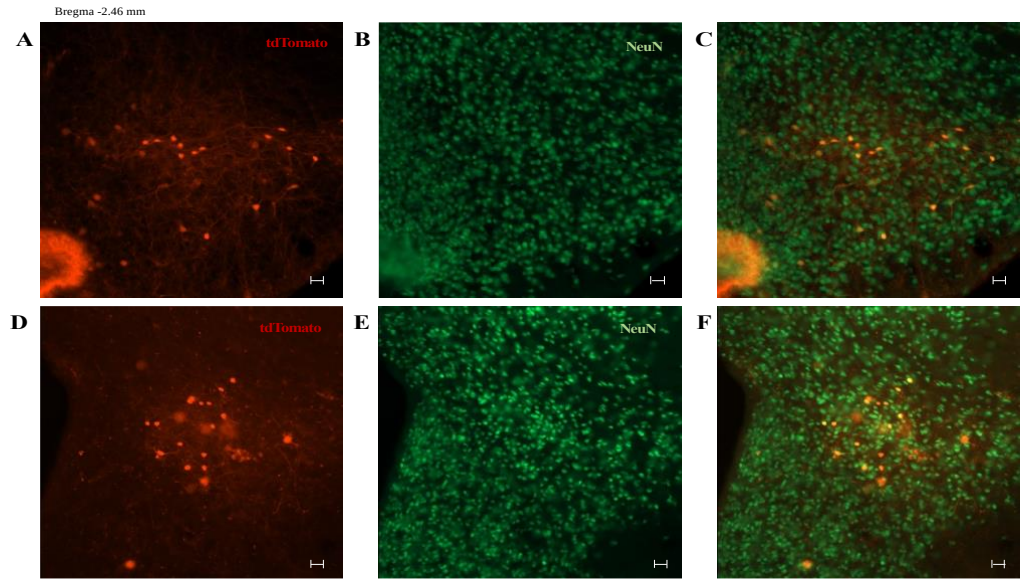

Supplementary Figure 1.

Panel 1. PMv-DAT$^+$ Cells Axonal Morphology, stained with NeuN, after 500 nL AAV-CAG-DIO-taCaspase3-TEVp bilaterally virus injection. (A) Image representative of a PMv section of a control mice female Ai9 (RCL-tdTomato) DAT-IRES-Cre flox/wt cre/wt, where tdTomato is visible in the DAT$^+$ cells. Axonal shape is regular. (B) Image representative of a PMv section of a control mice female Ai9 (RCL-tdTomato) DAT-IRES-Cre flowx/wt cre/wt stained with NeuN marker. (C) Merge of the A and B images. (D) Image representative of a PMv section of a mice female Ai9 (RCL-tdTomato) DAT-IRES-Cre flox/wt cre/wt with 500 nL AAV-CAG-DIO-taCaspase3-TEVp bilaterally virus injection and perfused after 3 weeks, where tdTomato is visible in the DAT$^+$ cells. Axonal morphology is altered by the presence of puncta/beads. (E) Image representative of a PMv section of a mice female Ai9 (RCL-tdTomato) DAT-IRES-Cre flox/wt cre/wt 500 nL AAV-CAG-DIO-taCaspase3-TEVp bilaterally virus injection, perfused after 3 weeks, stained with NeuN marker (SQL-03206). (F) Merge of D and E images.

Panel 2. PMv-DAT^{+} Cells Axonal Morphology, stained with NeuN, after 1 uL AAV-CAG-DIO-taCaspase3-TEVp bilaterally virus injection. (A) Image representative of a PMv section of a control mice female Ai9 (RCL-tdTomato) DAT-IRES-Cre flox/wt cre/wt, where tdTomato is visible in the DAT+ cells. Axonal shape is regular. (B) Image representative of a PMv section of a control mice female Ai9 (RCL-tdTomato) DAT-IRES-Cre flowx/wt cre/wt stained with NeuN marker. (C) Merge of A and B images. (D) Image representative of a PMv section of a mice female Ai9 (RCL-tdTomato) DAT-IRES-Cre flox/wt cre/wt with 1 uL AAV-CAG-DIO-taCaspase3-TEVp bilaterally virus injection and perfused after 3 weeks, where tdTomato is visible in the DAT+ cells. Axonal morphology is altered by the presence of puncta/beads. (E) Image representative of a PMv section of a mice female Ai9 (RCL-tdTomato) DAT-IRES-Cre flox/wt cre/wt 1 uL AAV-CAG-DIO-taCaspase3-TEVp bilaterally virus injection, perfused after 3 weeks just stained with NeuN marker (SQL-03202). (F) Merge of D and E. Images were acquired using a Zeiss AxioImager M2 microscope (20X magnification). Scale bar: 50 um.

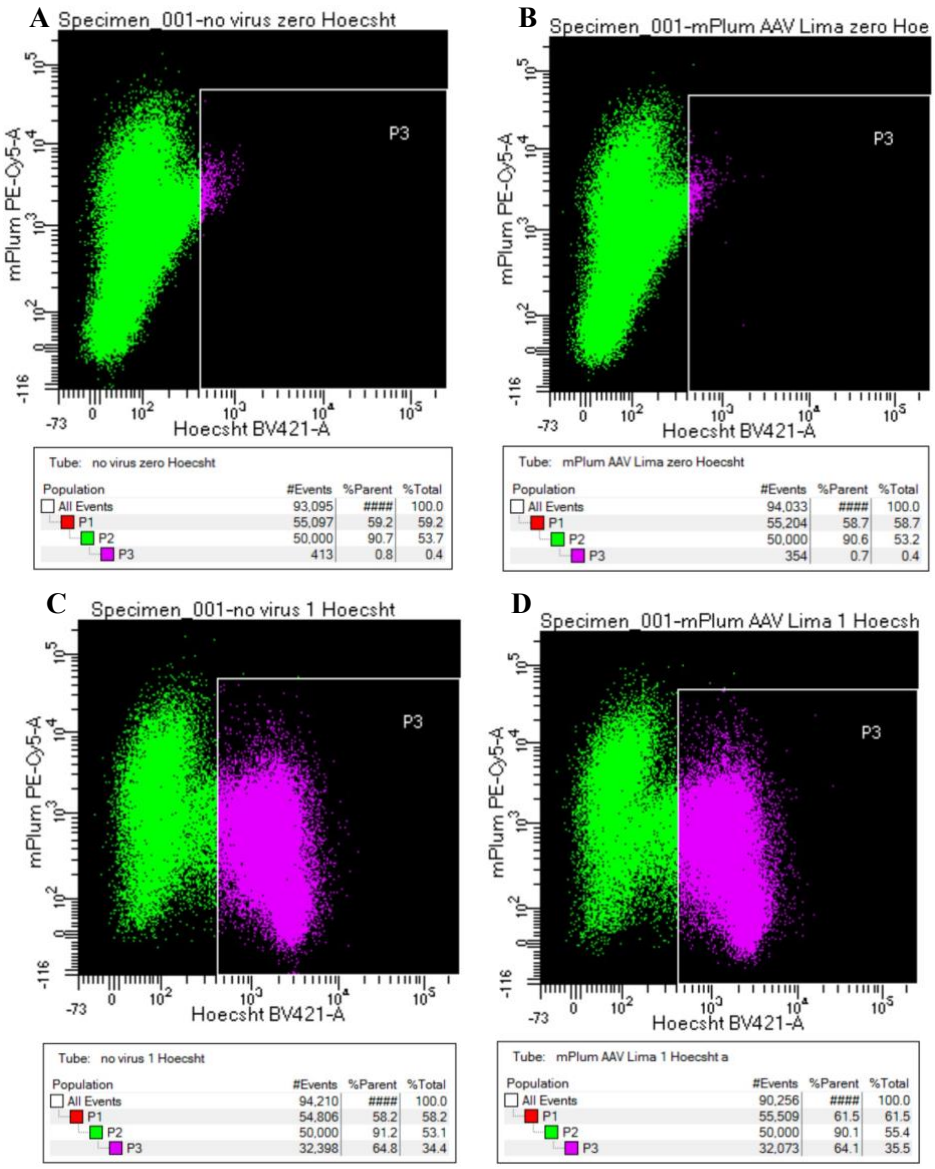

Supplementary Figure 2. *In vitro* quantification of 293T Cre cell death after one-week of virus infection. P2 (green) represents the fluorescence intensity of live cells and P3 (purple) represents death cells. (A) Fluorescence-Activated Cell Sorting quantification of cells, without Hoecsht 3258 marker (cell death marker). (B) Fluorescence-Activated Cell Sorting quantification of cells infected with AAV2-CAG-DIO-taCaspase3-TEVp and without Hoecsht 3258 marker (cell death marker). (C) Fluorescence-Activated Cell Sorting quantification of cells with Hoecsht 3258 marker. Cell death percentage is around 65%. (D) Fluorescence-Activated Cell Sorting quantification of cells infected with AAV2-CAG-DIO-taCaspase3-TEVp and stained with Hoecsht 3258 marker. Cell death percentage is around 64%.

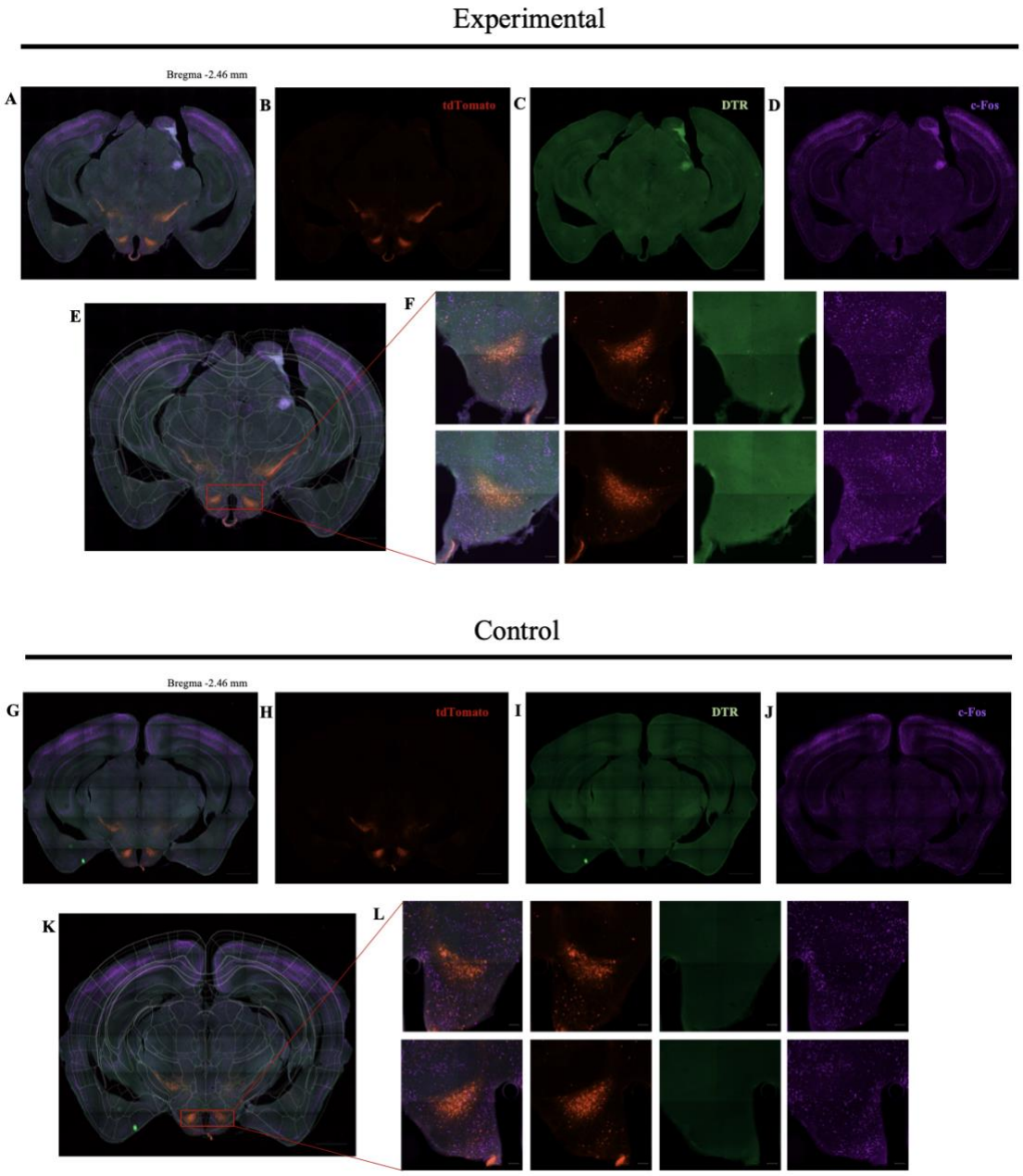

Supplementary Figure 3.

Panel 1. Representative microscopy results of Ai9(RCL-tdTomato) DAT-Cre females injected with DTR receptors and DTx, after sexual behavior performance. Animals were transfected with AAV2-FLEX-DTR-GFP bilaterally in the PMv and injected intraperitonially with Diphtheria Toxin two weeks after. Female natural estrous cycling was monitored afterwards, and they were allowed to interact and performed sex with an experienced male during their receptive phase of the cycle (proestrus/estrus). (A-D) Representative brain slice (bregma: -2.46 mm) with the PMv region, in 10X magnification; scale bar: 1000 um. (E) Representation of the same brain slice (bregma: -2.46 mm), with 10X magnification, embedded in the mouse brain atlas configuration; scale bar: 1000 um. (F) ROI images of the PMv, with 20X magnification, in both hemispheres; scale bar: 100 um.

Panel 2. Representative microscopy results of Ai9(RCL-tdTomato) DAT-Cre females with DTx after sexual behavior performance (control group). Animals were submitted to a craniotomy and injected intraperitonially with Diphtheria Toxin two weeks after. Female natural estrous cycling was monitored afterwards, and they were allowed to interact and performed sex with an experienced male during their receptive phase of the cycle (proestrus/estrus). (G-J) Representative brain slice (bregma: -2.46 mm) with the PMv region, in 10X magnification; scale bar: 1000 um. (K) Representation of the same brain slice (bregma: -2.46 mm), with 10X magnification, embedded in the mouse brain atlas configuration; scale bar: 1000 um. (L) ROI images of the PMv, with 20X magnification, in both hemispheres; scale bar: 100 um.

PMv-DAT$^+$ are represented in red by the fluorophore tdTomato. In green (Alexa 488) are the Diphtheria Toxin Receptor (DTR) positive cells and, in purple (Alexa 647), are represented the c-Fos immediate early gene positive cells. Females were exposed 5 minutes to a male mouse before perfusion to allow the activation of social brain regions. Images were acquired using a Zeiss AxioImager M2 microscope.

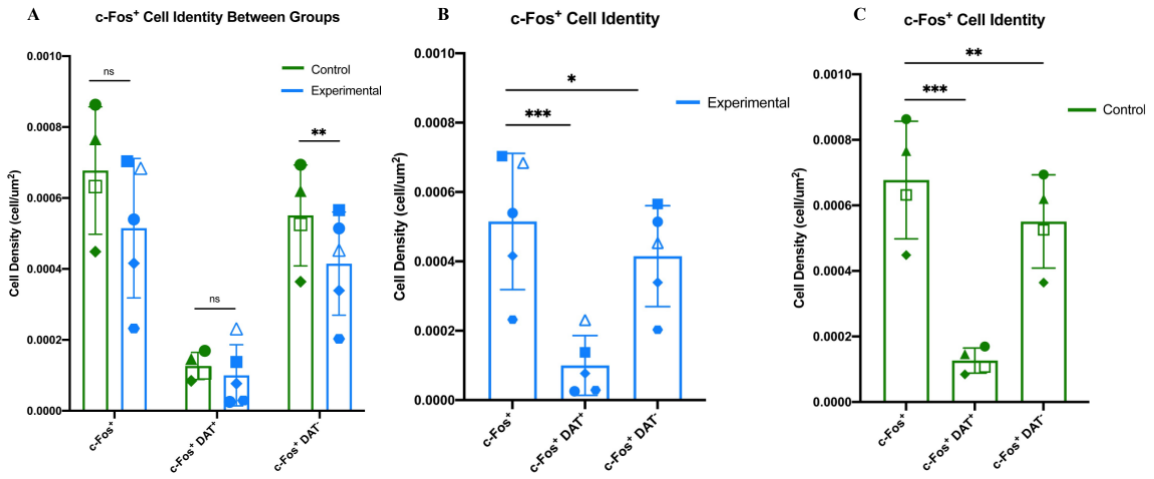

Supplementary Figure 4. c-Fos$^+$ cell density in experimental and control females. (A) Cell number per area in experimental (n=5) and control females (n=4). (B) Cell number per area in experimental animals. (C) Cell number per area in control females. Each point type represents a different animal. Open symbols represent animals that were not counted in the behavioral analysis as they did not perform sexual behavior (triangle in experimental group and square in control group). Normality was tested in all groups. T-Test for two independent sample was used for access statistical significance. Error bars represent mean ± SD. Significance was noted as *p < 0.05, **p < 0.01, ***p < 0.0005.

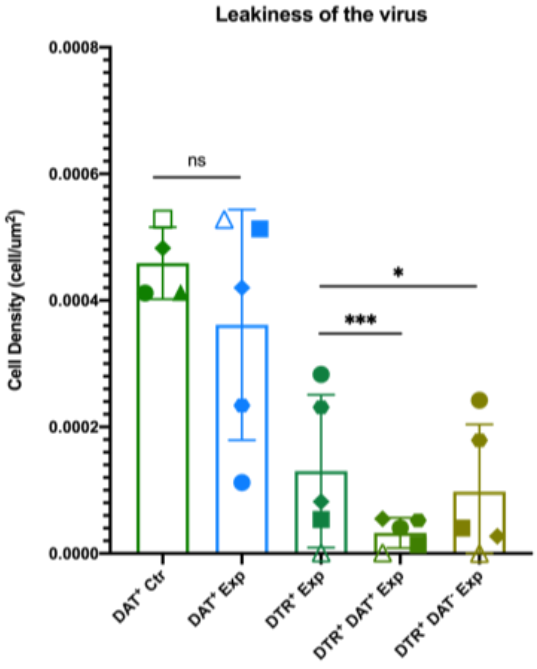

Supplementary Figure 5. Viral leakiness in experimental females. Cell density (number of cells per area) for DAT$^+$, DTR$^+$ and co-localization between DAT$^+$ and DTR$^+$. Normality was tested in all groups. Each point type represents a different animal. Open symbols represent animals that were not counted in the behavioral analysis as they didn't perform sexual behavior (triangle in experimental group). T-Test for two independent sample was used for access statistical significance. Error bars represent mean ± SD. Significance was noted as *p < 0.05, **p < 0.01, ***p < 0.0005.

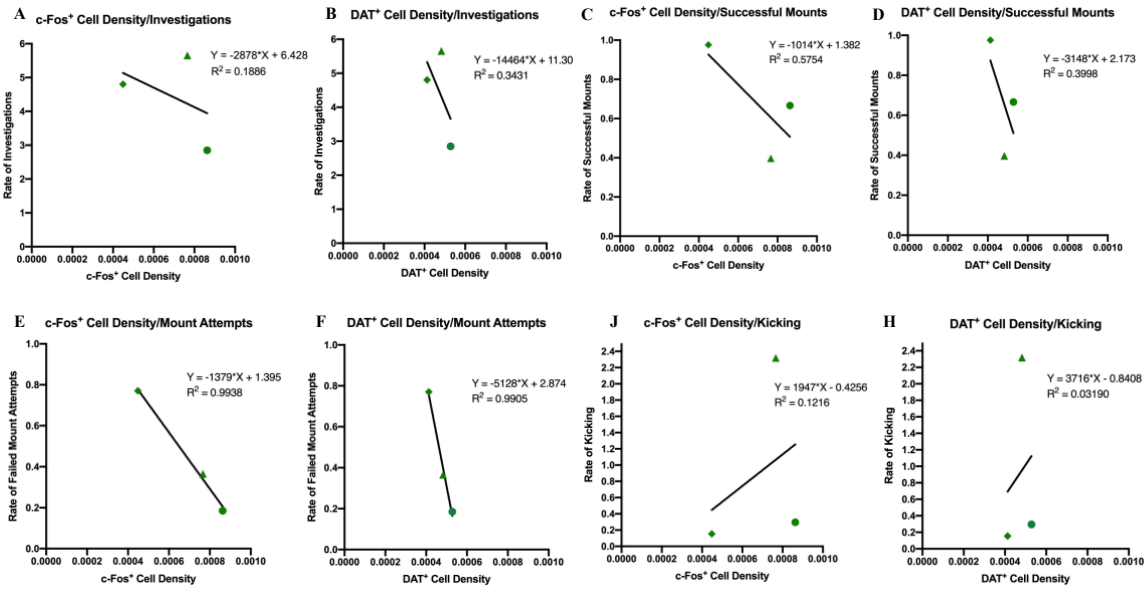

Supplementary Figure 6. Correlation between c-Fos$^+$ and DAT$^+$ cell density with sexual microbehaviors in control females (n=3). (A) Rate of investigations during all session correlated with c-Fos$^+$ cell density. (B) Rate of investigations during all session correlated with DAT$^+$ cell density. (C) Rate of successful mounts during all session correlated with c-Fos$^+$ cell density. (D) Rate of successful mounts during all session correlate with DAT$^+$ cell density. (E) Rate of failed mount attempts during all session correlate with c-Fos$^+$ cell density. (F) Rate of failed mount attempts during all session correlate with DAT$^+$ cell density. (G) Rate of kicking during all session correlate with c-Fos$^+$ cell density. (H) Rate of kicking during all session correlate with DAT$^+$ cell density. Each point represents a different animal.